Universidade de Évora - Instituto de Investigação e Formação Avançada

Programa de Doutoramento em Ciências da Terra e do Espaço

Área de especialização | Física da Atmosfera e do Clima

Tese de Doutoramento

Global and Direct Solar Radiation at Surface over Iberian Peninsula: Variability, Trends and Forecasting

João Carlos de Carvalho Branco Perdigão Marquês

Orientadores | Rui Paulo Salgado

Maria João Costa

Évora 2021

Universidade de Évora - Instituto de Investigação e Formação Avançada

Programa de Doutoramento em Ciências da Terra e do Espaço

Área de especialização | Física da Atmosfera e do Clima

Tese de Doutoramento

Global and Direct Solar Radiation at Surface over Iberian Peninsula: Variability, Trends and Forecasting

João Carlos de Carvalho Branco Perdigão Marquês

Orientadores | Rui Paulo Salgado

Maria João Costa

Évora 2021

A tese de doutoramento foi objeto de apreciação e discussão pública pelo seguinte júri nomeado pelo Diretor do Instituto de Investigação e Formação Avançada:

Presidente	António José Candeias (Universidade de Évora)
Vogais	Ana Maria Guedes de Almeida e Silva (Universidade de Évora) Carlos Alberto Leitão Pires (Universidade de Lisboa - Faculdade de Ciências) Dina da Conceição Nunes dos Santos (Instituto Português do Mar e da Atmosfera) Inmaculada Foyo Moreno (Universidad de Granada) Rui Paulo Salgado (Universidade de Évora) (Orientador)

Évora 2021

“Nunca temos uma ideia do que podemos conseguir. Tudo o que fazemos é perseguir uma interrogação e ver até onde ela nos conduz.”

Jonas Salk

Este trabalho é dedicado aos meus pais.

The work in this thesis is my own, with the exception of references to other researchers (and respective work) which has all been appropriately referenced.

Preface

This thesis, in which three scientific papers are presented, is submitted to acquire the doctoral degree in Earth and Space Sciences with specialization in Atmosphere Physics and Climate, by the University of Évora.

This work is the result of a laborious journey between my full-time work (High school Teacher) and research (reading, writing, programming ...) at the Institute of Earth Sciences (Évora), and at Portuguese Institute for Sea and Atmosphere (IPMA), in Lisbon. During the first four years of this PhD I also participated in seminars with oral or poster presentations:

- Online workshop on Earth and Space Sciences with focus on Atmospheric Physics and Climate, with a short communication: "Assessment of Direct Normal Irradiance Forecasts based on IFS/ECMWF data and observations in the south of Portugal" (Évora, June/2020)
- 8ª Assembleia Luso-Espanhola de Geodesia e Geofísica, com apresentação de um Poster: "Climatology, variability and trends in solar radiation at the surface in the Iberian Peninsula using the $WRF-ARW$ model", (Évora, Jan/2014)
- Workshop em Ciências da Terra e do Espaço, com apresentação intitulada:"Analysis of $WRF-ARW$ model performance to estimate shortwave downward radiation in Spain", (Évora, Fev/2013)
- 7th Portuguese-Spanish Assembly of Geodesy and Geophysics, com apresentação de comunicação intitulada: "Numerical modeling of incident short wave radiation over Iberian Peninsula with WRF model", (Donostia/Spain, Jun/2012)
- Fifth Meeting of Post-Graduation in Physics and Earth Sciences of University of Évora, with a short communication:"Variabilidade da Radiação Solar à Superfície em Portugal", (Évora, Set/2011)
- Global Conference on Global Warming, with a short communication "Inter Annual Variability of Surface Solar Radiation over Iberian Peninsula", (Lisboa, Jul/2011)
- XIV Congresso Latino-Americano e Ibérico de Meteorologia, com apresentação de comunicação intitulada "Variabilidade Inter-Anual da Radiação Solar à Superfície na Península Ibérica", (Setúbal, Mar/2011)

As result of previous meetings I wrote three conference papers:

- **Perdigão, J**., Salgado, R., Prasad, H., Costa, MJ., 2013, Analysis of WRF-ARW model performance to estimate shortwave downward radiation in Spain, Livro de Actas, ISBN: 978-989-98196-2-7
- **Perdigão, João**, Dasari, Hari, Salgado, R., Costa Maria João, 2011. Numerical modeling of surface radiation over Iberian Peninsula with special reference to Portugal. Proceedings of the Global Conference on Global Warming 2011, 11-14 July, 2011, Lisbon, Portugal.
- **Perdigão, J**., H. Dasari, R. Salgado, 2011. Variabilidade inter-anual da radiação solar à superfície na Península Ibérica. In: 7º Simpósio de Meteorologia e Geofísica da APMG; 12º Encontro Luso-Espanhol de Meteorologia; XIV Congresso Latino-Americano e Ibérico de Meteorologia. Setúbal-Portugal. Anais da APMG.

I also participated, as a co-author, in the article:

- Dasari, H. P., Salgado, R., **Perdigao, J**., Challa, V. S., 2014. A Regional Climate Simulation Study Using WRF-ARW Model over Europe and Evaluation for Extreme Temperature Weather Events. International Journal of Atmospheric Sciences, Article ID: 704079, 22 p.

In a first stage, the work leading to this thesis was supervised by Professor Rui Salgado, Professor Maria João Costa and Doctor Hari Prasad. After returning to the doctoral course, Doctor Hari Prasad was no longer in Évora and the thesis was concluded under the supervision of Rui Salgado and Maria João Costa.

Évora, 16 November 2020

João Perdigão

MSc. Astronomy and Astrophysics

Acknowledgments

I would firstly like to thank my supervisors Prof. Dr. Rui Salgado, Doctor Hari Prasad and Prof. Dra. Maria João Costa for supporting and encouraging me during this Ph.D. work. I am also thankful to Prof. Dr. Paulo Canhoto. There are no words to express my gratitude for their continuous support specially to Prof. Rui Salgado.

To the IPMA who received me during a short period of this work and, in particular, to Dr. Manuel Mendes, who guided and supported me during that journey.

I am also grateful to all my friends and family that supported me through this project, during both ups and downs as well as for helping me having a somewhat normal social life.

Abstract

Besides being the key to Earth's climate, global solar radiation at the surface ($SW\downarrow$) is one of the most valuable renewable resources. This way, an adequate knowledge of the solar resource is critical as an assessment for a strategic planning of projects related to the production of solar energy. Therefore, the main goals of this thesis is to analyze past changes and variability of solar radiation fluxes in Portugal and Iberia Peninsula (IP) using observational available measurements, ERA–40 and NCEP/NCAR reanalysis datasets and, predict and characterize the solar radiation at the surface over Iberian Peninsula based on numerical weather prediction models.

In a first part, this study is dedicated to the analysis of temporal and spatial variability of $SW\downarrow$ based on ground-based stations, as well as in ERA–40 and NCEP/NCAR reanalysis. Parametric and non-parametric tests are applied to detect trends in both reanalysis and ground-based observations. Cloud cover obtained from reanalysis is also used to examine the possible causes of the observed long-term changes in $SW\downarrow$. In a second stage, is presented an assessment of the $SW\downarrow$ WRF model at high resolution ($5\,km$) against observations and with another WRF configuration. After a bias removal process, a $SW\downarrow$ and cloud cover climatology was obtained for IP (1950–2010 period). Finally, the performance of IFS/ECMWF is evaluated to predict Direct Normal Irradiance (DNI) over Évora city at very short (1 hour) and short term (1 to 3 days), for one year period. It is also described a new methodology to compute DNI attenuation using *in situ* observational data in order to estimate the transparency of the atmosphere in the absence of cloud cover datasets. To improve IFS/ECMWF outputs is also tested a bias correction methodology.

Keywords: Iberian Peninsula; Solar Radiation; Reanalysis products; Dimming/brightening periods; WRF model

Resumo

A Radiação Solar Global e Direta à Superfície na Península Ibérica: Variabilidade, Tendências e Previsão

A radiação solar é um dos recursos energéticos renováveis mais valiosos. Na Península Ibérica (PI) estão em instalação muitos sistemas comerciais e de investigação para o aproveitamento da energia solar. Neste contexto, o conhecimento do fluxo de radiação solar que incide na superfície terrestre e da sua evolução torna-se de extrema importância.

Pretende-se com este trabalho estudar a distribuição espacial, a variabilidade e as tendências da radiação solar de pequeno comprimento de onda ($SW\downarrow$) à superfície, na PI e em Portugal, a partir de dados observacionais e das reanálises ERA–40/NCEP assim como, prever e caracterizar a radiação com base em modelos de previsão numérica do tempo.

Na primeira parte deste estudo, efetua-se uma análise da variabilidade temporal e espacial da radiação $SW\downarrow$ recorrendo a estações terrestres, bem como a dados de reanálise ERA–40 e NCEP/NCAR. Para o efeito utilizam-se testes paramétricos e não paramétricos a fim de detetar tendências nas séries em estudo. A cobertura de nuvens obtida a partir das reanálises é também usada para avaliar as possíveis causas da variabilidade da radiação $SW\downarrow$ observada.

Numa segunda etapa do estudo, obteve-se uma climatologia a 5 km de resolução da radiação solar à superfície com base em simulações com o modelo regional $WRF-ARW$, para a PI, e para o período 1950–2010. Os resultados das simulações foram validados recorrendo a estações de observação e a uma outra simulação WRF, com outra configuração, previamente validada. Na construção da climatologia $SW\downarrow$ e de nuvens foi aplicado um método de pós-processamento para remoção do viés. Finalmente, avalia-se o desempenho do modelo IFS, do ECMWF na previsão da radiação DNI a curto e médio prazo, sobre a região. Propõe-se uma nova metodologia para estimar a transparência da atmosfera e testa-se uma metodologia de correção de viés.

Palavras Chave: Península Ibérica; Radiação solar; Produtos de reanálise; Períodos *Dimming* e *Brightening*; modelo WRF

Table of Contents

List of Figures

List of Tables

List of Acronyms, Symbols and Abbreviations

AEMET Spanish Meteorological Agency

AOD Aerosol Optical Depht

APREN Deloitte and Portuguese Renewable Energy Association

AR5 Fifth Assessment Report

ARW Advanced Research WRF

BIAS Bias Error

BC Bias Correction

CAM Community Atmospheric Model

CDF Cumulative Distribution Function

CERES Clouds and the Earth's Radiant Energy System

CV Coefficient of Variation

CSP Concentrated Solar Power Plants

DAI DNI attenuation index

DNI Direct Normal Irradiance

DTR Diurnal Temperature Range

ECMWF European Center for Medium Time Weather Forecasting

ERA–40 ECMWF reanalysis data set for 1957-2001 period

EU European Union

GHI Global Horizontal Solar Irradiance

IFS/ECMWF Integrated Forecasting System of European Centre for Medium- Range Weather Forecast

IP Iberian Peninsula

IPMA Portuguese Institute for Sea and Atmosphere

IPCC Intergovernmental Panel on Climate Change

IRENA International Renewable Energy Agency

LW Longwave radiation

MAE Mean Absolute Error

MAPE Mean Absolute Percentage Error

MBE Mean Bias Error

MK Mann-Kendall test

MOS Model output Statistic

NAO North Atlantic Oscillation

NBIAS Normalized BIAS

NCEP/NCAR Centers for Environmental Prediction/National Center for Atmospheric Research

NWP Numerical weather prediction models

PBL Planetary Boundary Layer

PV Photovoltaic

RCM Regional Climate Model

RMSE Root Mean Square Error

RSR Ratio between the Root Mean Square Error and the observations Standard Deviation

SD Sunshine Duration

SSRD Downward Global Solar Radiation at the Surface (variable available from ECMWF); Physically means the same as Downward Global Solar Irradiance at the Earth's surface.

SW Shortwave Radiation

SW↓ Downward Global Solar Irradiance at the Earth's surface

SWRCLF Shortwave Radiative Cloud Fraction

TCC Total cloud cover

WMO World Meteorological Organization

WRDC World Radiation Data Centre

WRF Weather Research and Forecasting

σ Standard Deviation

$\boldsymbol{X}$ Mass Fraction of Hydrogen

$\boldsymbol{Y}$ Mass Fraction of Helium

$\boldsymbol{Z}$ Mass fraction of metals

$\boldsymbol{Z_{MK}}$ Statistical value of the Mann-Kendall test

$\boldsymbol{u_{\alpha}}$ α-th percentile of a standard normal variate

$\boldsymbol{\mu}$ mean

1.

Introduction

"The world is a dangerous place to live,

not because of the people who are evil,

but because of the people who don't do anything about it."

Albert Einstein

1.1. Motivation

The Fifth Assessment Report (AR5) of the Intergovernmental Panel on Climate Change (IPCC, 2014), gives us a dramatic picture of the planet Earth as a consequence of climate change, with several implications such as: at the level of wildlife – with the extinction of some species; at the level of agriculture – farmers without means of economic survival; with rising sea levels – coastal cities to be submerged, among others issues.

The main contributor of climate change seems to be identified for a long time – human activity. According to the above-mentioned report, "*Anthropogenic greenhouse gas emissions have increased since the pre-industrial era, driven largely by economic and population growth, and are now higher than ever. This has led to atmospheric concentrations of carbon dioxide, methane and nitrous oxide that are unprecedented in at least the last 800 000 years. Their effects, together with those of other anthropogenic drivers, have been detected throughout the climate system and are extremely likely to have been the dominant cause of the observed warming since the mid-20th century*." (IPCC, 2014)

The theme of climate change has led organizations such as the United Nations or the European Union (EU) to pressure the global community through concerted and planned policy measures (eg, Kyoto protocol) as well as in energy and technology adaptations. In the AR5, we can read

the following: "*Effective implementation depends on policies and cooperation at all scales and can be enhanced through integrated responses that link mitigation and adaptation with other societal objectives.*" In this way, renewable energy sources are part of the solution for the near future, specially the solar energy whose demand is increasing and becoming a reliable and competitive source of energy and simultaneously contributing to the decarbonization.

In 2019, from data obtained in the International Renewable Energy Agency (IRENA), China comes as the first country with the largest installed solar capacity (photovoltaic and thermal), with an annual production of $\sim 205\, TWh$, followed by the United States of America ($\sim 66\, TWh$) and Japan ($\sim 62\, TWh$). Concerning to European countries, Germany arises in fourth place with $\sim 49\, TWh$, as can be seen in Figure 1.1.

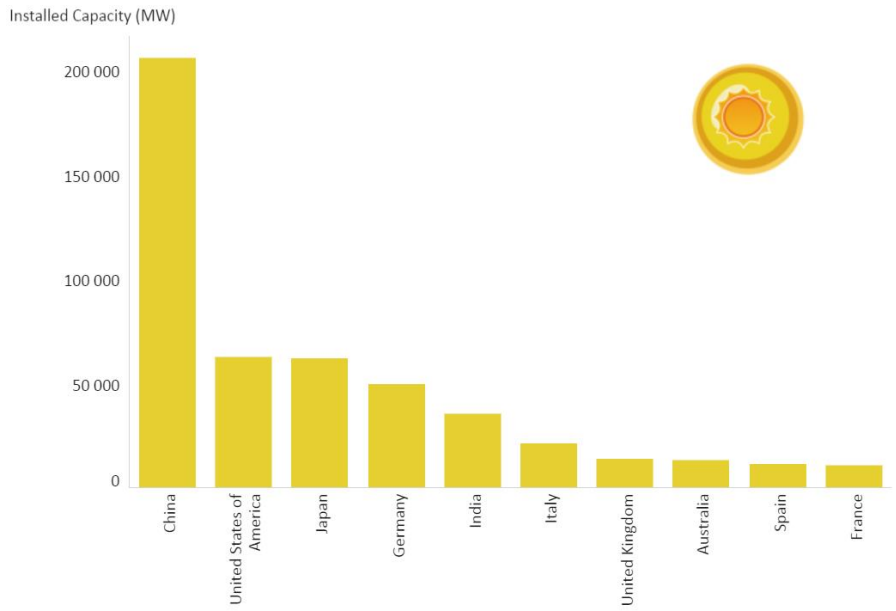

Figure 1.1. Ranking of the ten countries with the largest installed solar capacity.

Figure obtained from the website of International Renewable Energy Agency.

According with the latest statistics report from Statistical office of the European Union (EUROSTAT), and relative to the countries of the EU, in 2016, the greenhouse gas emissions were reduced by more than 20% compared with the beginning of the nineties of the last century. For instance, in Portugal, in 2018, electricity production from renewable sources was 29 877 GWh (corresponding to 52.6% of total electricity production), contributing to a saving of 189 million euros in CO_2 allowances. These values allowed a reduction of 12 megatonnes of CO_2 emissions (APREN, 2019).

Regarding data from IRENA, for Portugal, and for the last two decades, it's evident the grow of solar energy (above 20%), making it at as a practical and sustainable alternative source in the production of electric energy (see Figure 1.2). In this way, it is imperative to analyze the economic and operational viability of future systems that use solar energy in a specific region. For example, for Portugal, and in what concerns to the impact of renewable energy study in gross domestic product, according with the study developed by Deloitte and Portuguese Renewable Energy Association (APREN), in 2030, it is expected that the contribution of electricity generation from renewable energies will be around 11 billion euros (APREN, 2019). On the other hand, there is an implicit need to quantify the solar potential and its evolution on a scale of several years or decades (in the past and future), as well as obtaining reliable forecast in a very short period, short (48 to 72 hours) and in the medium term (up to 10 days).

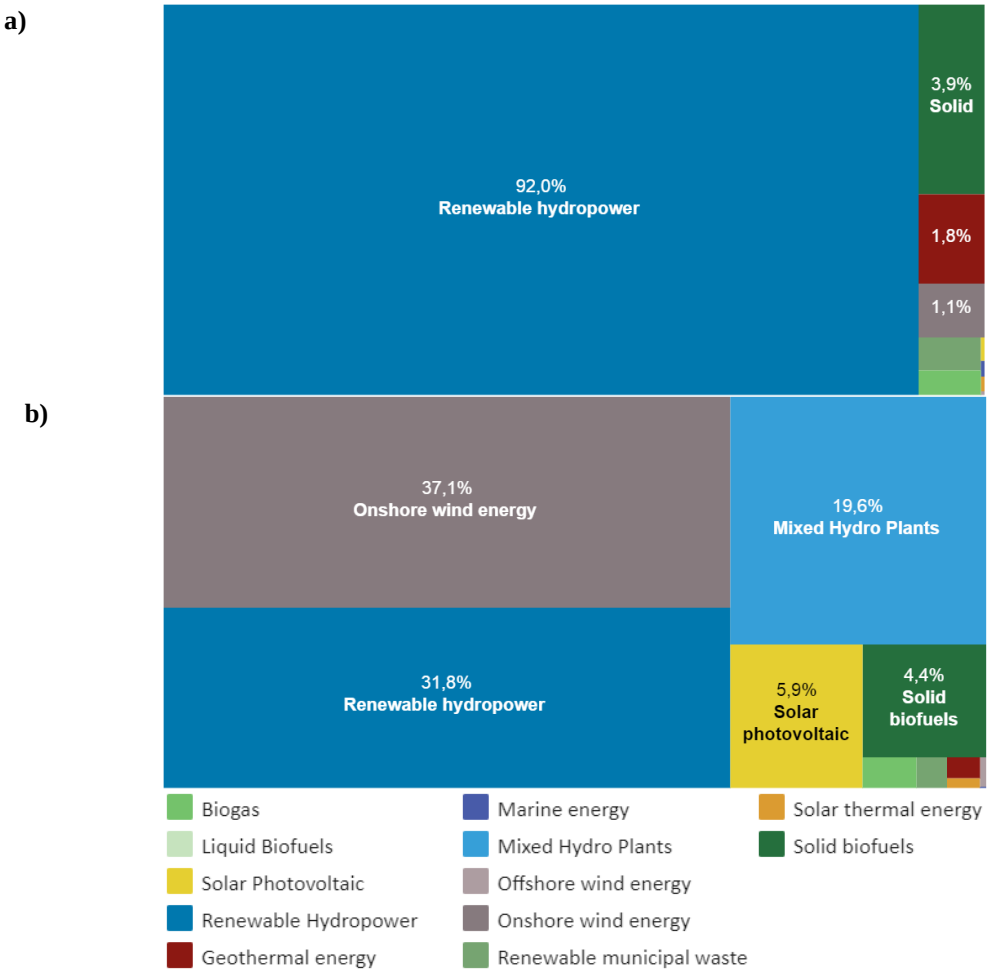

Figure 1.2. Percentage of the installed capacity in Portugal for renewable energy sources between 2000 (Figure 1.2a) and 2019 (Figure 1.2b).

Figures obtained from the website of IRENA.

Studies on the variability of solar radiation are limited due to low availability of global radiation data in certain regions of the globe such as Africa, South America and the Maritime Continent

(i.e., Southeast Asia countries), and particularly the entire ocean areas (Wild, 2016). On the other hand, the regions where solar radiation data exist, have other problems, such as the size of the series and the fact that many of them are incomplete, or even some of the measurements obtained may be dubious, due to the lack of calibration of the measuring instruments (see for instance, García *et al*., 2014).

In recent decades, methods and models were developed in order to overcome some of these constraints, such as using climate data like sunshine duration (SD) or the diurnal temperature range (DTR) as proxies for solar radiation analyses (e.g., He *et al*., 2018; Rahimzadeh *et al*., 2015, Sanchez-Lorenzo *et al*., 2007, among others); application of reanalysis products such as ERA–40 (European Center for Medium Time Weather Forecasting reanalysis data set for 1957–2001 period), MERRA (Modern-Era Retrospective analysis for Research and Applications) or NCEP/NCAR (Centers for Environmental Prediction/National Center for Atmospheric Research) (Zhao *et al*., 2013; Wild and Schmucki, 2011; Träger-Chatterjee *et al*., 2010); application of numerical weather prediction models (NWP) (Magarreiro *et al*., 2014; Jimenez *et al*., 2016;); analyses from images/data from satellite observations (e.g. Ayeta and Tandeo, 2018; Pfeifroth *et al*., 2018a); application of statistical/physical methods (Angstrom, 1924; Chineke, 2008; Noorian, *et al*., 2008) or artificial neural networks (Dorvlo *et al*., 2002; Reikard, 2009; Mellit and Pavan, 2010; Qazi *et al*., 2015).

IPCC in its 2014 report stated that Climate models have improved since the fourth Assessment Report (AR4) and summarizes some of the accomplishments made, such as changes in upper-ocean heat content, continental-scale patterns of precipitation, global mean surface temperature, climate phenomena (such as monsoons or El Niño-Southern Oscillation, …). According with AR5 these improvements were achieved because recent models integrate better cloud and aerosol parametrizations, carbon cycle, among other schemes.

As seen previously, the knowledge of incoming solar radiation is an important factor in our society in an economic, social (health, employability, ...) and meteorological perspective. On the other hand, the study of variations and trends in climatic series (radiation and clouds, among others climatic variables) allows us to study the trends in the past and helps us to predict the possible scenarios in the near future. In this context, the major reasons and motivation for this study are:

(1) The lack of direct measurements, or very short time series of global solar radiation and clouds in Portugal;

(2) The absence of solar radiation studies to assess and quantify the errors associated to the European Center for Medium Time Weather Forecasting (ECMWF) and National Centers for Environmental Prediction/National Center for Atmospheric Research (NCEP/NCAR) reanalysis in order to reproduce radiative fluxes and clouds in Portugal and Spain;

(3) The number of studies with reference to solar radiation climatology with good resolution over Iberian Peninsula, and in particular, over the Portuguese territory, are limited;

(4) Few studies to assess to the capacity of Advanced Research – Weather Research and Forecast ($WRF - ARW$) regional model to predict solar radiation in IP for a long period. Some studies using this model are restricted to some Spain areas;

(5) The number of ongoing projects for the construction of Concentrated Solar Power Plants (CSP) over IP (and in the Évora region).

1.2. Objectives and structure of the thesis

The present work aims to contribute to the evaluation of the solar resource in two specific domains: analysis of the trends of global solar radiation at the surface in particular for Portugal and in the Iberian Peninsula, in the context of ongoing climate change; and in the prediction of solar radiation (global and direct) on the Earth's surface based on the results of numerical weather forecasting models and models of radiative transference in the atmosphere.

The specific objectives are:

(1) To study global solar radiation at the Earth's surface in Portugal, using data from ground-based stations, as well as the reanalysis products of ECMWF and NCEP/NCAR. The cloud cover obtained from the ECMWF is also considered in order to assess the possible causes of the changes observed (in the past) on solar radiation.

(2) To characterize the solar resource in the IP using the Weather Research and Forecasting (WRF) model to predict the downward global solar irradiance at the Earth's surface.

(3) To evaluate the quality of the Integrated Forecasting System of the European Center for Medium-Range Weather Forecast (IFS/ECMWF) model to forecast the direct normal irradiance at the Earth's surface, in Évora, for different time horizons of weather forecasting.

In order to achieve the specific objectives, the main body of this thesis comprises three publications, presented as individual chapters.

In ***chapter two***, from ERA–40 and NCEP/NCAR reanalysis, the evolution of the downward global solar irradiance at the Earth's surface and of the cloud cover in the atmosphere over Iberian Peninsula and specially Portugal for the past 50 years is investigated. A monthly and annual analysis of the solar radiation variability was carried out and the trends of the the global solar irradiance reaching the Earth's surface were studied from parametric and non-parametric methods. The reanalysis data were validated and compared with time series obtained for solar radiation at the surface, measured at observation stations on the Iberian Peninsula. A climatology of downward global solar irradiation at the Earth's surface and of the cloud cover is obtained using ERA–40 reanalysis. (***article 1:*** *Perdigão, J. C., Salgado, R., Costa, M. J., Dasari, H. P., Sanchez-Lorenzo, A., 2016. Variability and trends of downward surface global solar radiation over the Iberian Peninsula based on ERA–40 reanalysis. Int. J. Climatol., 36, 3917–3933. doi:10.1002/joc.4603*)

In ***chapter three***, a set of numerical experiments was performed with the $WRF-ARW$ atmospheric model with a horizontal resolution of $5\,km$, covering 60 continuous years (1950–2010), using NCEP reanalysis as initial and boundary conditions. The model grid includes the Iberian Peninsula and adjacent areas to adequately represent coastal circulation and the influence associated with cloud development. The model was run in re-initialization time-slices mode and a bias correction methodology was applied. The results obtained by the atmospheric model were analyzed and validated by comparison with observational data over 65 ground-based stations covering the entire IP and with another $WRF-ARW$ simulation, performed and validated by Soares *et al*., (2012). After validation it was possible to quantify the model's ability to correctly predict solar radiation over IP and, after bias removal, create a climatology of downward global solar irradiation at the Earth's surface and of the cloud cover that could serve as a basis for future projects in the area of power plants. (***article 2*: *Perdigão, Joao, Salgado, Rui, Magarreiro, C., Soares, Pedro M.M., Costa, M.J., Dasari, H.P., 2017. An Iberian climatology of solar radiation obtained from WRF regional climate simulations for 1950–2010 period, Atmospheric Research 198, 198, 151–162.DOI10.1016/j.atmosres.2017.08.016***)

In ***chapter four***, the IFS/ECMWF predictions of direct solar radiation were analyzed. The errors associated with the forecast of this radiative variable were quantified at very short (1 hour) and short term (1 to 3 days), for one year period of data using observations taken at the ground based station of Évora. The quality of the forecast and error quantification were obtained by using a set of statistical parameters. A bias correction (BC) approach is included and it is also developed and tested a method for estimating sky conditions. (***article 3*: *Perdigão, J.; Canhoto, P.; Salgado, R.; Costa, M.J., 2020. Assessment of Direct Normal Irradiance Forecasts Based on IFS/ECMWF Data and Observations in the South of Portugal. Forecasting, 2, 130-150. https://doi.org/10.3390/forecast2020007).***

In the next sections is described briefly the state of the art on solar radiation variability and forecasting, particularly over IP.

1.3. Solar Radiation in Atmosphere: a synthesis

The Sun is the star that sustains the planet's physical, chemical, and biological phenomena and is the main source of energy on planet Earth. It is a gaseous sphere of radius ~ 109 times greater than the Earth and has a mass of ~ 333000 times greater. From an astronomical point of view, it is a star of the main sequence, with a spectral class of $G2V$ type and with a chemical composition of $X = 0.7381$, $Y = 0.2485$ and $Z = 0.0134$ (Asplund *et al.*, 2009), whose energy production occurs via proton-proton reaction (see for instance, Carrol and Ostlie, 1996).

Our Sun is made by several layers: the Core, the radiative and convective layer, the photosphere, the chromosphere, the transition region and the Corona (Zeilik and Gregory, 1998). The surface of the Sun is called the photosphere, has a thickness around 330 km and a temperature around the 5800 K (Carrol and Ostlie, 1996). The total energy emitted by the surface layer of the Sun is approximately equivalent to a blackbody emitter at ~ 5800 K whose theoretical spectrum is given in Figure 1.3a.

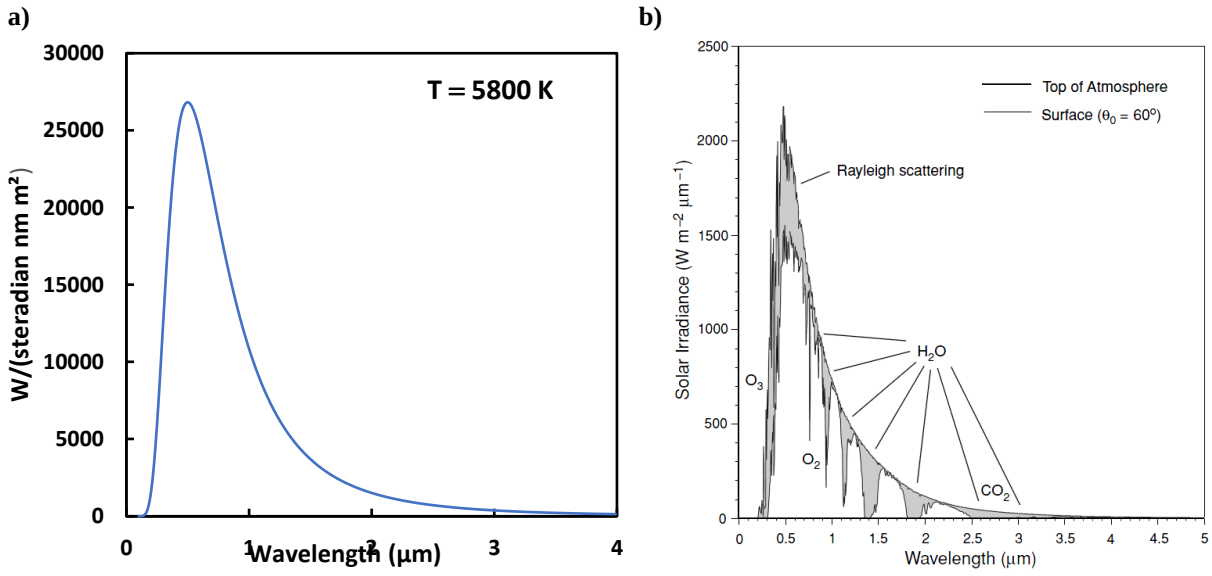

Figure 1.3. Spectral irradiance: (a) blackbody curve of an emitter at $5800K$ assuming an atmosphere without aerosols or clouds and (b) from the Sun at top of atmosphere and surface for a zenithal angle of 60º.

Blackbody spectrum elaborated from online data obtained at SpectraPlot (http://www.spectraplot.com/blackbody). Image (b) taken from Liou (2002).

Figure 1.3b) depicts irradiance spectrum of the Sun for an atmosphere without aerosols or clouds. The differences between irradiances at the top of the atmosphere and the surface are

evident and shows at surface the absorption by atmosphere constituents (specially ozone and water vapor).

One of the interesting features of photosphere layer is the appearance of sunspots (cooler regions) in a cycle of approximately eleven years (see Figure 1.4).

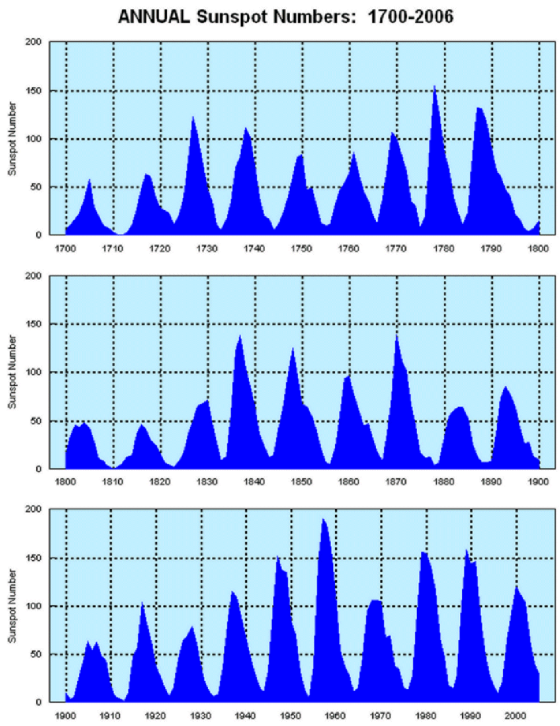

Figure 1.4. Annual mean sunspot number since the beginning of XVII century until present day.
Image was obtained from website of National Oceanic and Atmospheric Administration (NOAA). (https://www.ngdc.noaa.gov/stp/solar/ssn.html).

Some studies try to associate this sunspots phenomenon with climatic variations on the planet. There are records which seem to support that the absence of this phenomenon in the late sixteenth century was associated with a period which is designated by the small ice age and known as the Maunder minimum (Eddy, 1976; Wilson, 1994). It's important to notice that these sunspots are observable since Galileo's era.

Electromagnetic radiation interacts with the atmosphere medium through different processes that depend on its wavelength, the chemical composition and the size of the particles that compose the medium.

Clouds and water vapor are the main responsible for changes in solar radiation at surface (Liou, 2002). On the other hand, aerosols (anthropogenic or natural origin) can affect radiation in a direct or indirect way. In the first case, the aerosols scatter and absorb shortwave radiation and

emit longwave radiation (LW), while in the second case, aerosols also have the ability to interact with the clouds by modifying their structure, properties and longevity (Albrecht, B., 1989; Hansen *et al*., 1997; Lohmann and Feitcher, 2005; Streets *et al*., 2006; among others), known as indirect aerosols effects. The scheme that illustrate the indirect aerosols effects can be seen in Figure 1.5.

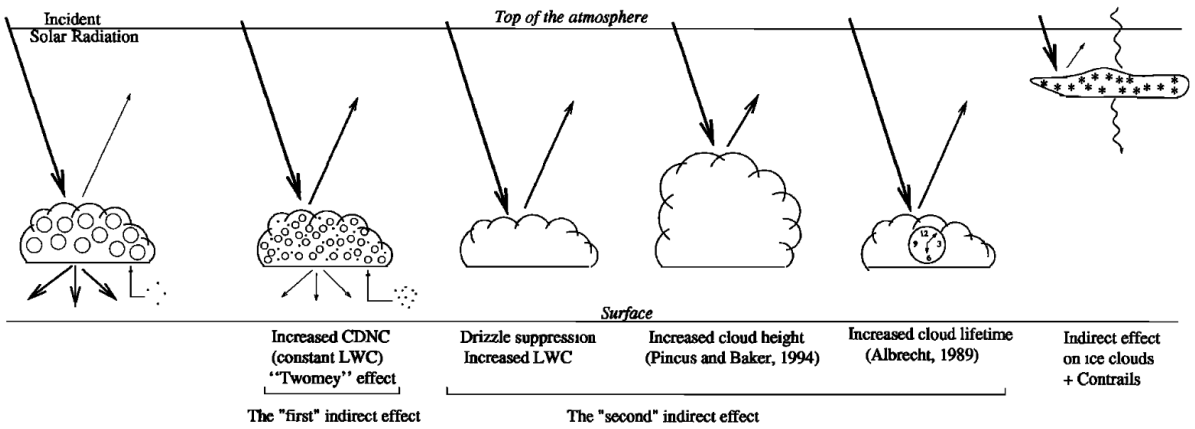

Figure 1.5. Aerosols impact in cloud properties. CDNC and LWC means cloud droplet number concentration and liquid water content, respectively.

Image taken from Haywood and Boucher (2000).

In Earth Sciences and in the theory of radiative transfer it is usual to divide the electromagnetic spectrum into two parts: short (SW) and LW radiation. Radiation whose wavelength is in the range of 0.1 to 4 μm is called SW and is associated with the energy that comes from the Sun (known as Global Radiation). Radiation whose wavelength range is between 4 to 100 μm is called LW and is associated with the energy that is emitted by the surface of the planet and its atmosphere constituents.

Global solar radiation is the algebraic sum of direct and diffuse solar radiation. Direct solar radiation (DNI) is defined as the downward solar radiation coming from the Sun that reaches the earth's surface directly. Diffuse solar radiation (DIF) is the component of downward radiation scattered by constituents (gases, aerosols and clouds) in the Earth's atmosphere. These components are depicted in Figure 1.6.

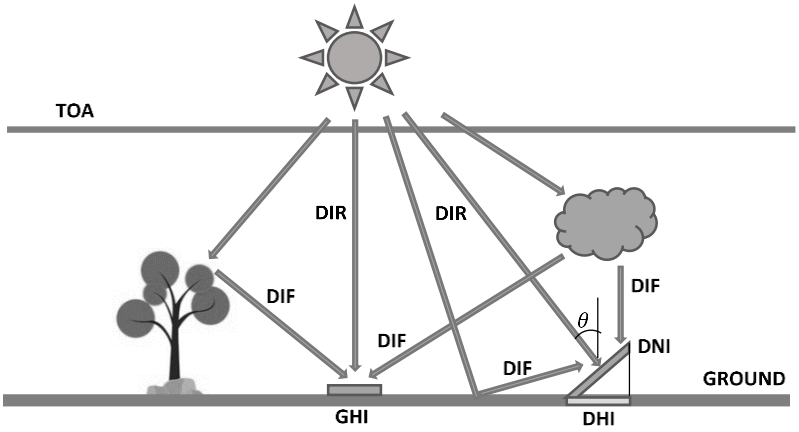

Figure 1.6. Components of solar radiation between the top of atmosphere (TOA) and the ground for a horizontal and tilted plane: Direct Horizontal Solar Irradiance (DHI), Direct Normal Solar Irradiance (DNI), Global Horizontal Solar Irradiance (GHI).

Scheme elaborated from Chan, 2013. The drawing is not to scale.

Measurements of Global Horizontal Irradiance (GHI), also known as surface downward solar radiance ($SW\downarrow$), the DNI and DIF are made with a pyranometer mounted horizontally, by a pyrheliometer mounted in an automatic solar tracker and by a pyranometer shaded from the direct sunlight, respectively. The relation between these quantities is given by

$$GHI = DNI \times cos(\theta) + DIF_{Horizontal} \tag{1.1}$$

where θ refers to the solar zenith angle (Liou, 2002).

One of the first models used for estimating global radiation was proposed by Angstrom (1924) and was a linear relation between sunshine hours (theoretical and real) in the form,

$$\frac{H}{H_c} = \alpha + (1 - \alpha)\frac{n}{N} \tag{1.2}$$

where α is an empirical constant with a value of 0.2 related to the mean proportion of radiation received on a totally overcast day, and n and N are actual and maximum theoretical sunshine durations, respectively. Both quantities H and H_c in Eq. 1.2 should be specified as well as their relation with the previous quantity GHI. Originally H_c was the maximum downward solar irradiance at the surface on a clear day, which was later substitute by H_0 in the Angstrom-Prescott Equation 1.3 being H_0 the maximum extraterrestrial irradiance. Although, we do not

intend to discuss this equation since this diverges from the essential focus of this thesis, one of the problems of its application was the necessity of knowing the solar radiation under clear sky days (H_0).

The equation (1.2) was slightly modified by Prescott (1940) and, nowadays, is known as Ångström-Prescott equation,

$$\frac{H}{H_0} = a + b\frac{n}{N} \tag{1.3}$$

In equation (1.3) a and b are constants to be determined (experimentally) and are specific for each region.

Several types of regression models (and empirical coefficients) have been evaluated and proposed in literature using equation (1.3) (see Prescott, 1940; Hinrichsen, 1994; among others). For instance, Stanhill *et al*. (2014) using Angstrom-Prescott equation found absence of significant changes in values of a and b, caused by aerosols, and concluded that cloud cover played the major role in dimming and brightening phenomena as discussed in the next section.

Accurate forecast of solar components at a given location is of great importance for many solar radiation projects. This way, a solar quantification is necessary for CSP or photovoltaic (PV) power plants that require the knowledge of direct normal solar irradiance and of the global solar irradiance at the Earth surface, respectively.

The production of electricity from CSP systems is obtained from the conversion of DNI into heat by concentrating solar radiation through parabolic mirrors (see Figure 1.7), while PV systems convert solar energy in (direct current) electricity using specific materials (semiconductor), by photovoltaic effect. These systems require the knowledge of global radiation. In what concerns to CSP systems there are different power plant operational schemes to obtain heat from DNI radiation. Figure 1.7 shows a diagram of different types of CSP systems.

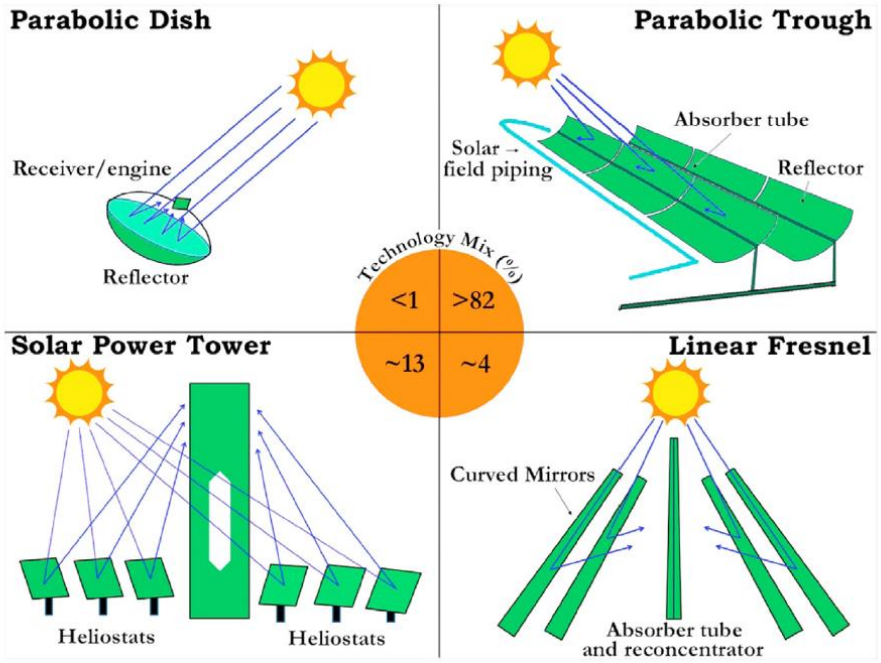

Figure 1.7. Different types of CSP technologies.

Scheme obtained from Islam *et al*. (2018).

A comprehensive review of state-of-the-art concentrated solar power can be seen in Islam *et al*. (2018), among others. In the literature there are several articles focus on the assessment and review of predictions in solar components, such as Bijarniya *et al*. (2016), who presented a review of concentrate solar power technology; Qazi *et al*., (2015), who compare artificial neural networks with other empirical models, or Inman *et al*. (2013) which also analyzed extensively solar forecasting methods and applications. This study of Yang *et al*. (2018) showed a history and trends in solar irradiance and PV power forecasting by establishing the technological infrastructure and identifying the key innovations in recent advances in solar forecasting.

Several authors already mentioned the importance of knowing DNI component of solar radiation with at least one day-ahead of forecasting for purpose of maximizing profit (Lopes *et al*., 2018; Nonnenmacher *et al*., 2016; Law *et al*., 2014, among others). Vick *et al*. (2012) mentions in their article that: "*To estimate how well CSP plants can meet utility electrical loading, the monthly insolation and diurnal accuracy of the DNI models should also be evaluated to determine what sky conditions, times of the year, and locations that the DNI models still need improvement*". According with Kraas *et al*., (2013), for CSP stations in Spain, "*…a 38h forecast is required to calculate the electricity production for sale on the market by means of a power plant model*". Nowadays, there are several methods to obtain the different

components of solar radiation. For example, a recent study made by Ayeta and Tandeo (2018), showed a computationally and efficient method to predict GHI. After a simple pos-processing BC, the authors reached a conclusion that the methodology is adequate for operational applications in different geographical regions. This study of Lee *et al*. (2017) also compared and evaluated models (ten) in order to convert GHI in DNI, for Korea, in 2007–2009 period, and reported one of the models (Reindl-2 model) as the most suitable. Nevertheless, in the same work, the authors proposed a new method and found that errors ($Bias$ and root mean square error – $RMSE$) were significantly lower (in order of 10%) than found with the other models.

The incoming solar radiation that is absorbed by the atmosphere and by the surface of the Earth (i.e that is absorbed by the system Globe+atmosphere) has to be balanced by the outgoing longwave radiation emitted by the system Globe+ atmosphere at the Top of the atmosphere (TOA), due to the principle of conservation of energy. This balance between the incoming (↓) energy from the sun and the outgoing (↑) energy from the Earth is known as energy budget. The net Radiation Budget at the Earth's Surface (E_{net}) is given by

$$E_{net} = (SW_{\downarrow} - SW_{\uparrow}) + (LW_{\downarrow} - LW_{\uparrow}) \tag{1.4}$$

Over the last few decades a number of studies have been carried out and various schemes have been developed and published in an attempt to establish this energy budget for the Earth (see for instance Wallace and P. Hobbs, 1977, Ramanathan, 1987, Kiehl and Trenberth, 1997 or Stephens *et al*., 2012; among others).

A comparison of recent values referent to global annual mean energy balances estimations have been made by Wild (2017), who reported: "*Increasing consensus thus emerges on a global mean surface downward shortwave radiation near* $185\ Wm^{-2}$*, as well as a global mean surface downward and upward longwave radiation slightly above* $340\ Wm^{-2}$ *and below* $400\ Wm^{-2}$*, respectively*."

Figure 1.8 shows a scheme of the annual mean of Earth's global energy budget and was obtained by Wild *et al*., 2015. A schematic detailed overview of recent determination of global annual energy budgets obtained for different authors can be found in Figure 4 of Wild (2017).

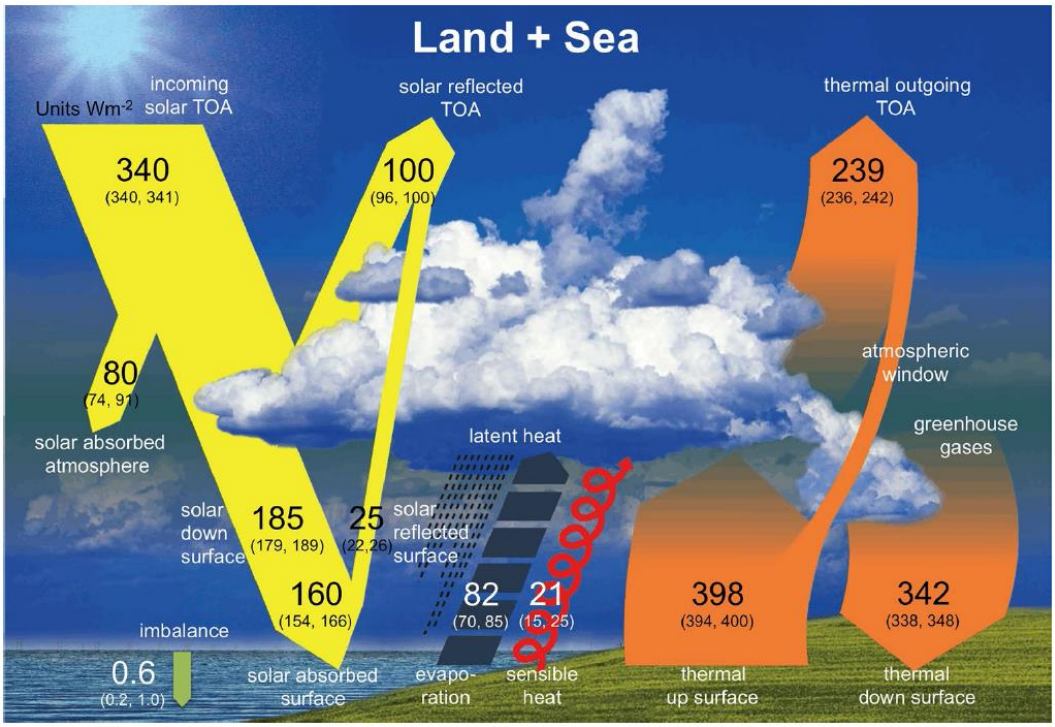

Figure 1.8. Scheme of global annual mean energy budget taken from from Wild *et al*. (2015).
All values are in Wm^{-2}, and uncertainty values are in parentheses. Shortwave fluxes are presented at yellow color and longwave fluxes at orange color.

According with a recent energy budget estimate by Wild *et al*. (2015), from the incoming solar radiation at the top of atmosphere ($340\ Wm^{-2}$), $75\ Wm^{-2}$ is reflected by clouds and aerosols back to space (see Figure 1.8), $80\ Wm^{-2}$ is absorbed by clouds and aerosols.

Without this induced $LW\downarrow$, surface average temperature on Earth would be approximately $255\ K$ (18 ℃) (Coakley and Yang, 2014). Therefore, $185\ Wm^{-2}$ of shortwave incoming radiation reach the Earth surface, although with an amount of $25\ Wm^{-2}$, that is reflected by the surface, back to space, and $160\ Wm^{-2}$ that is absorbed by surface. In order to maintain the balance of energy in the atmosphere + globe system, the outgoing longwave radiation at the top of atmosphere, $\sim 240\ Wm^{-2}$, must be equal to the difference between the incoming radiation at top of atmosphere minus the amount reflected by atmosphere and surface ($100\ Wm^{-2}$), i.e.,the total shortwave radiation absorbed by the atmosphere ($80\ Wm^{-2}$) and surface ($160\ Wm^{-2}$), $= 240\ Wm^{-2}$. With regard to detailed knowledge of the Earth's global energy budget, in Table 1, of Wild (2017), is presented a review of the main radiative components of the annual global mean energy budget obtained in the last two decades from different sources (models, observations, …), and is presented the state of the art relative to this subject as well as

points out some challenges (still) to overcome, such as the partitioning of surface net radiation into nonradiative fluxes of sensible and latent heat, uncertainties of surface albedos, among others.

In the next sections the state of art in what concerns to global solar radiation forecast is presented (main focus of this work).

It is important to notice that, in the present thesis, particularly in the chapters two and three, the terms solar radiation at surface, global radiation, solar radiation or another term related with radiation means Downward Global Solar Irradiance at the Earth's Surface and will be represented by $SW\downarrow$.

1.4. Dimming and Brightening periods

The translation movement of Earth around Sun produces daily variations (sun altitude, length of day and angle of incidence of the sun's rays at the earth's surface) in solar energy received by the Earth. These variations are also dependent from the latitude where the measurements are made.

Solar radiation has a variability on an astronomical scale (thousands of years) as a consequence of variation of the eccentricity of the Earth's orbit, the precession and the obliquity of the Earth's axis, and these factors conjugated leads, periodically, to extreme climate events on Earth – *Milankovitch theory* (see for instance, Imbri and Imbrie, 1980; Berger and Loutre, 1991).

However, on a much shorter time scale, several studies around the world showed that the Earth has experienced two opposite periods known as "*global dimming*", a decrease in downward solar radiation at the Earth's surface from 1960 to 1990" (Ohmura and Lang, 1989; Stanhill and Moreshet, 1992; Gilgen *et al.*, 1998; Stanhill and Cohen, 2001, Liepert, 2002), and a "*global brightening*", an increase in global irradiance since 1990 (Wild *et al.*, 2005, Wild *et al.*, 2009; Wild, 2009; Wang and Wild, 2016). These phenomena were discovered at the beginning in some regions over Europe and later on over other parts of the world (Gilgen *et al.*, 1998).

Relatively to the magnitude of dimming and brightening periods, observations indicate a decrease in surface solar radiation with absolute trend of ~ -2 to $-9\ Wm^{-2}decade^{-1}$ for dimming (Gilgen *et al.*, 1998, Stanhill and Cohen, 2001; among others), followed by an increase between $+1$ to $+9\ Wm^{-2}decade^{-1}$ after the nineties (Wild, 2016; Wild, 2009; Wild *et al.*, 2005, among others).

According to Wild (2009, 2012), although this phenomenon has been identified in many regions of the world (see Table 1 of the review paper of Wild, 2009), the term global was used inadequately since it was referring to global solar radiation and not to planetary (global) scale. Currently, the term "global" has been replaced by "period".

The principal candidates to explain dimming and brightening periods are variations in atmospheric transparency, changes in aerosol concentration (natural/anthropogenic), urbanization factors (anthropogenic air pollution) or variability of cloud cover. (Ohmura and Lang, 1989; Liepert and Tegen, 2002; Alpert *et al.*, 2005; Stanhil and Cohen, 2008; Norris and

Wild, 2007; Liley, 2009; Sanchez-Lorenzo *et al*., 2009; Wild, 2009; Wang *et al*., 2015; among others).

During the last decades, many authors have studied these phenomena over different regions of the world and some explanations were presented. Ohmura and Lang (1989) proposed cloud changes as the main factor for explaining global dimming. Liepert (2002) proposed changes in cloud amount and optical properties as explanation. Wild *et al*. (2005) stated that changes in aerosols were the main factor to explain the brightening period. Alpert *et al*. (2005) and Alpert and Kishcha (2008) argued that solar dimming was reflex of an urbanization effect (local effect instead a worldwide effect). Norris and Wild (2007), from clear sky data, found that the cloud cover effects are insignificant for the dimming over Europe. Ruckstuhl *et al*. (2008) found over Germany and Switzerland (after 1980) a solar brightening and showed that the direct aerosol effect had approximately five times more impact on climate forcing than the indirect aerosol and other cloud effects. Ohmura (2009) showed that the direct and indirect effects of aerosols are responsible for the variability of solar radiation at surface. After, Norris and Wild (2009) reported that direct aerosol effects or changes in cloud optical properties were the major causes of dimming. Zhou (2011) showed that the interdecadal variability of seasonal mean surface solar radiation over Northwest China may be associated with an increased low cloud cover. Wild (2012) argued that the reversal from dimming to brightening was caused by an increase in the transparency of the atmosphere due to a reduction in cloud cover and anthropogenic aerosol concentrations.

Variations of sunshine duration and DTR was studied by Rahimzadeh *et al*. (2015) over Iran, between 1961 and 2009, and they found a nonsignificant trend from the mean annual sunshine series over the entire period. Nevertheless, a slight decrease in sunshine duration was observed after 2000 with a strong decline in 2009. Annual DTR showed a significant drop until the beginning of the 1990s and after, no relevant variations were found. They showed that these results where a consequence of changes in aerosols concentrations. Wang *et al*. (2015) argued that dimming cannot be considered as an urban effect. Based on sunshine duration over China, Wang *et al*. (2017) found a regional phenomenon over the dimming period (decline in SD) dependent of changes in urbanization. Nevertheless, their analysis showed that rather than local effects, the decadal variations in SD, in China, over the period 1960–2013, were observed at large scale instead as a local effect. Cusworth *et al*. (2017), investigate the relation between aerosols, clear sky and downward surface solar radiation over the central and southeastern United States (US), for the 2000–2014 period, and found, from *in situ* $SW\downarrow$ measurements and

using the column version of the rapid radiative transfer model for general circulation (RRTMG–SW) driven by aerosol optical depth (AOD), an increase of solar radiation $\sim 1\ Wm^{-2}year^{-1}$. The authors concluded that the behavior observed was a consequence of the reductions in aerosols concentrations in the atmosphere. Jahani *et al*. (2017), studied global solar radiation and its relationship with cloud cover for 1998–2015 over Iran and found a dimming in the referred period. The authors reached the conclusion that dimming shows a strong dependence of an increasing amount of aerosols over the region but, they don't rule out the relationship between both clouds and aerosols. Mao *et al*. (2017) analyzed several variables related with radiation (e.g., water vapor, among others) from satellite during monsoon season, over India (2006–2015 period), and found that the increase in AOD was inconsistent with solar radiation. However, they established that the decreases in water vapor amount and clouds could significantly contribute to solar brightening and to the surface warming.

Pfeifroth *et al*. (2018b), compared and evaluated surface data in Europe, for the period 1983–2015, with records of two satellites from the CM-SAF (Climate Monitoring Satellite Application Facility), in order to assess their accuracy and ability to capture temporal and spatial variability of Surface Solar Radiation in Europe. The authors reported an overall brightening period after the 1980s (with values between 1.9 and 2.4 $Wm^{-2}decade^{-1}$). The results also showed that, the strongest Brightening was found in eastern Europe (specially over Spring season). Concerning to north and southern Europe, the trends were not completely reproduced by satellites, in particularly over southern area. The authors reached the conclusion and reported that "*the observed trends in surface solar radiation in Europe is caused by changes in clouds and that remaining differences between the satellite- and the station-based data might be connected to changes in the direct aerosol effect and in snow cover*".

According with Wild (2016), the brightening phenomena has been somewhat less coherent than the preceding dimming, with trend reversals at widespread locations. On the other hand, and in this century, there are locations (like China or India) where dimming or brightening periods are still visible. For example, Padma *et al*. (2007) estimate, using ground-based stations, over India, and for the period of 1981 to 2004, a pronounced dimming with a strongest negative trend of $\sim 0.9\ Wm^{-2}year^{-1}$. Zhou *et al*. (2019) related that the main influencing factor of decadal variability of surface solar radiation across China between 1984 and 2015 are aerosol optical depth and aerosol-cloud interaction rather than clouds. On the other hand, Yang *et al*. (2019), related that clouds had played two opposite roles in the surface solar radiation changes over China in 1958–2016 period. They showed that clouds played two opposite roles in the last 30

years since compensate the decline in solar radiation under clear sky conditions for 1985–1999 period and counteracting the increasing in solar radiation under cloud free conditions in 2008–2016 period. However, they reported that aerosols loading had been increasing before 2000 and started to decline around 2008 and are the main possible cause of dimming and brightening periods.

Recent studies reveal that in the beginning of the twentieth century there was also an early brightening. Manara *et al*., 2015 (over Italy) and García *et al*. (2014), (over Canary Islands-Spain), have found for the period between ~1930 and 1950, an increase in sunshine duration.

As seen before, there are a number of studies on the subject, and for several regions around the world, although the majority of researcher (as seen previously) claims that aerosols are the main responsible by dimming and brightening periods (Stanhill and Moreshet, 1992; Wild *et al*., 2005; Norris and Wild, 2007; Ruckstuhl *et al*., 2008; Augustine and Dutton, 2013; Persad *et al*., 2014; Nabat *et al*., 2014; among others). According with Wild (2016), "*the majority of the studies since AR5 thus appear to support the general picture that since the mid-20th century aerosol effects dominate on the longer (multidecadal) timescales, whereas cloud effects become more relevant on shorter decadal/subdecadal timescale*."

Schwarz *et al*. (2020), address that: "*changes in clouds and aerosol are the prime potential causes for the phenomenon, but the scientific community has not yet reached a consensus about the relative role of the different potential forcing agents"*.

The causes of these solar radiation variations are not entirely understood and the transition to brightening also need explanation as seen in previous examples.

1.5. Forecasting model, ERA–40 and NCEP/NCAR reanalysis

The first attempts to predict the weather appeared with the Babylonians and later with the Greek philosophers such as Theophrastus (371–287 b.C.) or Aristotle (384–322 b.C.). Some centuries later, in the early part of twentieth century, Lewis Richardson (1881–1953), made important contributions to weather forecasting but, without computers, the time necessary to produce a forecast wasn't practical. It was necessary more than four decades after Richardson, at the beginning of the fifties, for a group of scientists using the Electronic Numerical Integrator and Computer (ENIAC) to forecast the geopotential height of the atmosphere one day ahead. Nowadays, there are several methods and models for forecast climate variables and, in particular, to forecast solar radiation parameters.

Concerning reanalysis, Betts *et al*. (2006) stated that: "… is a way to produce a dynamically consistent global analysis of the state of the atmosphere over an extended period of time (many years or decades) with no gaps in space or time".

In this section, a special emphasis will be given to $WRF - ARW$ model, ERA–40 and NCEP/NCAR reanalysis.

1.5.1. ERA–40 and NCEP/NCAR reanalysis

Atmospheric reanalysis products are used for assessing different meteorological parameters when datasets are not available for a region. Reanalysis, such as ERA–40, The Japanese 55-year Reanalysis (JRA55), NCEP/NCAR, ERA–Interim, among others has been widely used in the assessment of several climatic variables by numerous researchers. These products are the result of the assimilation of observational data (obtained by several ways), and using a global numerical weather prediction model, in order to reproduce the state of the atmosphere at any given time, and thus providing us a large number of climatic variables. The reanalysis has the advantage that they are characterized by long time series, at different temporal scales (hourly, daily, …) and at different resolutions, with global spatial coverage. This is one reason why they are also used by the NWP models as initial conditions. ERA–40 is a reanalysis of the ECMWF containing data for 45 years 1957–2001 period (Uppala *et al*., 2005), while NCEP/NCAR is the

reanalysis project for the period of 1948 to the present day (Kalnay *et al*., 1996). It's important to notice that ERA–40 solar radiation parameters (doesn't provide direct solar irradiance) are generated by the assimilation of observational data (see Figure 1 of Uppala *et al*., 2005) and the ECMWF numerical weather prediction model. Lately, the European Centre for Medium–Range Weather Forecast (IFS/ECMWF) also provides forecasts of the direct solar radiation.

ERA–40 and NCEP/NCAR products have been widely used in atmospheric studies and are also used to run RCM. Relative to solar radiation variability, the reanalysis was also used by some researchers, since these products provided variables such as downward global solar irradiance (NCEP/NCAR), clear sky downward global solar irradiance (NCEP/NCAR), net shortwave radiation (NCEP/NCAR), downward global solar irradiance at the surface (ECMWF), surface net solar radiation clear sky (ECMWF), top solar radiation (ECMWF), among others radiative variables.

There are several studies that use reanalysis to assess climate conditions over specific regions. For example, Betts *et al*. (2006) evaluated temperature, relative humidity, precipitation, sensible and latent heat flux as well as downward shortwave and longwave radiation using ERA–40 and NCEP/Department of Energy (DOE) Atmospheric Model Intercomparison Project reanalysis, and found that both variables obtained with reanalysis were well captured when compared with the second International Land-Surface Climatology Project (ISLSCP-II) dataset from ECMWF. They also found that incoming solar radiation estimated by ERA–40 presented the lowest bias. Bromwich *et al*. (2007) assessed the performance of ERA–40 (and other reanalysis products) over polar regions and found that clouds (in ERA–40) were too optically thin. Thus, the real impact of clouds on the radiation would compromise the results. However, these authors refer to reanalysis products as "*powerful tools"* in climate studies. Wild *et al*. (1998) had already referred to the fact that the performance of the ERA–40 was more accurate in clear sky conditions. Träger─ Chatterjee *et al*. (2010) evaluated the downward solar radiation at surface of the ERA–40 and ERA–Interim reanalysis over Germany and adjacent regions and concluded that both products have limitations. For example, and with respect to ERA–40, in regions with low/higher cloud indices ERA–40 underestimate/overestimate downward solar radiation at surface. They attribute these results to limitations in the representation of clouds by ERA–40. You *et al*. (2010) assessed the variability of downward solar radiation at surface over Tibetan Plateau, for 1961–2005 period, in a monthly basis, using ERA–40 reanalysis data and sunshine duration. In this study, it was found a

brightening/dimming before/after the eighties, in opposition to major results previously seen in section 1.4. This was explained as changes in transmittivity of atmosphere due to a decrease (brightening period)/increase (dimming period) of anthropogenic aerosols concentration. However, Wild and Schmucki (2011) verified that ERA–40 fails to reproduce the major decadal changes in solar surface radiation, specially over regions heavily polluted since a monthly mean distribution of aerosols are presented and not actual values. Nevertheless, their analysis showed that ERA–40 reveals dimming and brightening periods although induced by changes in cloud cover and with an extent smaller than in observations. In the same study, Wild and Schmucki (2011), carried out an analysis using 23 climatic models, over five climatic regions (Europe, Japan, Southeast China, Northwest China and India), where dimming and brightening were observed *in situ*, and they found strong variations in surface solar radiation. On the other hand, they discovered that only half of the models used in the study could qualitatively describe the observational solar variations.

Relatively to NCEP/NCAR reanalysis, Xia *et al*. (2006) assessed solar radiation at surface in China using two satellite-based surface insolation data sets and relative to the results obtained, the authors found an overestimation that exceeded surface observations between 40 Wm^{-2} to more than 100 Wm^{-2}. This overestimation was explained by inaccurate representation of clouds and aerosols in the reanalysis model. A similar overestimation was found by You *et al*. (2013) over the Tibetan Plateau with a bias of $+31.3\%$ relative to the annual observations. The authors also found that the all-sky and clear-sky SSR trends derived from both NCEP/NCAR and ERA–40 does not capture the decadal variations seen in surface observations. The previous bias was assigned to inaccuracies related to clouds and aerosols assimilation. Tahir *et al*. (2020), stated that the surface solar irradiance obtained from NCEP/NCAR for two observational stations in Sind province (Pakistan) were overestimated as a consequence of deficiencies in the radiative transfer model (inappropriate cloud fraction and aerosols). Zhang *et al*. (2016), assess six current representative global reanalysis (included NCEP/NCAR) using surface measurements from different observation networks worldwide (647 sites) and found an overestimation, caused by a bias in cloud fraction, between 11.25 Wm^{-2} and $\sim$49.80 Wm^{-2}. On the other hand, Silva *et al*. (2010), using NCEP/NCAR reanalysis data and sunshine duration measurements over northeastern Brazil, for 1958–2009 period, found a reasonable correlation between datasets as well as evidence of global dimming. Pinto *et al*. (2010), also found a good spatial representation of the solar radiation at surface in several regions over South America from reanalysis products (ERA–40 and NCEP/NCAR).

1.5.2. Weather Research and Forecasting model (WRF−ARW)

In the last decades, RCM have played a key role in research of different variables (such as temperature, precipitation, wind, ...), or energy budgets (Folini and Wild, 2011; Wild and Schmucki, 2011).

The Weather Research and Forecasting model is one of these regional climate models and is a powerful and versatile tool in climate simulations, since it presents a great flexibility in parameterizations, including microphysics, cumulus schemes, surface layer physics, planetary boundary layer (PBL) and atmospheric radiation physics.

WRF is the world's most used atmospheric model with more than 36 000 registrations distributed across 162 countries and with over 26 500 citations in peer-reviewed journals, with an average of over 10 citations per publication, and an average of 510 publications per year for the 2011−2015 period (Powers *et al*., 2017). For instance, and relative only to Iberian Peninsula (or part of it), the WRF was widely used to perform downscaling in different atmospheric areas, such as:

(i) to evaluate the capacity of WRF to simulate Spanish ***precipitation*** *and to determine its adequacy for future climate simulations (Argüeso et al., 2012); (ii) to reproduce the* ***surface wind direction*** *over complex terrain located in the north-eastern of IP (Jimenez and Dudhia, 2013); (iii) to evaluate four PBL schemes and the impacts of* ***air quality*** *outputs over Catalonia (Banks and Baldasano, 2016); (iv) the behaviour of the* ***sea breeze*** *along the north coast of Spain (Arrillaga et al., 2016); (v) to evaluate trends of* ***extreme temperature*** *indices over Iberian Peninsula (Fonseca et al., 2016);* (*vi) to describe the* ***wind*** *resource for the present and future using the RCP4.5 and RCP8.5 emission scenarios (Soares et al., 2017); (vii) to assess the* ***future changes in precipitation*** *over the Iberian Peninsula (Cardoso et al., 2019); (viii) to forecast different surface and near-surface variables (temperature,* ***downward longwave radiation*** *over a region in Eastern Spain (Caselles et al., 2018);(ix) to estimated the spatiotemporal distribution of* ***moisture recycling*** *(González-Rojí et al., 2020);* among other considerable references in literature over the last decade.

In the next paragraphs a short-detailed description is made of WRF model based on the NCAR technical note (Skamarock *et al*., 2008) and in the description of the NCAR Community Atmosphere Model (Collins *et al*., 2004).

The WRF model contains two dynamic cores: The Non-hydrostatic Mesoscale Model (NMM) developed at the National Centers for Environmental Prediction by Janjic (2003), and the Advanced Research WRF (ARW) core, developed at the National Center for Atmospheric Research by Skamarock *et al*. (2005).

The WRF version used in this thesis was the 3.3.1, with the dynamical core ARW. The main components of WRF are presented in Figure 1.9. The equations that govern the core of $WRF - ARW$ model are based on the Eulerian solutions for compressible and non-hydrostatic equations and use a vertical coordinate system (Skamarock *et al*., 2008). Figure 1.9. shows schematically the system components in WRF model.

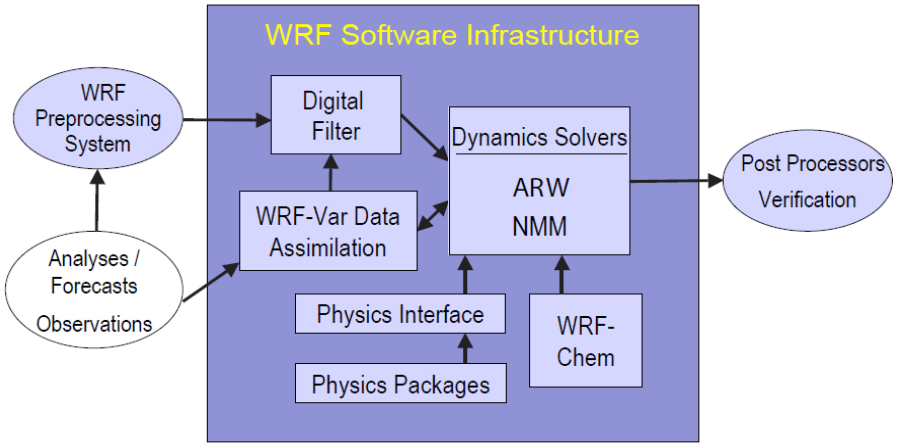

Figure 1.9. Scheme of the system components in the WRF model.

Image taken from pg. 2 of Skamarock *et al*. (2005).

The core consists on a set of modified differential equations, with terms that consider air humidity, Coriolis force and cartographic projection, in order to simulate the atmosphere. In terms of temporal discretization, WRF uses a time–split scheme known as Runge-Kutta of 3rd order, which integrates a set of ordinary differential equations with a formulation of the type predictor-corrector. Relative to spatial discretization, WRF model uses the Arakawa C-type grid. These specifications are described in Skamarock *et al*. (2008).

A short description of the parametrizations used in this work is made in the next paragraphs.

The microphysical scheme has the role of solving, for each grid point, the processes associated with water vapor, clouds (with or without ice) and precipitation. In this work the *microphysics scheme* used was the *WSM-3 Class Simple Ice Scheme* (Hong *et al*., 2004). This scheme is a

routine where water coexists in three categories: water vapor, water/ice clouds and rain/snow, and where is assumed that, above the freezing point, the clouds exist in the form of water and rain and below freezing point in the form of ice and snow (Skamarock *et al*., 2008).

In what concerns to *cumulus parameterization*, the routine of the cloud processes, our choice was the computationally efficient *Grell-Devenyi ensemble scheme* (Grell, G.A. and D. Devenyi, 2002), in which multiple cumulus schemes and variants are run within each grid box and then the results are averaged to give the feedback to the model. The cumulus parameterization provides the vertical profile of heating, humidity and precipitation associated to convection. This scheme determines updraft (and downdraft), mass flux and other fluxes (Skamarock et al., 2008).

The *surface layer* parameterization plays a vital role in the interaction between surface and atmosphere (exchange of energy, momentum and water between these two systems). The scheme selected for surface layer was the *thermal diffusion scheme* which aims to determine the friction velocity and the turbulent transfer coefficients in order to predict the fluxes of heat, water vapor and momentum between the lowest model level and the surface. In this scheme the soil mixture is fixed with a land use and season-dependent constant value and is represented by five layers with thicknesses of 1, 2, 4, 8 and 16 *cm*, without explicit vegetation (Skamarock *et al*., 2008).

Regarding to the parameterization of the *PBL*, the *Yonsei University–YSU* (Hong *et al*., 2006) routine was chosen. The PBL is the region associated to human activities (atmosphere adjacent to the earth's surface), and for this reason, a source of natural and anthropogenic aerosols. The PBL schemes determine the flux profiles within the well-mixed boundary layer and the stable layer, and thus provide atmospheric tendencies of temperature, moisture (including clouds), and horizontal momentum in the entire atmospheric column (Skamarock *et al*., 2008).

Relative to radiation schemes, they are responsible for reproducing the shortwave and the longwave radiation fluxes at the surface and the scattering and absorption of shortwave and longwave radiation and emission of longwave radiation in the atmosphere. In this thesis, *radiation* parametrization was, for both shortwave and longwave, parameterized with the Community Atmospheric Model – *CAM* (Community Atmospheric Model) *scheme* (Collins *et al*., 2004).

CAM *SW* scheme is a spectral band with 19 discrete spectral intervals (seven in the ultraviolet band, three in the photosynthetic active region band and nine in the near-infrared band).

CAM LW is a spectral scheme with 8 longwave bands (wavenumber range between 500 to 1500 cm^{-1}) which interacts with ozone, carbon dioxide, cloud fraction, gases and aerosols. According with Collins *et al*. (2004), CAM scheme includes five chemical species of aerosol (sea salt, soil dust, black and organic carbonaceous aerosols, sulfate and volcanic sulfuric acid) with a monthly mean aerosol profile. It also worth noting that CAM scheme imposes the direct and semi-direct effects of tropospheric aerosols on shortwave fluxes and heating rates. This radiation scheme is a one-dimensional column scheme. Details of the several parametrizations in WRF model are available in Skamarock *et al*. (2008).

In this work, NCEP/NCAR reanalysis data provides the initial and lateral boundary conditions for simulations at 6–hour interval. A complete description of WRF setup used in this thesis can be seen in section 3.2.1.

Solar radiation predictions were obtained from WRF model over Xinjiang (China), for two days with different radiation schemes by Chen *et al*. (2017) who showed that the results were strongly dependent on the radiative scheme and that Rapid Radiative Transfer Model (RRTM) and CAM are the most appropriate under clear sky days. Wilmot *et al*. (2014) found an overestimation of incoming radiation over southeastern coastal Texas. According with previous authors, and taking in account the fifth-generation Penn State/National Center for Atmospheric Research mesoscale model (MM5) and the Weather Research and Forecasting (WRF) models, biases for outgoing radiation were smaller with WRF. This later study revealed that other variables (such as water vapor, latent heat flux, sensible heat flux, friction velocity, ...) were also assessed and in most of them the best score was found with WRF model predictions.

Wild (2016) argued that global climate models generally simulate the observed dimming/brightening qualitatively but underestimate the corresponding magnitude over several regions. On the other hand, the majority of state-of-the-art RCM tends to overestimate the surface solar radiation flux as compared to ground observations (e.g. Lara-Fanego *et al*., 2012a; Ruiz-Arias *et al*., 2015). Hence, a common practice to the majority of climate researchers is to apply bias removal technics in order to reduce biases errors. In the case of solar radiation predictions, NWP models alone are not sufficiently accurate for predict solar radiation for the majority of solar applications (Jimenez *et al*., 2016).

Diagne *et al*. (2014) found a significative improvement over Reunion Island in hourly basis for global horizontal irradiance outputs, obtained by WRF model, after application of a Kalman

Filter. According with these authors, post-processing methods remove bias without the necessity of long climatological series.

Lima *et al*. (2016) established a methodology for obtaining solar irradiances over northeastern region of Brazil and found that, WRF model adjusted by an artificial neural network lowers the $BIAS$ and $RMSE$ and increase the correlation coefficients between ground-based stations and WRF outputs.

Based on two regional climate models (WRF and Regional Atmospheric Modeling System – RAMS), Avolio *et al*. 2016, evaluated the performance of the models to predict shortwave irradiances and wind speed for two stations in Southern Italy (Lamezia Terme and Leccethe). Their analysis showed that the errors were reduced up to 20% after application of a multi-model approach. Rincón *et al*. (2018) using a Kalman filter with model output statistics improved WRF outputs obtained for global horizontal irradiances over Paraguay and found a reduction of 97% in annual $BIAS$ and 13% of annual $RMSE$.

The WRF model has also been used in Iberian Peninsula to simulate solar radiation. For example, by Lara-Fanego *et al*. (2012b) that used the model to evaluate direct normal radiation during a year and they found that the model is more accurate in forecasting DNI over clear sky conditions and these results were also improved after the application of a post-processing correction. Over the southern half of IP, Santos-Alamillos *et al*. (2012), using daily wind and solar radiation obtained for 2007, found the existence of a complementarity between those two renewable energies. Ruiz-Arias *et al*. (2016) evaluated the WRF to predict shortwave downward total solar radiation flux for Spain over a ten years period. They found an overestimation relative to observations as consequence of a very low cumulus cloud amount due to a possibly misrepresentation of the radiative impact of that type of cloud. Subsequently, they proposed an original method to correct this bias based on concurrent radiometric ground observations (known as optimal interpolation), their results provided global and direct irradiances with a nominal uncertainty of $\sim 5\%$. According with these authors, lower biases are found when a large number of ground-based stations were used. Later, Ruiz-Arias *et al*. (2016), investigated the overestimation found in shortwave total down radiation and found that these errors are tied to a deficient representation of cumulus cloud and/or their radiative impact, in particular during spring and summer and in northern mountains. Magarreiro (2016) evaluated the reliability of WRF to forecast global radiation with a combination of statistical bias correction methods and found an overestimation, on a daily basis, over the entire IP. This

overestimation was also explained as a result of a systematic underestimation of cloud fractional coverage by the model.

2.

Variability and trends of downward surface global solar radiation over the Iberian Peninsula from ERA–40 reanalysis

This chapter is a transcription of the paper published with the following reference:

Perdigão, J. C., Salgado, R., Costa, M. J., Dasari, H. P., Sanchez-Lorenzo, A., 2016. Variability and trends of downward surface global solar radiation over the Iberian Peninsula based on ERA–40 reanalysis. Int. J. Climatol., 36, 3917–3933. doi:10.1002/joc.4603

Abstract

A climate study of the incident downward surface global solar radiation (SSRD) in the Iberian Peninsula (IP) based primarily on ERA–40 reanalysis is presented. NCEP/NCAR reanalysis and ground-based records from several Portuguese and Spanish stations have been also considered. The results show that reanalysis can capture a similar interannual variability as compared to ground-based observations, especially on a monthly basis, even though ERA–40 (NCEP/NCAR) annual values tend to underestimate (overestimate) the observations with a mean relative difference of around 20 Wm^{-2}(40 Wm^{-2}). On the other hand, ground-based

measurements in Portuguese stations during the period 1964–1989 show a tendency to decrease until the mid–1970s followed by an increase up to the end of the study period, in line with the dimming/brightening phenomenon reported in the literature. Nevertheless, there are different temporal behaviors as a greater increase since the 1970s is observed in the south and less industrialized regions. Similarly, the ERA–40 reanalysis shows a noticeable decrease until the early 1970s, followed by a slight increase up to the end of the 1990s, suggesting a dimming/brightening transition around the early 1970s, earlier in the south and center and later in the north of the IP. Although there are slight differences in the magnitude of the trends, as well as the turning year of the dimming/brightening periods, the decadal changes of ERA–40 fairly agree with the ground-based observations in Portugal and Spain, in contrast to most of the literature for other regions of the world, and is used to perform a climatology of the SSRD in the study area. NCEP/NCAR reanalysis do not capture the decadal variations of SSRD in the IP. The results show that part of the decadal variability of the global radiation in the IP is related to changes in cloud cover (represented in ERA–40).

Keywords: Radiation variability; Radiation trends; Downward surface global solar radiation; Total cloud cover; ERA–40; NCEP/NCAR; Ground-based observations; Iberian Peninsula

2.1. Introduction

It is well known that the most important factor that shapes the climate of our planet is the solar radiation that reaches the Earth, so any changes in radiation will induce modifications on temperature, humidity, rainfall, etc. Meanwhile, renewable energies constitute a vital resource for the near future. In particular the solar energy is increasingly becoming a reliable and competitive source of energy and the correct evaluation of this resource and estimation of its trends, in the present and in the near future, is critical in assessing the viability of projects of solar power plants (e.g., Hammer *et al.*, 2003; Wild *et al.*, 2015).

In recent decades the scientific community has dedicated some attention to surface solar radiation and to its variation all over the globe. Some studies reported that between the 1950s and mid 1980s there was a decrease of the surface solar radiation, a phenomenon known as the "global dimming" (Ohmura and Lang, 1989; Stanhill and Moreshet, 1992; Stanhill and Cohen, 2001, among others). Later on it was observed the opposite effect, which is known as the "global brightening" (e.g. Wild *et al*., 2005).

During the last years, many authors have dedicated their attention to the study of surface solar radiation decadal variations over different regions of the globe, such as, for example, China (Xia, 2010; Liu *et al.*, 2010; Wang *et al.*, 2015), the Tibetan Plateau (You *et al.*, 2013), Northeast Brazil (Silva *et al.*, 2010), the whole of Europe (Chiacchio and Wild, 2010; Sanchez-Lorenzo *et al.*, 2015), Northern Europe (Stjern *et al.*, 2009), Southern Europe (Sanchez-Lorenzo *et al*., 2013a; Mateos *et al*., 2014a; Manara *et al.*, 2015), or the United States (Liepert, 2002; Augustine and Dutton, 2013) .

Many attempts have been conducted to explain these effects and the major candidates are the changes in the amount and properties of clouds in the atmosphere (Liley, 2009; Stjern *et al*., 2009; Russak, 2009; Chiacchio *et al.*, 2010, among others) and aerosol concentrations (Norris and Wild, 2007; Sanchez-Lorenzo *et al.*, 2009, among others). For example, Liley (2009) found for New Zealand an increasing trend of cloudiness until the end of the eighties and then an opposite trend, in line with the observed dimming/brightening phenomenon observed in surface solar radiation series. Chiacchio *et al.,* (2010) found, in Alaska, changes in decadal solar radiation and explained the same as a result of changes in clouds and atmospheric circulation patterns over the Pacific. Russak (2009) distinguished two different periods over Estonia

between 1950 and 2007 and found correlations between changes in solar radiation and the amount of low clouds, as well as the transparency of the atmosphere.

Other studies explain the dimming/brightening periods as the result of the changes in aerosol effects in the atmosphere (e.g., Liepert and Tegen, 2002; Wild *et al.*, 2005; Norris and Wild, 2007) due to their ability to affect directly and indirectly the solar radiation that reaches the surface of the Earth (e.g., Lohmann and Feichterm 2005; Yu *et al.*, 2006). Thus, for example, Qian *et al*., (2007) suggested that in China the increase of aerosols in the period 1960 to 1980 was the main factor that led to a decrease in solar radiation in clear sky conditions.

On the other hand, Alpert *et al.*, (2005) and Alpert and Kishcha (2008) revealed higher rates of solar radiation decrease during the dimming period in urban areas relatively to rural areas, which was attributed to an impact of urbanization on the trends of surface solar radiation. Nevertheless, a recent study by Wang *et al.*, (2015), using 105 pairs of stations with collocated measurements of surface solar radiation, concluded that on a global scale the dimming period cannot be considered an urban effect. For an extensive analysis on the dimming/brightening subject, see review papers of Wild (2009, 2010; 2012).

Regarding the use of reanalysis products to study the climatology and changes in surface solar radiation, it is worth mentioning that Kaurola *et al*. (2010) describe that ERA−40 data on a monthly basis reduced the bias on the surface radiation as compared to the records on a daily basis, especially when temporal variations related to cloud radiative effects are studied. Similarly, Betts *et al*. (2006) verified that ERA−40 reproduced the most important variations associated with clouds and shortwave radiation. However, Wild and Schmucki (2011) found that the strong ERA−40 simulated decline in cloud amount over Europe is not observed in the same extent in ground-based records, as well as that reanalysis product fails to reproduce the dimming/brightening phenomenon. Träger-Chatterjee *et al*. (2010) assessed the downward surface solar irradiation for Germany from reanalysis products and found some limitation to adequately represent the clouds, especially in summertime. However, reanalysis products have some advantages over historical observed series since a variety of meteorological data obtained by different instrumentation (surface observations, satellites, aircraft, etc.) is assimilated, allowing a consistency in the data obtained by the quality control of the model, while presenting a regular spatial and temporal resolution.

The North Atlantic Oscillation (NAO) is a major phenomenon that influences the weather and climate variability of Europe (Hurrell 1995, 1996). The NAO is related to precipitation (Hurrell,

1995, Trigo *et al*., 2002) and influences the temporal and spatial variability in the Iberian Peninsula (IP). Specifically, the positive (negative) phase of NAO explains a reduction (increase) of precipitation and a decrease (increase) in the percentage of cloud fraction over the south of Europe. In Portugal, high values in the NAO index correlate with low values of precipitation and cloudiness (Trigo *et al*., 2002). Sanchez-Lorenzo *et al.* (2009) described that cloud cover and sunshine duration over IP are linked to NAO, especially during winter. Pozo-Vázquez *et al*. (2004) found for IP high correlations between the NAO index and the monthly sums of sunshine duration.

Sanchez-Lorenzo *et al*. (2009) describe that clouds show a decreasing trend in the IP between 1960 and the mid of 2000, where as sunshine duration series shows a decrease from the 1950s to the mid–1980s (dimming), with a subsequent increase until the 2000s (brightening). Sanchez-Lorenzo *et al*. (2013a) found from the analysis of 13 Spanish observational stations a positive trend for the global radiation in the 1985–2010 period with a value of $+3.9\ Wm^{-2}$ per decade, in line with the sunshine durations trends since the 1980s. Mateos *et al*. (2014a) found a strong brightening in IP for the period 2003–2012 as a result of a decrease of clouds and aerosols in the region. The decreasing trends observed for shortwave radiation was explained in 75% by clouds and the remaining 25% by the effect of aerosols.

The main objective of this work is to study the patterns, evolution and trends of downward surface global solar radiation at the surface in the IP with ERA–40 reanalysis data and explore its relationship with clouds. Section 2.2 and 2.3 presents the data, the study area and describes the methodology used for this study; in section 2.4, shortwave radiation reanalysis data were compared to the common period to the measurements taken at Portuguese and Spanish meteorological stations. In section 2.5, annual and monthly area averaged values of downward surface global solar radiation and total cloud fraction are computed for ERA–40 reanalysis product and analyzed for the IP region. Temporal averages of shortwave radiation and total cloud cover were carried out over the entire ERA–40 period. Finally, conclusions are presented in section 2.6.

2.2. Data and Methods

2.2.1. Data and Area of Study

The daily downward surface global solar radiation (SSRD, in Wm^{-2}) data measured at Portuguese meteorological stations (Bragança, Porto, Évora and Faro) were obtained from the World Radiation Data Centre (WRDC, http://wrdc-mgo.nrel.gov/). SSRD from other Portuguese stations, also available at the WRDC was not considered for this study due to insufficient data (Table 2.1). For Lisbon, the monthly data were obtained directly from the Portuguese Institute of Ocean and Atmosphere (IPMA).

Table 2.1. Location and data availability for the Portuguese stations.
Bold stations refer to stations used in this study.

STATION	PERIOD	LAT (N)	LON (W)	ALTITUDE (m)	MISSING MONTHLY DATA (%)
Lisbon	*58-89*	*38.43*	*-9º.09*	*77*	*0*
Monte Estoril	*64-89*	*38.42*	*-9.24*	*31*	*90.7*
Porto	*64-89*	*41.08*	*-8.36*	*93*	*2.2*
Coimbra	*64-89*	*40.12*	*-8.25*	*141*	*10*
Faro	*64-86*	*37.01*	*-7.58*	*7*	*0.4*
Évora	*64-89*	*38.34*	*-7.54*	*309*	*1.0*
Penhas Douradas	*64-89*	*40.25*	*-7.33*	*1380*	*19*
Castelo Branco	*64-89*	*39.50*	*-7.29*	*386*	*82.4*
Bragança	*64-89*	*41.48*	*-6.44*	*691*	*4.8*

The analysis was done on a monthly mean basis obtained from the daily values. A month was considered only if the data available corresponded to at least two thirds of that month. In the absence of data for a month at a given station and a given year, the average of all corresponding months in the series was used. The annual average was calculated taking into account those values. The percentage of missing monthly values in the period under study is indicated in Table 2.1, which contains also the locations of the stations used. In addition, a collection of 13 Spanish series available since 1985 were considered in this study. For more details about the dataset, we refer to Sanchez-Lorenzo *et al*. (2013a).

SSRD and total cloud cover (TCC) variables from ERA−40 and NCEP/NCAR reanalysis are also used in this study on an annual and seasonal basis. ERA−40 is the 45 year second generation reanalysis based on the European Centre for Medium-Range Weather Forecast (ECMWF) operational three-dimensional variation assimilation system, making comprehensive use of satellite data and conventional observations (Uppala *et al.*, 2005). It covers the period from September 1957 to August 2002 and the model uses 60 vertical levels and a T159 spectral resolution. The shortwave radiative variables were computed by the Fouquart and Bonnel (1980) scheme. The data were extracted from the ECMWF portal. The spatial resolution used in the present study is $0.25° \times 0.25°$, every 6 hours. NCEP/NCAR data (Kalnay *et al.*, 1996) covers the period from 1948 until present and has horizontal resolution of $2.5° \times 2.5°$ (T62 Gaussian grid $\sim 209\ km$), with 17 pressure level and 28 sigma levels. Monthly mean data was downloaded from National Oceanic and Atmospheric Administration (NOAA) portal.

In section 2.4, annual and monthly averaged trends for SSRD and TCC are computed from ERA−40 and for the IP region (36N−44N; 10W−4E), and for the period from 1958 to 2001. The seasons are defined according to the World Meteorological Organization (WMO) nomenclature i.e., winter (DJF), spring (MAM), summer (JJA) and autumn (SON).

2.2.2. Homogenization methods

Climatological series sometimes contains temporal inhomogeneities. In this study, the Standard Normal Homogeneity Test (SNHT, Alexandersson, 1986), Buishand Range Test (Buishand, 1982), Pettitt Test (Pettitt, 1979) and Von Neumann Ratio Test (Von Neuman, 1941) were used for testing the homogeneity of the Portuguese series. The absolute homogeneity tests were applied for each station separately (Wijngaard *et al.*, 2003; Morozova and Valente, 2012; Hakuba *et al.*, 2014) since observational stations have a low density (only five) and are considerably spaced from each other. Specifically, the Pettitt Test, SNHT, and Buishand test suppose that tested values are independent and identically normal distributed (null hypothesis), while under alternative hypothesis, tests assume inhomogeneous series as consequence of a break or a shift. On the other hand, for the Von Neumann Ratio Test the null hypothesis is that the data are independent and identically distributed random values, and with alternative hypothesis that the values in the series are not randomly distributed.

For each of the tests description, let be n the length of a time series to be tested, where x_i is *i-th* element of the series with mean μ and standard deviation σ.

Statistic $T(k)$, in SNHT test, compares the mean of the first k observations with the mean of the last $(n-k)$ observations,

$$T(k) = k\left[\frac{1}{k}\sum_{i=1}^{k}\frac{x_i-\mu}{\sigma}\right]^2 + (n-k)\left[\frac{1}{(n-k)}\sum_{i=k+1}^{n}\frac{x_i-\mu}{\sigma}\right]^2, k = 1, \dots, n \qquad (2.1)$$

The null hypothesis is rejected if $T_0 = \underset{1\le k\le n}{max}T(k)$ and if T_0 is above a certain level given in a table of Khaliq and Ouarda (2007).

The Buishand statist test, $S(k)$, is defined as

$$S(k) = \sum_{i=1}^{k}(x_i-\mu), \qquad k = 1, \dots, n \qquad (2.2)$$

with, $S(0) = 0$, and R statistic given by

$$R = \left(\underset{0\le k\le n}{max}S(k) - \underset{0\le k\le n}{min}S(k)\right)/\sigma \qquad (2.3)$$

Critical values for $R/\sqrt{n}$, were obtained, from Buishand (1982).

$Y(k)$ statistic test, for Pettitt test, is calculated as

$$Y(k) = 2\sum_{i=1}^{k} r_i - k(n+1), \qquad k = 1, \dots, n \qquad (2.4)$$

Since Pettitt test is a non-parametric test, $r_1 \dots \dots . . r_n$ is the rank of the $x_i \dots . . x_n$. The critical value of the test $Y(k)$ is calculated for a probability level α as

$$Y_{k\alpha} = \sqrt{-ln\alpha(n^3+n^2)/6} \qquad (2.5)$$

and a change point will occurs when,

$$Y_k = \max_{1 \le k \le n} |Y(k)| \tag{2.6}$$

Von Neumann ratio test (VNRT) is defined as

$$N = \frac{\sum_{i=1}^{n-1}(x_i - x_{i+1})^2}{\sum_{i=1}^{n}(x_i - \mu)^2} \tag{2.7}$$

Critical values was calculated, with probability level α, as

$$N_\alpha \sim 2 - 2u_\alpha \sqrt{\frac{n-2}{(n-1)(n+1)}} \tag{2.8}$$

According to Wijngaard *et al*. (2003) and Hakuba *et al*. (2014), three classes were considered: Class I: Useful – one or zero test reject the null hypothesis; Class II: Doubtful – two tests reject the null hypothesis; Class III: Suspect – three or four tests reject the null hypothesis. In this work, the null hypothesis was rejected at 1% level. The series in Class I and II may be considered homogeneous, whereas inhomogeneous for Class III (Wijngaard *et al.*, 2003).

2.3 Statistical methods

The parameters used to evaluate the data model and meteorological data were the mean bias ($BIAS$), root mean square error ($RMSE$), the correlation coefficient (r) and coefficient of variation (CV). For a series with x_i values, with mean (μ) and standard deviation (σ), the CV (in percentage) is defined as:

$$CV(\%) = \frac{\sigma}{|\mu|} \times 100 \tag{2.9}$$

This parameter measures the variability in the values of a series relative to de population mean.

Normalized $BIAS$, in percentage, is defined as:

$$NBIAS(\%) = \frac{BIAS}{\frac{1}{n}\sum_{i=1}^{n} x_i} \times 100 \tag{2.10}$$

A simple linear regression model (including the determination coefficient – R^2), as well the nonparametric statistical method of Mann-Kendall (Mann, 1945), were applied to find possible trends in annual and monthly data. The method of Mann-Kendall (MK test) has been widely used by several authors in meteorological studies. (Silva *et al*., 2010, Obot *et al*., 2010; Cislaghi *et al*., 2005 among others) to statistically assess if there is a monotonic upward or downward trend of the variable of interest over time and it is recommended by the World Meteorological Organization (WMO).

Specifically, for a time series containing a set of observations ($x_i, \ldots . x_n$), the MK test is given by

$$S = \sum_{i=1}^{n-1} \sum_{j=i+1}^{n} sign(x_i - x_j) \tag{2.11}$$

where:

$$\begin{aligned} sign(x_i - x_j) &= 1, \qquad if(x_i - x_j) > 0 \\ sign(x_i - x_j) &= -1, \qquad if(x_i - x_j) < 0 \\ sign(x_i - x_j) &= 0, \qquad if(x_i - x_j) = 0 \end{aligned} \tag{2.12}$$

The statistical value of the test is the Mann-Kendall index (Z_{MK}), given by

$$Z_{MK} = \begin{cases} \dfrac{S-1}{\sigma} & if \quad S > 0 \\ 0 & if \quad S = 0 \\ \dfrac{S+1}{\sigma} & if \quad S < 0 \end{cases} \tag{2.13}$$

with

$$\sigma = \sqrt{\frac{1}{18}\left[n(n-1)(2n-5) - \sum_{p=1}^{q} t_p\,(t_p - 1)(2t_p + 5)\right]} \tag{2.14}$$

A positive value in equation (2.11) indicates that there is a positive trend in the observations, a very large value of S reveals that the latest observations correspond to higher values than the first, for the same series; on the other hand, if the result of equation (2.11) gives a negative value, it can be assumed that there is a negative trend. In this work is considered a significant α level of 5%, which corresponds to $|Z_{MK}| \geq 1.96$. The α level value is obtained from the standard normal distribution table.

The sequential version of MK test (with the acquisition of two series – one regressive and another progressive), slightly modified by Sneyers (1975), allows to determine the point in time when the trend starts and when it becomes meaningful. In this version of the MK test, original values of a set of observations ($x_i, \ldots . x_n$) are replaced by their ranks y_i in ascending order. The magnitude of $y_i, (i = 1, \ldots, N)$ are compared with $y_j, (i = 1, \ldots, N)$, and a statistic test is defined as

$$t_i = \sum_{j=1}^{i} n_i \tag{2.15}$$

where, n_i represents the sum of a temporal series whose values $y_i > y_j$. Assuming that there is a trend (null hypothesis is rejected), the series presents a normal distribution and variance given by:

$$E_{(t_n)} = \frac{n(n-1)}{4} \tag{2.16}$$

$$VAR(t_n) = \frac{n(n-1)(2n+5)}{72} \tag{2.17}$$

The sequential values of the statistic are given by:

$$u_{(t_n)} = \frac{\left(t_n - E_{(t_n)}\right)}{\sqrt{VAR(t_n)}} \tag{2.18}$$

The progressive series (forward direction) is determined from equation (2.18), starting from the value $i = 1, \dots, N$, generating the statistical $u_{(t_n)}$. The regressive series is determined backward from the last term of the series $i = N, \dots, i$, generating the statistical $u'(t_n)$. The intersection between the progressive $u(t_n)$ and regressive $u'(t_n)$ series should occur within the confidence intervals and representing the beginning of the trend. The series became significant when the values of statistical data exceed the confidence intervals of 95% level.

2.4 Comparison of shortwave radiation data from ground-based and reanalysis datasets in Portugal and Spain

2.4.1. Changes of shortwave radiation in ground-based observation of Portugal

Due to the lack of studies dealing with the decadal changes of SSRD over Portugal using ground-based measurements (e.g., see Sanchez-Lorenzo *et al.*, 2015), in this section we first introduce their main characteristics. For more details about decadal changes in Spain, we refer to Sanchez-Lorenzo *et al.* (2013a).

As detailed in Section 2.2.2, the annual SSRD series for Portuguese stations were tested by means of four homogeneity tests. The results confirm that the five series can be considered homogeneous. Specifically, Bragança, Porto and Lisboa series obtained classification of Class I, whereas Évora and Faro were classified as Class II since null hypothesis was not rejected for the Buishand and Von Neumann tests. Consequently, we have used the five series for the subsequent analyses. Figure 2.1 shows the mean annual SSRD series in the five observational stations of Portugal.

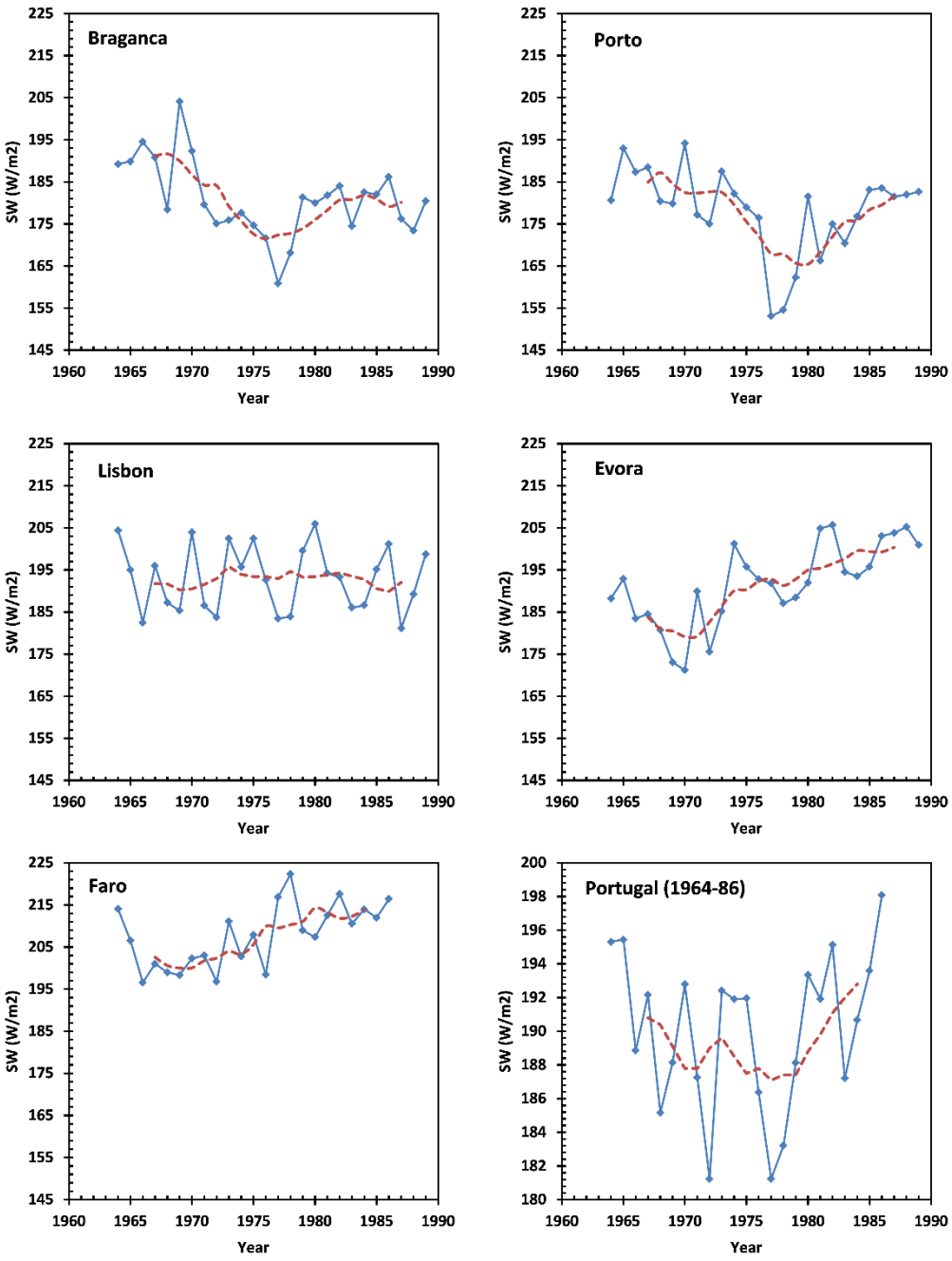

Figure 2.1. Mean annual global incident radiation observed in Portuguese stations.
In the bottom right plot, a mean of five Portuguese series is represented. The red dashed line corresponds to a five-year-centred moving average.

As can be seen from Table 2.1, the length of time series varies from station to station. In order to smooth the data and facilitate trend detection and qualitative analysis, a five-year centered moving average was applied. Table 2.2 shows the some climatological parameters on annual basis for the five Portuguese stations under analysis.

Table 2.2. Annual climatology for meteorological station in Portugal with mean ($\bar{X}$), standard deviation (σ), slope (b), coefficient of determination (R^2) and *MK* indice (Z_{MK}) with a α level of confidence of 5%.
Bold values means significant trends.

STATIONS	Period	$\bar{X}$	σ	b	R^2	Z_{MK}
Braganca	*1964-89*	*181.0*	*9.0*	*-0.5*	*0.2*	*-1.5*
Porto	*1964-89*	*178.2*	*10.1*	*-0.4*	*0.1*	*-1.1*
Lisbon	*1964-89*	*192.5*	*7.8*	*-0.1*	*0.0*	*-0.3*
Évora	*1964-89*	*191.6*	*9.8*	*0.9*	*0.5*	***3.7***
Faro	*1964-86*	*207.7*	*7.5*	*0.7*	*0.4*	***2.9***

Porto series clearly shows a decrease of the SSRD by the end of the 1970s with a maximum annual average value observed in 1970 of $194\ Wm^{-2}$ and the minimum in 1977 of $153\ Wm^{-2}$. Similarly, Bragança reveals a decrease of radiation until the mid-70s followed by an increase. The maximum annual value was reached in 1969 ($204\ Wm^{-2}$) and the minimum value in 1977 ($161\ Wm^{-2}$). Évora and Faro present a similar behavior, contrasting to that observed in Porto and Bragança, i.e., an increase of SSRD is observed since the early 1970s, without any visible dimming period. Regarding Faro, the maximum annual value was registered in 1978 ($222\ Wm^{-2}$) and the minimum, in 1966, with an average value of $196\ Wm^{-2}$. Évora station recorded a maximum mean annual value of $205\ Wm^{-2}$ in 1982, and a minimum annual value of $171\ Wm^{-2}$ in 1970. Finally, in Lisbon there are no relevant decadal variations in the series, which is in contrast with the changes observed in the other stations from Portugal.

Nevertheless, it is worth mentioning that the use of individual series is questionable, especially when the homogeneity testing of the series has been subjected to absolute methods due to the lack of reference series. For this reason, we have also computed the composite mean series of Portugal (Figure 2.1) that allows a higher signal-to-noise ratio, enabling a better identification of decadal variations than single station series and reduce the possible inhomogeneities remaining in the series. The SSRD mean values over Portugal range between $\sim 180\ Wm^{-2}$ and $\sim 200\ Wm^{-2}$. It is possible to identify two periods - until the end of the 1970s the behavior of SSRD is characterized by a decrease followed by an increase, in line with previous literature (e.g., Wild, 2009, 2012), although with an earlier turning year as compared to other regions of Europe (e.g., Wild, 2009; Sanchez-Lorenzo *et al.*, 2013b; Sanchez-Lorenzo *et al.*, 2015).

Figure 2.2 shows the standard deviation of the global radiation on a monthly basis (between the same months) during the period of analysis.

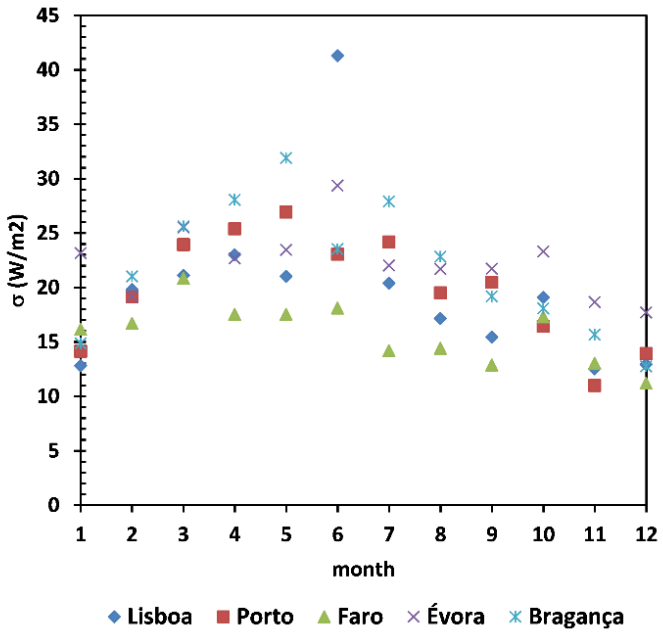

Figure 2.2. Standard deviations of the observed SSRD monthly means.

In general and in all months the highest values of variability corresponds to the cities of Porto and Bragança (in the north of Portugal), which in June presents the largest deviation. The inter-annual variability is greater in the cities of Évora and Porto with annual standard deviations of 10 Wm^{-2}. Faro station shows the lowest inter-annual value of 8 Wm^{-2} and has the maximum mean value of SSRD. The observed variability in the SSRD may be associated to inter-annual variability in cloudiness due to atmospheric circulation patterns such as NAO (Trigo *et al.*, 2002). On the other hand, due to the proximity of the IP to the north of Africa, it is expected that the SSRD is strongly affected by Saharan dust aerosol in particular in the spring and summer months, as well as by summer forest fires. Saharan dust aerosols increase the aerosol optical depth of the atmosphere and lead to a significant decrease of the solar radiation that reaches the ground (Antón *et al.*, 2012; Valenzuela et *al.*, 2012; Obregón *et al.*, 2015).

Lisbon and Porto are the major Portuguese cities and are located near the coast, where the majority of the Portuguese population and industries are concentrated. At the south of Tagus river the industrialization is less relevant (location of districts of Évora and Faro). An analysis of the population in Portugal shows that in the period under review (1960 –1990), the population grew in Lisbon (+53.8%), Porto (+40.5%) and Faro (+8.3%) and decreased in Évora (−20.7%) and Bragança (−20.8%) districts (Cravidão and Matos, 1990).

The SSRD pattern observed in Bragança and Porto (Figure 2.1) shows a decrease of SSRD that may be associated to the period commonly known as global dimming (Stanhill and Cohen, 2001). Still, the data shows that the increase in SSRD appears relatively earlier than that described in the literature, (e.g. Wild *et al*., 2005, Wild, 2009, 2012). Results seem to indicate that the locations where industrial, topography of region and demography is relevant are those where the increase of SSRD arises later or is not visible at all (like in Lisbon). In the remaining stations of Portugal, located in the countryside in the south, with a lower industrial and population density and almost flat topography, the measurements hint at an earlier increase of radiation.

Specifically, Évora and Faro stations (cities at south of Portugal) seem to indicate an increase of SSRD over the whole study period. These cities are located in regions with small industrial density and demographic growth and with only a few occurrences of forest fires when compared with northern Portuguese regions (Leite *et al.*, 2014). Therefore, it is reasonable to assume that the typical atmosphere was characterized by low aerosol loads (background atmospheric aerosol), with occasional events of desert dust or forest fire particle transports, which means that possibly the area did not experience enough aerosol influence to be part of the dimming phenomenon (Alpert and Kishcha, 2008).

Since the area in question had little industry and the dominant circulation brings air masses from the Atlantic Ocean, it does not seem that the concentration of strongly absorbing aerosols (from local areas or from another region) has increased significantly and triggered a pronounced indirect effect of aerosols (as described for example in Twomey *et al.*,1984 and Albrecht, 1989). Daily 120-h back-trajectory analyses of air masses for south-western IP, from 2005 to 2010, showed that the most frequent situations observed were the clean and maritime situations (Obregón *et al.*, 2012). This would, at least partly, explain the behavior of Évora and Faro series, which shows a stronger increase of SSRD than the other Portuguese stations.

Overall, the turning year from the period of decrease and increase if SSRD was around five years before in the stations in the south as compared to the stations in the north (especially Porto station). Results from winter and summer seasons confirm that the beginning of the brightening period is noticed over Portugal in the late seventies. SSRD in spring and autumn show an opposite behavior, i.e., autumn presents a positive trend without a decrease of SSRD, and spring season a negative trend without an increase (Figure 2.3).

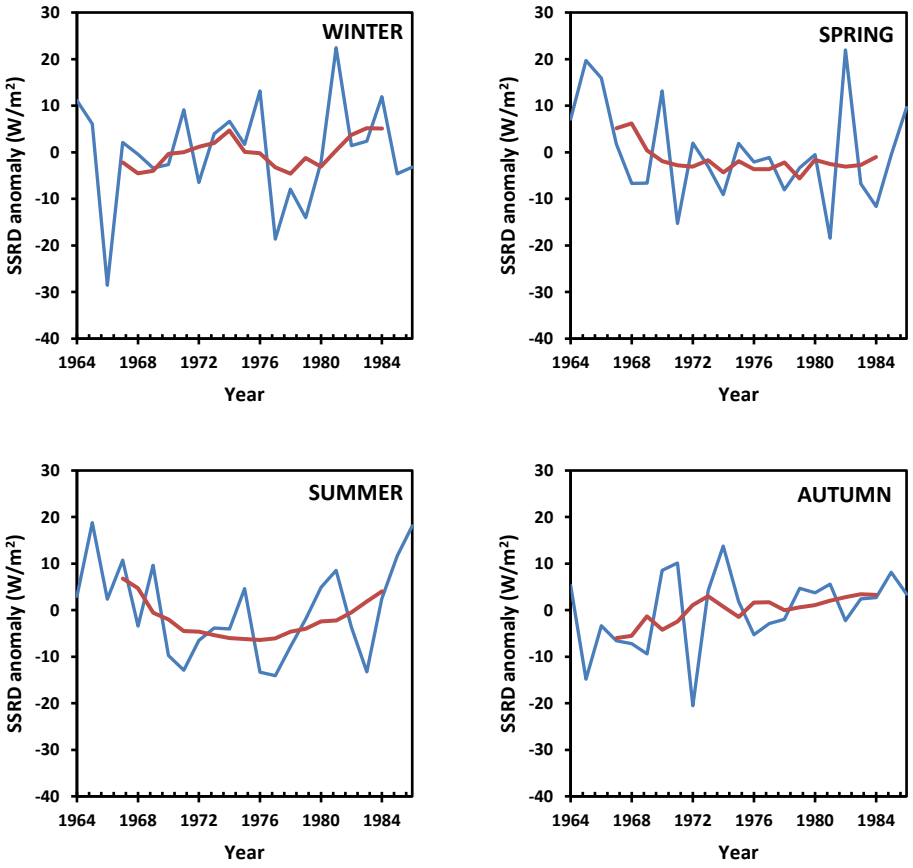

Figure 2.3. Evolution of seasonal mean SSRD in Portugal in the period 1964−86 (blue solid line).
A five year centred moving average was applied (dashed line). Series expressed in anomalies (observation minus mean of reference period).

Table 2.3 contains the seasonal trends over the periods for the mean of five series (Portugal).

Table 2.3. Seasonal linear trends for SSRD mean over Portugal for different periods. Trend values in $Wm^{-2}y^{-1}$. In parenthesis, is presented the α level of confidence obtained by *MK* test.
Bold values means significant trend and the values in parenthesis indicate the level of significance.

	Period		
	1964-86	**1964-77**	**1978-86**
DJF	*0.1*	*0.0*	*0.9*
MAM	*-0.4*	*-1.2 (80%)*	*1.1*
JJA	*-0.0*	***-1.6** (98%)*	*1.9 (80%)*
SON	*0.4 (80%)*	*0.5*	*0.5*

The linear trend in the majority of the seasons, over Portugal, is non-significant over the entire period. The dimming and the brightening trends are mainly observed during summer with

$-1.6\ Wm^{-2}year^{-1}$ and $1.9\ Wm^{-2}year^{-1}$, respectively. However, the highest level of confidence is only obtained for the observed dimming period.

2.4.2. Evaluation of ERA–40 and NCEP/NCAR reanalysis products against ground-based measurements

The mean annual cycle and interannual variability of ERA–40 and NCEP/NCAR SSRD are compared with the global radiation measured at the meteorological stations described in section 2.2.1. For the analysis, the nearest grid points of the reanalysis products are considered. It is worth noting that the comparisons present some limitations due to the large spatial scale between grid point of reanalysis and observations (e.g., Hakuba *et al.*, 2014). The mean correlation coefficients and the bias values for Portugal and Spain, on annual and monthly basis, are shown in Figure 2.4 and Figure 2.5 respectively, whereas in the Supplementary Material additional results for individual stations are presented (Figure 2.14; Table 2.7).

ERA–40 (NCEP/NCAR) annual and monthly averaged SSRD radiation values are always lower (higher) than the corresponding ground-based measurement values as indicated by the negative (positive) $BIAS$ (Table 2.7 – supplementary material, Figure 2.4 and Figure 2.5). The spatial distribution over IP (Figure 2.4) shows a tendency towards negative biases, except in the northern areas, with a performance of ERA–40 better than NCEP reanalysis data. For instance, ERA–40 database underestimates the SSRD in comparison to the observations with a mean $BIAS$ of around $20\ Wm^{-2}$ (or 10% in relative values) for Portugal, where NCEP/NCAR overestimation is around $40\ Wm^{-2}$ (or 20% in relative values).

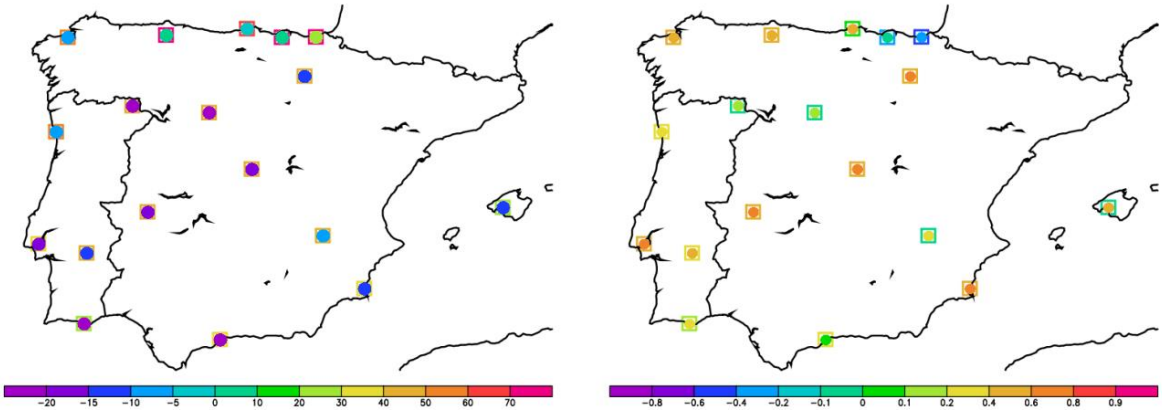

Figure 2.4. Annual spatial distribution of *BIAS* (left image) and correlation coefficient (right image) for Portuguese (1964−1986) and Spanish (1985−2001) stations.
Squares represent values from validation between NCEP/NCAR and observation data and filled circles results from ERA–40 and observations. *BIAS* values in Wm^{-2}.

It is known (Wild, 2001) that NCEP reanalysis is too transparent relative to surface solar radiation, and probably this is one of the reasons that may explain the highest bias found relative to ERA–40.

The correlation coefficient (*r*), on an annual basis (Figure 2.4), between the data measured at the selected stations and reanalysis products is relatively low, with mean values of $r = 0.4$ (ERA–40) and $r = 0.2$ (NCEP/NCAR). Spatial distribution of correlation coefficient is, for both reanalysis, worst at northern stations either in Portugal or in Spain. It is well known that clouds are structures of various dimensions. Due to the coarse spatial resolution of the reanalysis, cloud properties are not well represented (Kaurola *et al*., 2010), which may explain, at least partially, the biases, as also found by Träger-Chatterjee *et al.* (2010) in Germany and You *et al.*, (2013) in the Tibetan Plateau, especially for the NCEP/NCAR reanalysis.

The reliability of ERA–40 and NCEP/NCAR data to assess SSRD was also investigated on a monthly basis (Figure 2.5).

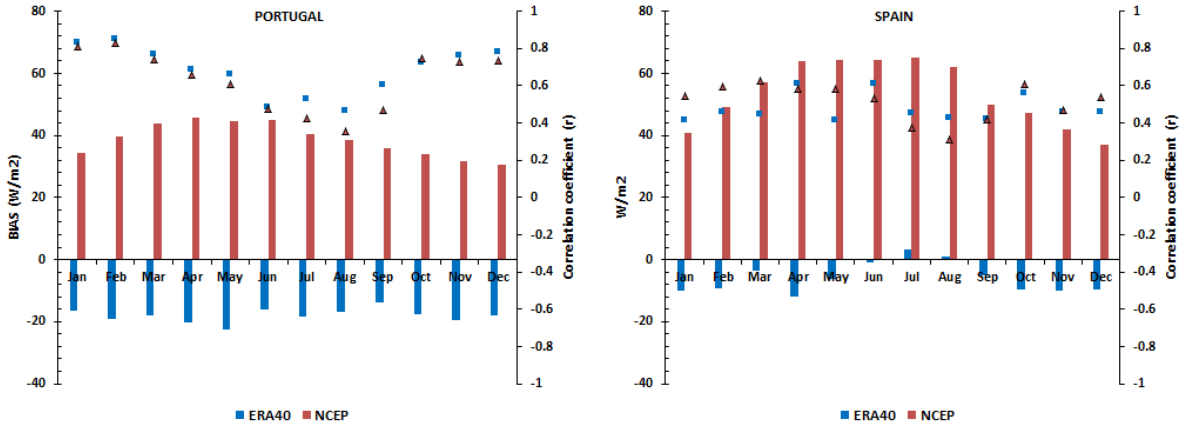

Figure 2.5. Mean correlation coefficients (triangles for NCEP and squares for ERA–40) and $BIAS$ (bars) for all stations in Portugal and Spain, between the monthly mean series of observed solar radiation at selected meteorological stations and simulated solar radiation at the nearest grid point of reanalysis product.

In the majority of the months, the values of the correlation coefficient are approximately above 0.6 for Portugal and Spain, indicating a good correlation (see supplementary material, Figure 2.14). The lowest correlations were obtained for the summer months. In those months the variance in the observations is much larger than in the reanalysis database probably due to the non-inclusion of the actual concentration of aerosols in the reanalysis process. For instance, the radiative fields of ERA–40 use a climatological aerosol profile and do not take into account the actual aerosol type and load (Uppala *et al.*, 2005). Thus, the decrease in the correlations during summertime can be explained by the fact that it is the season with the highest atmospheric aerosol loading over the IP (Alados-Arboledas *et al.*, 2003; Toledano *et al.*, 2007). Nevertheless, the inaccurate representation of clouds, especially the convective systems, can be also considered as another likely cause of the disagreement as compared to surface observations (Wild and Schmucki, 2011; Xia *et al.*, 2006; Enriquez-Alonso *et al.*, 2015).

The CV of the annually averaged observed series (see supplementary material, Table 2.7) is low (less than 5%), indicating a weak interannual variability of the mean incident global radiation, in line with the observed CV in sunshine duration series in IP (Gil *et al.*, 2015). The mean annual values of CV are slightly higher for observations than reanalysis products, since these products are based in radiative transfer model computations and not in radiation measurements contributing to smoothing the data series.

2.4.3. Trends of SSRD for Portugal and Spain from observations, ERA–40 and NCEP/NCAR data

The least square linear method was applied to the Portugal annual series (see Table 2.2) and the results indicate that for the whole period only two of the five stations studied (Évora and Faro) show a significant linear trend, whose confirmation was provided by MK test (Z_{MK} equal to 3.7 and 2.9, respectively). The result shows that in the 1964–1989 period, the trends are relatively strong with an increase in radiation of about $0.9\,Wm^{-2}year^{-1}$ in Évora and, $0.7\,Wm^{-2}year^{-1}$ in Faro. In the other stations the trends are not statistically significant, as confirmed by the *MK* test. It is worth mentioning that Évora and Faro show rates of increase in SSRD comparable with the nearest stations in Spain (Caceres and Malaga), as shown in Table 5 of Sanchez-Lorenzo *et al.*, (2013a).

Figure 2.6 shows the anomaly means of annual SSRD over Portugal and Spain from observations (mean series), ERA–40 and NCEP/NCAR data.

The anomaly series are expressed as differences relative to a common period for Portugal (1964–1986) and Spain (1985–2001). In Portugal, ERA–40 and NCEP/NCAR reanalysis replicate the general features of observations. ERA–40 captures better the dimming period than NCEP/NCAR, but both with a transition from dimming to brightening in the early 1970s (see Figure 2.6).

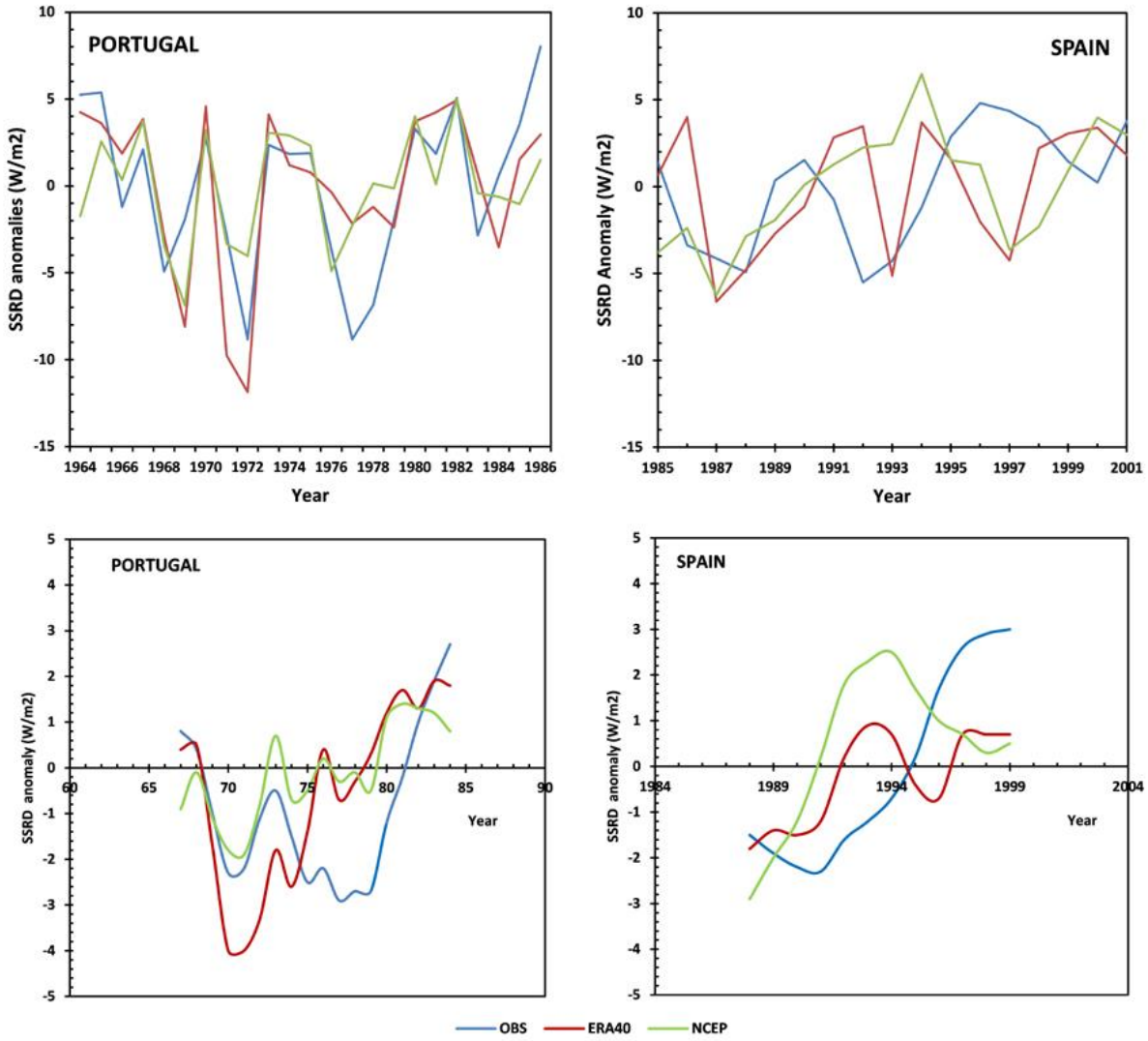

Figure 2.6. Anomaly mean of annual SSRD for Portugal (1964−86) and Spain (1985−2001) from observations (blue line), ERA−40 (red line) and NCEP (green line) data.
Bottom plots show five years centred moving averaged applied to Portugal and Spain data.

Relatively to Spain annual anomalies (1985−2001), ERA−40 and NCEP/NCAR show a general positive trend as the ground-based observations. Table 2.4 shows results for linear trends for different periods.

For Portugal, signals are similar in all periods (except for 1978−1986 period in NCEP/NCAR), although the magnitude of the trends present slight differences between ground based stations and reanalysis products, as well as the turning year of the dimming/brightening periods. In the case of observational Spanish data sets, only one period (1985−2001) is considered.

Table 2.4. Linear trends for annual mean SSRD over three periods in Portugal for observations, ERA–40 and NCEP data. All values in $Wm^{-2}year^{-1}$.

In parenthesis, is presented the α level of confidence obtained by *MK* test. Bold values means significant trend and the values in parenthesis indicate the level of significance.

	Portugal			Spain
	1964-86	**1964-77**	**1978-86**	**1985-2001**
OBS	*0.1*	*-0.5 (90%)*	*1.1 (90%)*	*0.4 (90%)*
ERA-40	*0.1*	*-0.3 (80%)*	*0.2*	*0.2*
NCEP/NCAR	*0.1*	*-0.1*	*-0.1*	***0.4** (98%)*

Linear regression applied to Portugal over the 1964–1986 period, is not statistically significant, as shown by the MK test (see Table 2.4). For subdivided periods, linear trends shows for Portugal significant values, with $-0.5\ Wm^{-2}year^{-1}$ for the dimming (1964–1977) period and $1.1\ Wm^{-2}year^{-1}$ for the brightening (1978–1986) period, taking into account a 90% of level of confidence. ERA–40 data, for the same locations, show only a decreasing trend over the 1964–1977 period but with approximately one half of that presented in Portugal and with non-significant for Spain. Results show that NCEP, in Spain, presents a trend of the same magnitude of observational series ($0.4\ Wm^{-2}year^{-1}$), both with a high significance level (above 90%). For a detailed SSRD trends over Spanish stations (1985–2001) see analysis in paper of Sanchez-Lorenzo *et al*. (2013a) who found a significant positive trend of around $4\ Wm^{-2}$ per decade.

Overall, the decadal changes of the reanalysis products fairly agree with the observations, especially for ERA–40, in contrast to literature for other regions of the world. The comparison between ERA–40 and observations of the SSRD shows a fairly good agreement in the analyzed period, especially on a monthly basis, where *r* values are relatively high. Results obtained from NCEP/NCAR reanalysis have a tendency to be higher than ground-based stations and ERA–40 reanalysis, as seen in biases and decadal changes of radiation shown previously.

This work suggests that the ERA–40 data may be used in order to study the climatology and evolution of the surface solar radiation and clouds, over the regions where aerosol concentrations have not changed significantly. Results obtained with NCEP/NCAR reanalysis are poorer when compared with observational data.

2.5. Assessing SSRD and TCC in the IP from ERA–40 reanalysis data

In this section, the variability and trends of the SSRD and TCC over the IP using ERA–40 reanalysis data from the ECMWF are examined and discussed. Monthly means of SSRD and TCC for the entire period are computed and analysed. The relation between the interannual SSRD over IP and TCC is also analysed.

2.5.1. General features of SSRD and TCC climatology

The ERA–40 data was used to create a climatology of the surface solar radiation for the IP. Figure 2.7 presents the spatial averages of SSRD and TCC from ERA–40 (1957–2002).

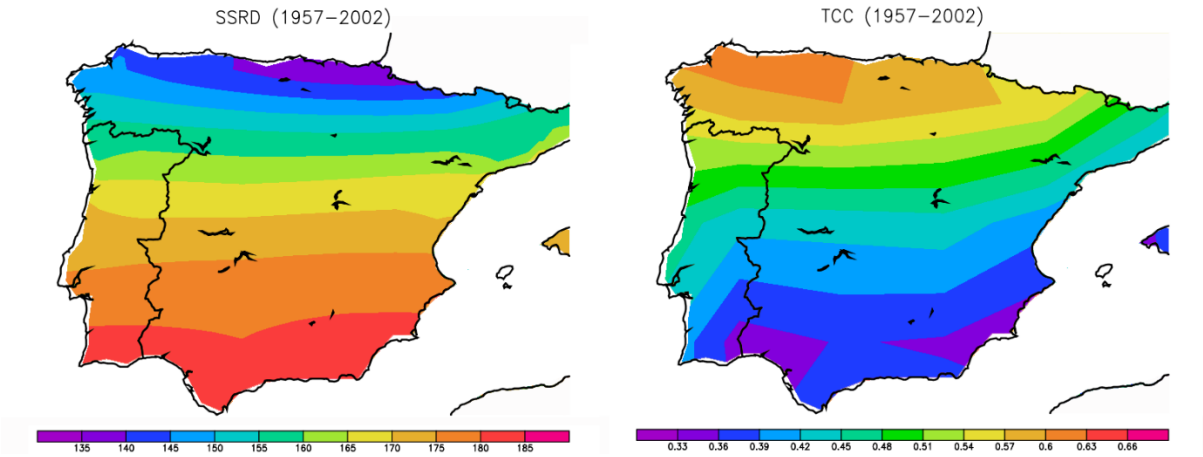

Figure 2.7. Mean values of SSRD (left image) and cloud cover (right image) from ERA–40. Radiation is expressed in Wm^{-2}.

As expected, the averaged SSRD presents a latitudinal gradient showing higher values at lower latitudes and lower values at higher latitudes. On the other hand, the mean TCC is larger for higher latitudes. In this period, the mean SSRD ranged from a minimum of 135 Wm^{-2} in the northern part of the IP to a maximum of 180 Wm^{-2} in the south. The spatial TCC pattern is in phase opposition with respect to SSRD. In addition to the latitudinal gradients, Figure 2.7 also shows longitudinal variations, mainly over the Mediterranean region, with a decrease of SSRD.

A relative maximum of SSRD in the southern IP is observed, covering the Algarve (Portugal) and Andalusia (Spain). The longitudinal gradient is more intense near the Portuguese West coast. The relation between SSRD and TCC was investigated in more depth for the period considered.

The IP annual mean values of the SSRD plotted as a function of the corresponding IP mean TCC values clearly illustrates that SSRD and TCC are negatively correlated, with a high coefficient of determination ($R^2 > 0.8$), as shown in Figure 2.15 (supplementary material). This result reveals a strong dependence of clouds on radiation in the ERA–40 and NCEP/NCAR reanalysis. This finding would be expected since the annual aerosol field is fixed, and so only the clouds and the water vapor may have a direct impact on the SSRD.

The spatial distribution of the mean and standard deviation of SSRD for two months (January/July) associated with two different seasons (winter/summer) were computed. Figure 2.8 depicts the results obtained.

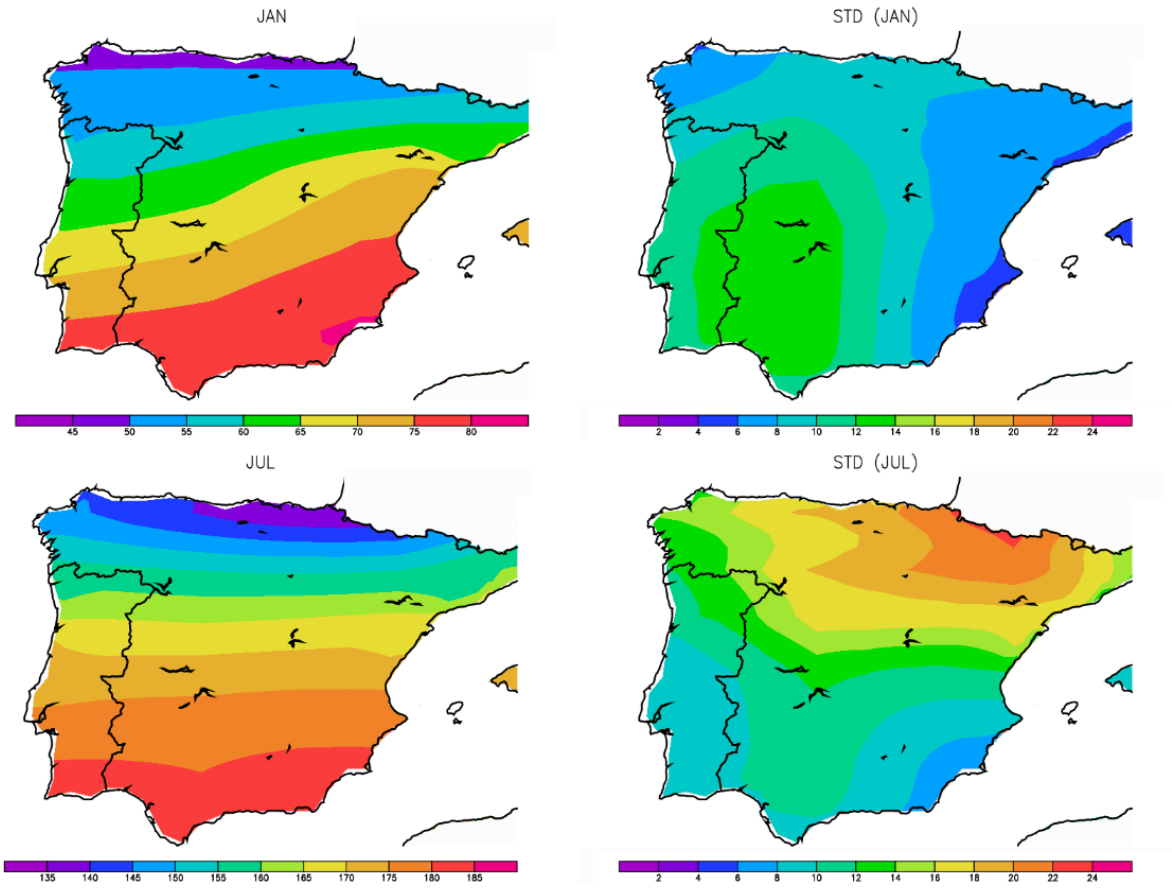

Figure 2.8. The mean ERA–40 SSRD for January and July and corresponding standard deviation.

In January, SSRD range from about 40 Wm^{-2} in the north to more than 80 Wm^{-2} in Murcia region, southeast of Spain. In July the mean SSRD values are almost four times higher, reaching values close to 300 Wm^{-2} in a wide region, including Alentejo and Algarve (Portugal), as well as Estremadura and Andalusia (Spain).

The variability (standard deviation) of the SSRD is larger in January over the southern and central regions of Portugal and Spain, particularly in Extremadura and Andalusia and lower in the same regions in the summer months. The lower absolute variability observed in the northern part of the IP (Galicia, Asturias, País Vasco) in January is in agreement with the lower values of SSRD in the region. In winter months, variability in precipitation (clouds) is usually associated to variability in the pathway of the frontal systems which arise from Atlantic Ocean (Trigo, 2006; Fragoso *et al.*, 2010; among others).

2.5.2. Trend analysis of SSRD and TCC

Figure 2.9 shows the time series of the spatially averaged annual SSRD and TCC in the IP from 1958 to 2001 and gives a general frame of the evolution of these two quantities in the region. The annual time series of SSRD and TCC reveal non-statistically significant trend in ERA–40 over IP for the 1958–2001 period as shown in Table 2.5 (low values of R^2).

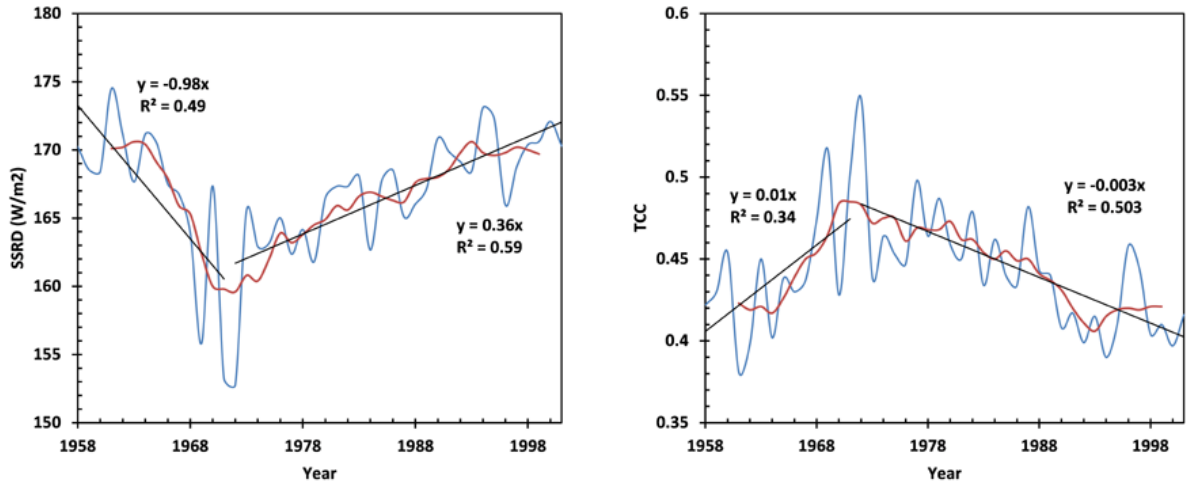

Figure 2.9. Temporal evolution of the annual mean values of the SSRD and of the TCC, over the whole IP, from ERA–40 data.

Red line is the five-year centered moving average. Black solid lines denote linear trends for two periods.

The spatially averaged ERA–40 SSRD mean values with a five-year centered moving average show two distinct periods for the IP (Figure 2.9): a decrease of SSRD in the beginning of the seventies (hereafter referred as ERA–40 dimming period) followed by a slight increase up to the end of the time series (hereafter referred as ERA–40 brightening period). In contrast, the TCC shows an opposite behavior with a decrease after 1971. Figure 2.9 allows identifying a maximum of SSRD over the IP in 1961 with a value of about 175 Wm^{-2} and a minimum in 1972 (153 Wm^{-2}). With respect to TCC, an opposite behavior is observed as referred before with the maximum obtained in 1972.

According to these results, trends for two separate periods were computed (before and after 1971) and are presented in Figures 2.9 and Table 2.5.

Table 2.5. Mean, standard deviation (σ), slope (b), $R - squared$ and time series trend obtained from the by MK test for SW and TCC in IP.

Bold Z_{MK} index means significant trend. In parenthesis, is presented the α level of confidence.

	Period	$\bar{X}$	σ	b	R^2	Z_{MK} ($\propto = 0.05$)
	1958-2001	*166.9*	*4.6*	*0.1*	*0.1*	*1.5*
SSRD	**1958-1971**	*166.9*	*5.8*	*-0.97*	*0.5*	***-3.0***
	1972-2001	*166.9*	*4.1*	*0.36*	*0.6*	***4.7***
	1958-2001	*0.44*	*0.0*	*-0.0*	*-0.0*	*-1.6*
TCC	**1958-1971**	*0.44*	*0.0*	*0.0*	*0.3*	*1.8*
	1972-2001	*0.44*	*0.0*	*-0.0*	*0.5*	***-4.1***

The annual evolution of SSRD series shows a statistically significant trend for both periods. In the first period, the SSRD shows a linear decrease of 1 $Wm^{-2}year^{-1}$ with a statistically significant Z_{MK}. In the second period, it is visible a slight increase of the radiation, with a slope of 0.4 $Wm^{-2}year^{-1}$ and with also significant Z_{MK} at 95% level of confidence. An opposite pattern is noticed for TCC with a significant linear trend only in the second period.

Results from sequential MK test analysis (Figure 2.10) show that in the first period (1958–1971) there is a decrease of the SSRD, which started around the late 60's (~1967) turning significant in the following year. This result is also consistent with the analysis done for the mean of five observational series in Portugal (section 2.4).

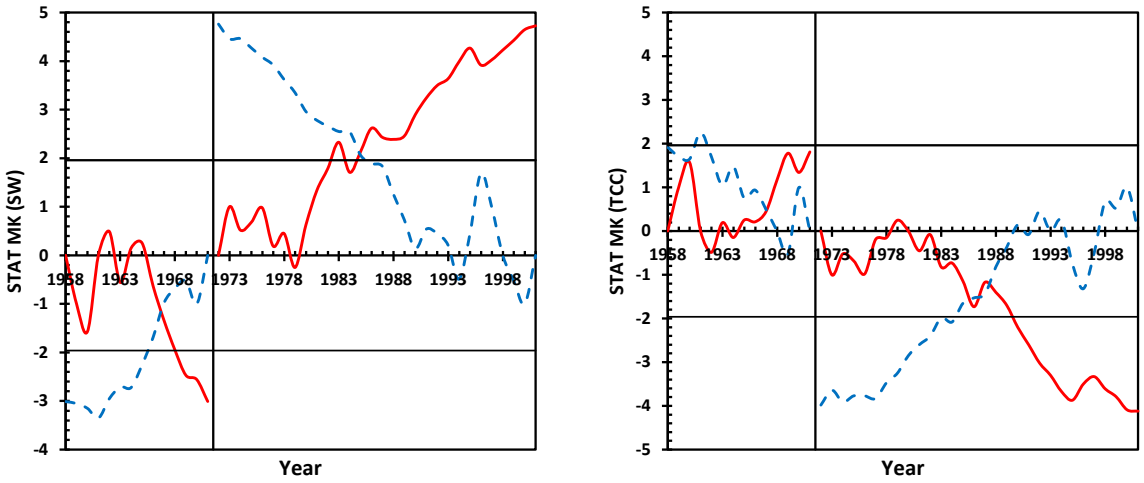

Figure 2.10. Sequential *MK* applied to IP data for *SW* (left panel) and TCC (right panel) divided in two periods (1958−1971) and (1972−2001).
The forward series is the solid line and backward series is the dashed line.

For TCC an opposite behavior is observed with an increase that began in the same year as the SSRD increase but without a statistically significant trend although positive. In the second period (1972–2001), there is an opposite behavior, with SSRD presenting a significant statistical increase after 1985 while the TCC decreases for the same year (see Figure 2.10 and Table 2.5). These results show that the dimming/brightening phenomena is present in the ECMWF ERA–40 dataset over IP, but that the transition occurred earlier than revealed by the majority of global or regional studies (e.g. Wild *et al.*, 2005; Wild and Schmucki, 2011). Anyway, it is possible to look at the dimming/brightening at a regional scale. Thus, the IP was divided into small areas (1° × 1°) and in each of these a five-year centered moving average was applied in order to compute the inflection point (minimum value of the centered moving average). The transition year, computed as the minimum of the centered moving average shows a latitudinal gradient (Figure 2.11), which suggests that the ERA–40 dimming period finished in 1970 in the south and center IP and a few years later (1973–1974) in the north, being the year of 1971 the average for the whole Peninsula.

The fact that ERA–40 does not consider the evolution of the aerosol concentration (Upalla *et al.*, 2005), may explain, at least partially, the anticipation of the inflection point in the reanalysis as compared to studies based on ground-observations. Note that the transition years in the ERA–40 data set are consistent with observations in Portuguese stations located in low industrialized regions (Faro and Évora), as shown before (see previously section).

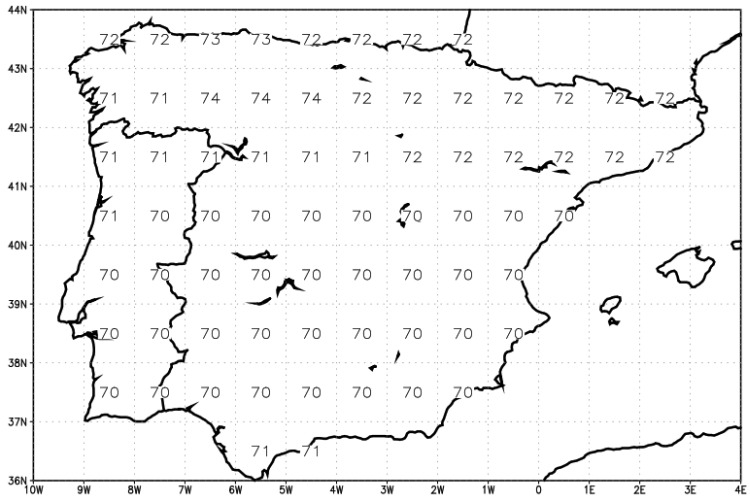

Figure 2.11. Dimming/brightening transition year computed from ERA–40 SSRD data-set on a 1º × 1º grid over IP.

These results show that part of the dimming/brightening phenomena in the Iberian Peninsula must be related with decadal changes in the cloud radiative effects and not only to changes in the aerosol loading, especially over south regions where brightening arise five to ten years earlier than shown in literature (Wild *et al.*, 2005), with a gradient that increase from southwest to northeast.

The SSRD linear trends were computed for the IP in both the ERA–40 dimming (1958–71) and brightening periods (1972–2001). Figure 2.12 shows the spatial distribution of the linear regression trends over the IP. For both periods, the pattern of SSRD trends shows a longitudinal gradient with an increase in the northeast direction. In the first period (1958–1971) trends are always negative with the highest values ($-1.8\ Wm^{-2}year^{-1}$) observed in Northeastern Spain, provinces of Navarra, Aragon and Catalonia. For Portugal, the maximum negative trend ($-1\ Wm^{-2}year^{-1}$) is found over the south (Alentejo and Algarve).

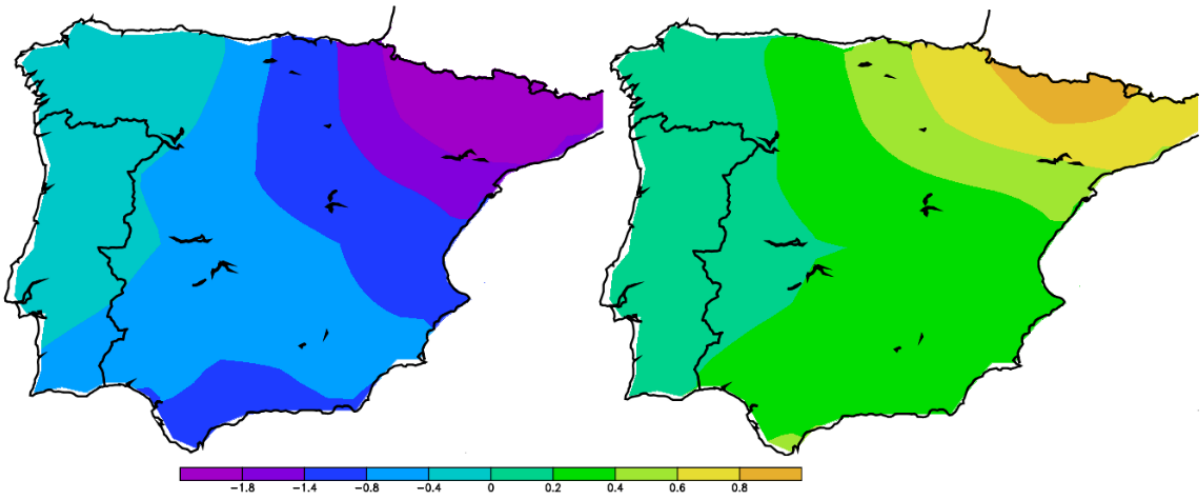

Figure 2.12. Spatial distribution of linear trends in SSRD for 1957−1971 (left) and 1972−2001 (right) periods.

Relatively to the second period (1972–01), linear trend values are always positive for entire IP with a maximum of $+1\ Wm^{-2}year^{-1}$ over the same region where in the first period the major negative trends were found (Northeast region). Although, the period of observational series "break" in different years, there is a tendency to underestimate the trend of the brightening in the reanalysis product as compared to the ground-based observations, with rates below the $4-6\ Wm^{-2}$ per decade reported in this study and in Sanchez-Lorenzo *et al*. (2013a) and in line with the results of Wild and Schmucki (2011). Equally, it is worth noting that during the dimming period, and especially for the ERA–40, there is a tendency to overestimate the rates of decrease as compared to surface observations, and in contrast to Wild and Schmucki (2011).

The monthly mean area averaged trends in IP for SSRD and TCC were computed for both periods and are presented in Figure 2.13. The results for the first period show that there is a clear decrease of radiation in 75% of the months. The maximum (negative) value of Z_{MK} is reached in August, although with other two months with negative Z_{MK} statistical significance (April and July). In the case of TCC, the MK test proved to be statistically significant for the months of April, July and August. However, results show an opposite behavior relatively to SSRD with an increase in all months with the exception of March, October and December.

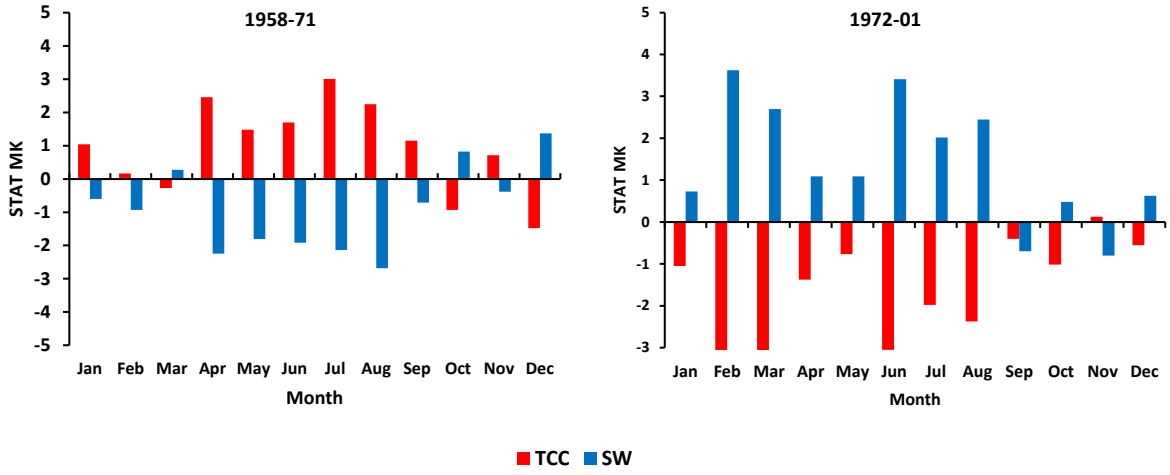

Figure 2.13. Monthly mean trends in ERA−40 dataset. Results from *MK* test for the SSRD and TCC over IP.

In the second period it is observed for both parameters and for almost all the months, an increase in SSRD (except in September and November) and a decrease in TCC (except for September). Table 2.6 summarizes the results of the monthly tendencies, where the grey colour indicates the existence of a statistically significant trend and the sign indicates positive (+) or negative (−) trends.

Table 2.6. *MK* test statistical analysis of the monthly averaged variability in the IP in various periods of study. The light grey indicates the existence of trends with a confidence level of 95%.

Period	Parameter	Jan	Feb	Mar	Apr	May	Jun	Jul	Aug	Sep	Oct	Nov	Dec
1958-71	**SSRD**	−	−	+	−	−	−	−	−	−	+	−	+
	TCC	+	+	−	+	+	+	+	+	+	−	+	−
1972-01	**SSRD**	+	+	+	+	+	+	+	+	−	+	−	+
	TCC	−	−	−	−	−	−	−	−	−	−	+	−

As expected, there are opposite trends in both parameters, especially visible for spring and summer periods. *MK* test shows an increase of SSRD in March, in both periods, statistically significant in the first period, which is consistent with that described by Miranda *et al*. (2006).

2.6. Conclusions

Both downward surface global solar radiation (SSRD) and total cloud cover (TCC) variabilities were studied in the Iberian Peninsula based on the ERA–40. NCEP/NCAR reanalysis data and global radiation data, for five Portuguese stations, obtained from WRDC and IPMA and processed in this study, and for 13 Spanish series available from Sanchez-Lorenzo *et al*. (2013a) were also used.

The SSRD mean series in Portugal show two distinct periods of decrease and increase during the study period, known as the dimming and brightening periods in the literature, although with an earlier turning year (around 5 years) than that described in the literature, in particular over south of Portugal. The observational data reveal an increasing trend of global radiation in the stations located in the South of Portugal, without a pronounced decrease before the 1980s, in the period 1964–1986.

Least square linear method shows for Évora and Faro a statistically significant increase in the SSRD of 1 $Wm^{-2}year^{-1}$, in the study period. This behavior has to be mainly explained by the interannual variability of clouds and respective synoptic patterns over North Atlantic Ocean. Overall, the observations suggest that the decadal evolution of SSRD may be influenced by local causes associated to human activities, particularly the emission of aerosols, as well as cloud changes.

ERA–40 database underestimates the SSRD in comparison to the observations for Portugal and Spain, whereas NCEP/NCAR overestimated the latter. The correlation coefficients (r) found between the ground-based stations for Portugal and Spain obtained from the nearest ERA–40 and NCEP/NCAR grid data points are relatively high for the monthly series. Specifically, the correlation coefficient values are above 0.7 with the highest values obtained during winter and autumn seasons.

From reanalysis and for Iberian Peninsula, it seems that ERA–40 captures better the decadal variability observed in ground-based SSRD records than NCEP/NCAR. Specifically, the time evolution of ERA–40 SSRD values for IP shows two distinct periods: a decrease of SSRD to the beginning of the seventies (ERA–40 dimming period), followed by a slight increase up to the end of the time series (ERA–40 brightening period), with a significant linear trends of

$-1\ Wm^{-2}year^{-1}$ and $+0.4\ Wm^{-2}year^{-1}$, respectively. For both periods, it is possible to see a longitudinal gradient toward the northeast direction. TCC shows an opposite behavior.

SSRD and TCC are negatively correlated with a fairly high coefficient of determination ($R^2 > 0.8$). This finding would be expected since the annual aerosol field is fixed (Uppala *et al.*, 2005). Results show that part of the dimming/brightening phenomena in the Iberian Peninsula must be related with decadal changes in the cloud radiative effects and not only to changes in the aerosol loading, especially over southern regions where brightening arise approximately 5 years earlier than reported in literature (Wild *et al.*, 2005).

ERA–40 reveals a reasonable ability to simulate the radiation, in particular on a monthly basis, considering the uncertainty in the observational data, the problem of fixed aerosols in the reanalysis data and its spatial resolution. It was thus possible to obtain a useful low resolution climatology of the surface global solar radiation over Iberian Peninsula based on ERA–40 reanalysis.

Acknowledgment

The authors acknowledge the funding provided by ICT, under contract with FCT (the Portuguese Science and Technology Foundation) and by the FEDER (Programa Operacional Factores de Competitividade COMPETE) and FCT in the framework of project FCOMP-01-0124-FEDER-041840 (EXPL/GEO-MET/1422/2013). ASL was supported by a post-doctoral fellowship JCI-2012-12508 and the projects CGL2014-55976-R, CGL2014-52135-C3-01-R from the Spanish Ministry of Economy and Competitiveness. The authors would also like to thank the ECMWF for providing ERA–40 data. *NCEP Reanalysis data was provided by the NOAA/OAR/ESRL through the website at http://www.esrl.noaa.gov/psd.* Authors would also like to thank to *AEMET (Spanish Agencia Estatal de Meteorologia) and IPMA (Instituto Português do Mar e da Atmosfera) for providing ground-based data.*

Supplementary Material

Table 2.7. Descriptive statistics of annual mean of downward surface global solar radiation for observed and reanalysis data over Portugal and Spain.

STATION	OBS	ERA-40	NCEP	NBIAS (ERA-40)	NBIAS (NCEP)	CV (OBS)	CV (ERA-40)	CV (NCEP)	r_{Obs} (ERA-40)	r_{Obs} (NCEP)
Lisboa	193.4	176.5	226.1	-8.7	16.9	4.0	2.4	1.2	0.6	0.5
Porto	177.7	168.6	228.5	-5.1	28.6	6.0	2.9	1.6	0.4	0.3
Faro	207.7	181.5	230.9	-12.6	11.2	3.6	3.2	1.1	0.3	0.2
Évora	190.1	177.9	237.6	-6.4	25.0	4.9	3.1	1.5	0.4	0.3
Bragança	181.5	159.0	225.8	-12.4	24.4	5.2	3.2	1.9	0.1	0
Albacete	188.2	178.4	233.4	-5.2	24.0	3.9	1.7	2.1	0.2	0
Bilbao	131.7	141.0	210.0	7.0	59.4	7.5	2.0	1.3	0	-0.3
Caceres	194.5	175.2	238.5	-10.0	22.6	2.4	2.0	2.3	0.6	0.5
Coruna	157.0	147.2	208.8	-6.2	33.0	3.2	2.2	1.1	0.5	0.5
Logrono	164.5	150.9	214.1	-8.3	30.2	3.4	2.4	1.5	0.6	0.4
Madrid	188.3	170.2	232.0	-9.6	23.2	2.9	2.3	2.0	0.7	0.5
Malaga	204.1	182.7	238.9	-10.5	17.1	3.0	2.5	2.1	0	0.3
Murcia	197.9	182.9	237.0	-7.6	19.8	2.6	1.1	1.7	0.8	0.5
Oviedo	137.8	143.0	209.2	3.8	51.8	4.5	1.9	1.2	0.4	0.5
Pmaiorca	187.3	175.2	210.0	-6.4	12.2	3.4	1.4	1.4	0.5	0
Ssebastian	138.2	161.6	231.1	16.9	67.2	4.8	1.8	1.9	-0.3	-0.4
Santander	142.3	141.2	210.0	-0.8	47.6	3.7	1.8	1.3	0.5	0
Valladolid	182.3	159.5	231.1	-12.5	26.8	3.3	2.2	1.9	0.2	0

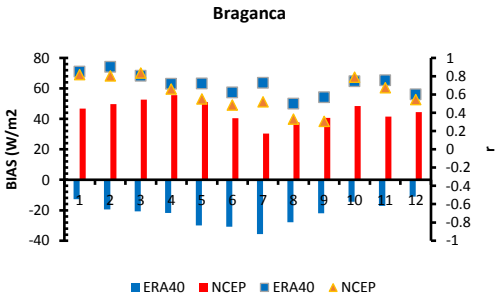
Braganca
BIAS (W/m2
r
ERA40 NCEP ERA40 NCEP

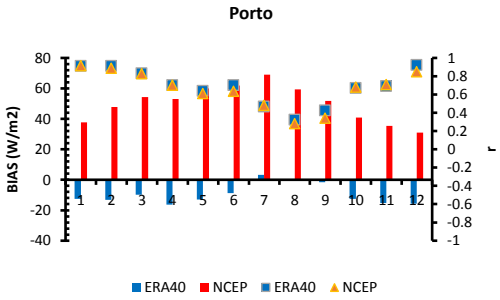
Porto
BIAS (W/m2)
r
ERA40 NCEP ERA40 NCEP

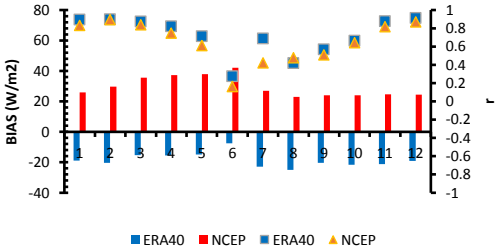
Lisbon
BIAS (W/m2)
r
ERA40 NCEP ERA40 NCEP

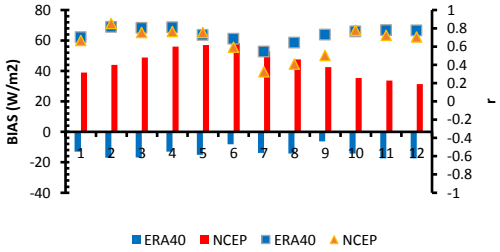
Evora
BIAS (W/m2)
r
ERA40 NCEP ERA40 NCEP

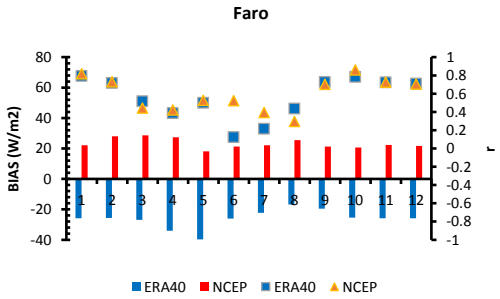
Faro
BIAS (W/m2)
r
ERA40 NCEP ERA40 NCEP

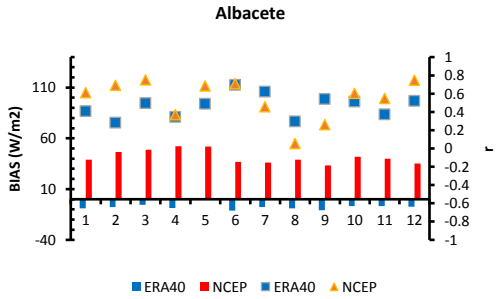
Albacete
BIAS (W/m2)
r
ERA40 NCEP ERA40 NCEP

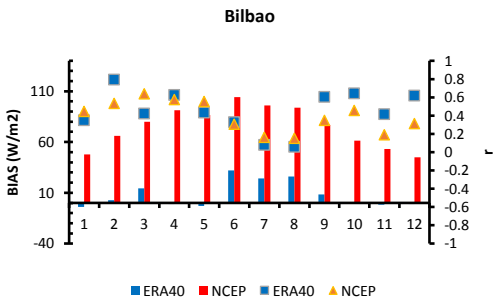
Bilbao
BIAS (W/m2)
r
ERA40 NCEP ERA40 NCEP

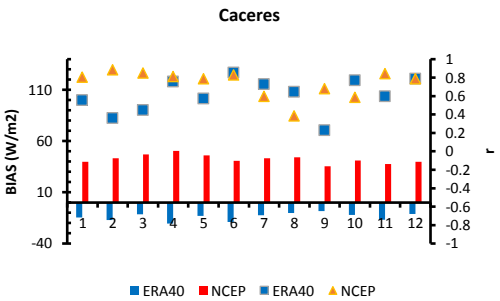
Caceres
BIAS (W/m2)
r
ERA40 NCEP ERA40 NCEP

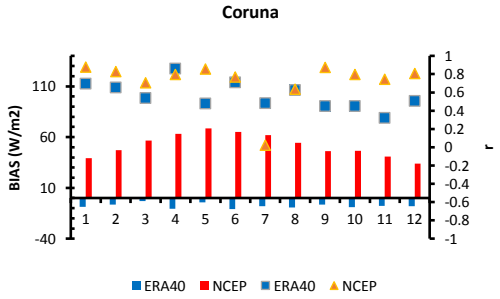
Coruna
BIAS (W/m2)
r
ERA40 NCEP ERA40 NCEP

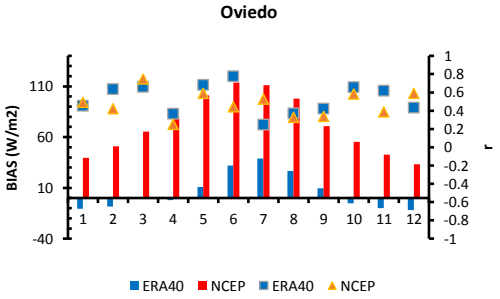
Oviedo
BIAS (W/m2)
r
ERA40 NCEP ERA40 NCEP

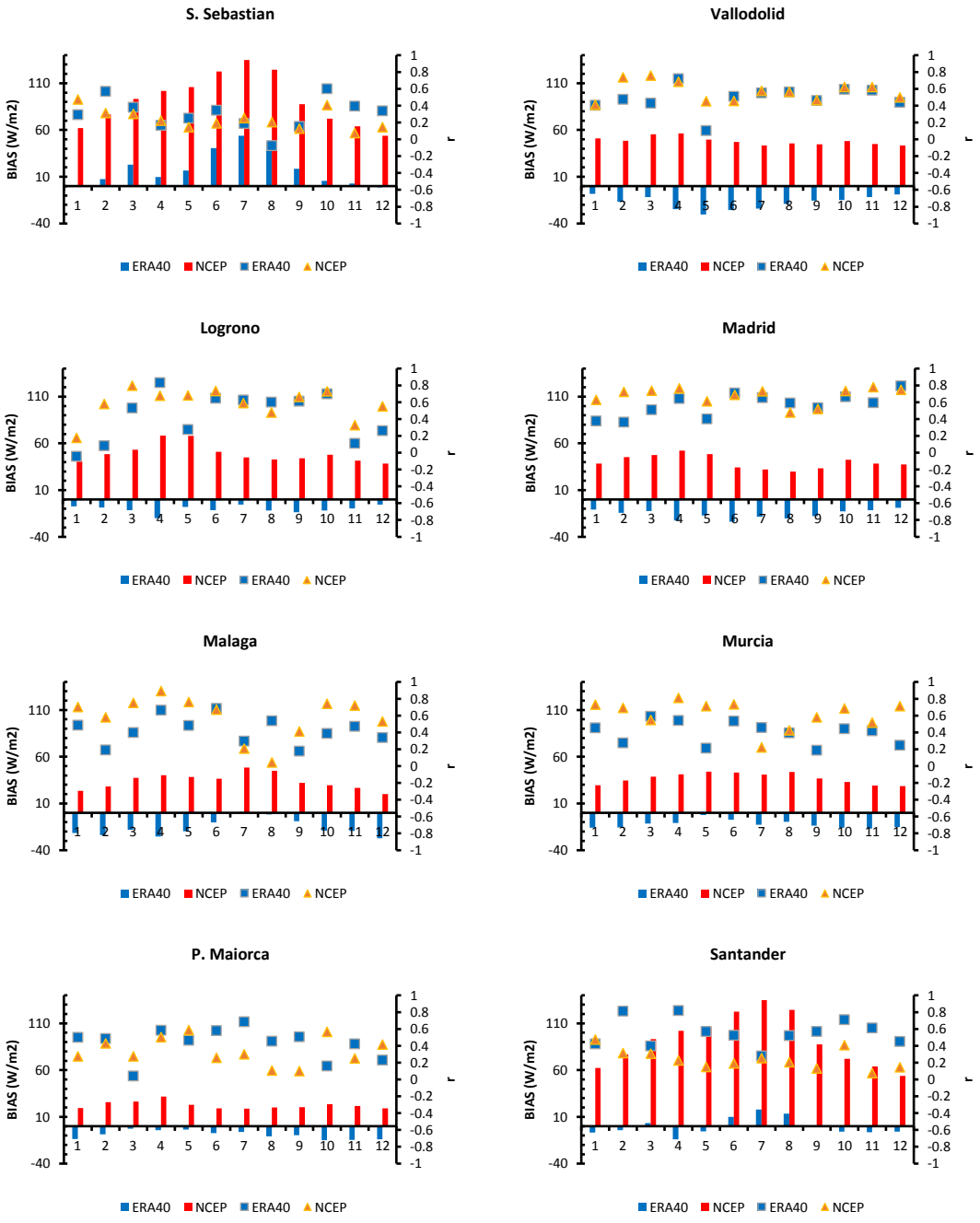

Figure 2.14. Correlation coefficients (dots) and *BIAS* (bars) between the monthly mean series of observed SSRD at selected meteorological stations (Portugal and Spain) and reanalysis products nearest grid point.

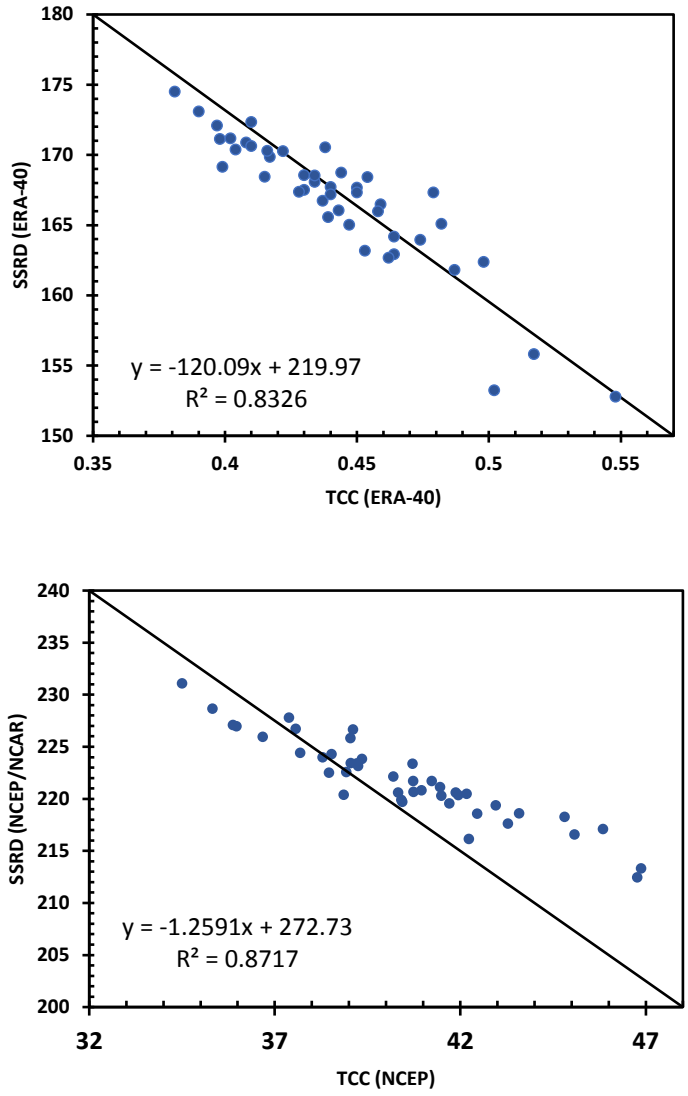

Figure 2.15. SSRD radiation versus TCC spatially averaged over IP, for ERA–40 (upper image) and NCEP/NCAR (down image).

SSRD in Wm^{-2}. TCC NCEP/NCAR data in percentage.

3.

An Iberian Climatology of Solar Radiation obtained from WRF regional climate simulations for 1950–2010 period

This chapter is a transcription of the paper published with the following reference:

Perdigão, Joao, Salgado, Rui, Magarreiro, C.,Soares, Pedro M.M., Costa, M.J., Dasari, H.P., 2017. An Iberian climatology of solar radiation obtained from WRF regional climate simulations for 1950–2010 period, Atmospheric Research 198, 198, 151–162.DOI10.1016/j.atmosres.2017.08.016

Abstract

The mesoscale Weather Research and Forecasting (WRF) Model is used over the Iberian Peninsula to generate 60 years (1950–2010) of climate data, at 5 km resolution, in order to evaluate and characterize the incident shortwave downward radiation at the surface ($SW\downarrow$), in present climate.

The simulated values of $SW\downarrow$ in the period 2000–2009 were compared with data measured in Spanish and Portuguese meteorological stations before and a statistical bias correction was

applied using data from Clouds and the Earth's Radiant Energy System (CERES), on board four different satellites. The spatial and temporal comparison between WRF results and observations show a good agreement for the analyzed period, although the model overestimates observations. This overestimation has a mean normalized bias of about 7% after bias correction (or 17% for original WRF output). Additionally, the present simulation was confronted against another previously validated WRF simulation performed with different resolution and set of parametrizations, showing comparable results. WRF adequately reproduces the observational features of $SW\downarrow$ with correlation coefficients above 0.8 in annual and seasonal basis.

60 years of simulated $SW\downarrow$ over the Iberian Peninsula were produced, which showed annual mean values that range from 130 Wm^{-2}, in the northern regions, to a maximum of around 230 Wm^{-2}, in the southeast of the Iberian Peninsula (IP). $SW\downarrow$ over IP shows a positive gradient from north to south and from west to east, with local effects influenced by topography and distance to the coast.

The analysis of the simulated cloud fraction indicates that clear sky days are found in more than 30% of the period at the southern area of IP, particularly in the Algarve (Portugal) and Andalusia (Spain), and this value increases significantly in the summer season for values above 80%.

Keywords: WRF model; Downscaling Climatology; Downward Solar radiation; Cloud fractions; Iberian Peninsula.

3.1. Introduction

Incoming solar radiation is an important variable from meteorological, economic and social perspectives. In the last IPCC report it is stated that "CO_2 emissions from fossil fuel combustion and industrial processes contributed about 78 % of the total greenhouse gas emission increase from 1970 to 2010, with a similar percentage contribution for the period 2000–2010" (IPCC, 2014). To reduce CO_2 emissions it is necessary to decarbonize the electricity generation. Detailed knowledge of the solar resource in the present and in the near future is essential for assessing the viability of projects related to the harnessing of solar energy.

Solar radiation studies carried out in various regions have revealed that, in the past century, the Earth has undergone two opposite periods regarding the variability of solar radiation: Global Dimming (Stanhill and Cohen, 2001), with a reduction in solar radiation at the surface until the mid-1980s and later the global Brightening (Wild *et al*., 2005), with an increase of global radiation at the surface. Based on observations and ERA–40 reanalysis, Perdigão *et al*. (2016) confirmed the existence of these two distinct periods in Portugal, known as dimming and brightening, but with an earlier turning year than the one described in the literature, in particular over the south of Portugal. This latter study revealed an increasing trend of surface global radiation located in the south of Portugal, without a pronounced decrease before the 1980s, in the period 1964–1986.

Before reaching the Earth's surface, incoming solar radiation is scattered, absorbed and reflected in the atmosphere. Clouds play a major role in spatiotemporal solar radiation variability. Hence, it is common that studies on solar radiation at Earth's surface include also an analysis of cloud cover. Sanchez-Lorenzo *et al*. (2009) analysed observational cloudiness series for Iberian Peninsula (IP) and found a decreasing trend in the IP between 1960 and mid 2000s. The authors report higher annual values over northern areas (4.5 $oktas$) and smaller values in southern areas (3.5 $oktas$), reaching minimum values in July and August (less than 3 $oktas$). According to the authors, the sunshine duration series show a decrease from 1950 to the mid–1980s that is not associated with total cloud cover. On the other hand, later on, Sanchez-Lorenzo *et al*. (2013b) found, for the 1985–2010 period, a positive trend in the global radiation in line with the sunshine duration trends since the 1980s.

Many commercial systems have been installed in the IP intended for solar energy power generation, particularly in the southern regions. In the study of Ridao *et al*. (2007), present and future of renewable solar energy was analyzed for Andalusia, with an average solar radiation energy of $4.6 \pm 0.3\, kWh/m^2\, day$, which qualifies the southern IP as a strategic region in Europe regarding solar energy technology implementation. In the European Union, solar energy presents itself as the main source of renewable energy investment until 2030 (APREN, 2014). Spain is the fifth country of the European Union in the production of photovoltaic energy, with more than $4\ GW$ of installed capacity (IDAE, 2016). In Portugal, the currently installed solar power capacity is more than $450\ MW$ (almost 3% of the energy produced) and it is expected to double that capacity by 2030. Alentejo and Algarve are the Portuguese regions with the highest installed solar capacity (APREN, 2014).

Santabàrbara *et al*. (1996) built annual and seasonal maps of solar radiation in and around Catalonia province (Spain), for the period 1964–1993, from daily *in situ* global solar irradiation datasets and found maximum values over the inner part of Catalonia and at the south coast. According to Jerez *et al*. (2013), IP shows a strong potential in terms of complementarity between solar and wind power. The authors combined simulated data obtained from the MM5 numerical model with a new developed algorithm to identify optimum spatial distributions for solar and wind power plants in order to guarantee a certain energy generation provided by renewable resources. Results show Valencia, Murcia and Andalusia provinces (Spain), as well as Algarve (Portugal), as optimal locations for solar power plants. Šúri *et al*. (2007) used a solar radiation model (Šúri and Hofierka, 2004) and showed that Portugal and the Mediterranean regions have the greatest potential for solar electricity production with maximum values in summer months. Also, Ruiz-Arias *et al*. (2012) showed similar conclusions. The authors evaluated the potential of renewable energies in electricity production for the province of Jaén (southern of Spain) and proposed a scenario where PV could produce up to 21% of the electricity demand in that region.

Due to the increasing demand of solar energy systems, an accurate knowledge of the solar resource plays a key role from an economic perspective. There are several methodologies and models to obtain solar irradiation maps and to predict solar radiation. For instance, Ehnberg and Bollen (2005) proposed a model based on cloud observations. Alsamamra *et al*. (2009) used a statistical methodology for mapping global solar radiation at the surface. Martín *et al*. (2010), applied several statistical methods based on observational time series to predict half daily values of global solar irradiances. Martín *et al*. (2010), proposed an empirical model to estimate the

solar energy as a function of other climatic variables. Ruiz-Arias *et al*. (2015) used an interpolation methodology to adjust global horizontal and direct normal irradiances obtained with WRF model with observational ground-based station data.

The application of Regional climate models (RCMs) in the evaluation of solar radiation features (trends, variability and climatology) in the past, present and future may overcome the problem of gaps in observational time series, the poor spatial coverage of ground-based stations and time series size. This approach allows for a detailed spatial characterization of any regions in order to select the one with best conditions to receive solar power plants, improving in that way the risk analysis of their implementations for political and economic decision-makers.

RCMs are used for downscaling of global climate simulations and have been extensively used in various regions (e.g. Feser *et al*., 2011; Soares *et al*., 2012). Reviews on RCMs can be seen in Dudhia (2014), Rummukainen (2010), Laprise (2008) or Giorgi and Mearns (1999). The mesoscale Weather Research and Forecasting (WRF) model (Skamarock *et al*. 2008) has been increasingly used as RCM. It is an open source tool, with considerable flexibility given the variety of parameterizations available, which makes it a very versatile tool for research in atmospheric physics. This model was used and evaluated over IP for different meteorological variables and by several authors such as Ruiz-Arias *et al*. (2015), Dasari *et al*. (2014), Rios-Entenza *et al*. (2014), Soares *et al*. (2014), Cardoso *et al*. (2013), Soares *et al*. (2012), Mercader *et al*. (2010), among others. For instance, Santos-Alamillos *et al*. (2012) proposed and evaluated a method to analyze the spatiotemporal balance between solar and wind resources over the southern part of IP, using the WRF model with a spatial resolution of $9km$. The results show the existence of complementarity between the solar and wind energy, but with a marked seasonality in strength and spatial coverage.

Lara-Fanego *et al*. (2012a) evaluated the reliability of WRF to predict global and direct irradiance over Andalusia (southern of Spain) and found that the model presents substantial quality. Nevertheless, their analysis showed that WRF tends to overestimate both irradiances with a relative seasonal bias of about 10% for global and twice higher for direct radiation.

The common practice in dynamical regional climate downscaling is to perform long continuous integrations with RCMs, starting from a single set of initial conditions, for a long period without re-initialization time slices. (e.g. Soares *et al*., 2012; Marteau *et al*., 2015). This technique allows the model to develop internal variability but it is computationally expensive. In this work, we used a WRF simulation of six decades with annual re-initializations to avoid such

computation costs (Dasari *et al*., 2014). This approach allows to perform model simulations simultaneously, resulting in a gain of execution time of the complete numerical experiment. This procedure is in agreement with other authors, namely Raju *et al.* (2015) and Xue *et al*. (2014). Lo *et al*. (2008) discuss advantages and disadvantages of this technique. According to these authors, the re-initialization approach is widely accepted in weather forecasting to mitigate the problems of systematic error growth in long integrations but it is rarely used in regional climate simulations. This happens because: (i) it is not easily portable; (ii) long spin-up time of RCMs constrains the re-initialization process and (iii) possible occurrence of discontinuity points between consecutive simulations. However, Lo *et al*. (2008) compared long-term continuous integration with short-term reinitialized simulations showing that the re-initialization runs outperform the continuous simulation runs.

Many authors pointed out the difficulties RCMs have in the representation of the large-scale features as they are forced at their boundaries (e.g. Jones *et al*., 1995; Yhang and Hong, 2011). Waldron *et al*. (1996) and Von Storch *et al.* (2000) firstly presented the nudging methodology. In the subsequent years nudging techniques were further developed and employed in many studies, but its use is not consensual (Alexandru *et al*., 2008; Miguez-Macho *et al*., 2004; Hong and Chang, 2012, Hong and Kanamitsu, 2014), due to disagreements regarding the advantage of reducing freedom from regional model's large scales and other potentially negative lateral consequences.

An important issue in NWP analysis is the evaluation of the model results. Usually, this evaluation is performed through the comparison between observational ground-based data with the nearest grid point of the model outputs. Bias correction (eg, Ruiz-Arias *et al*., 2015; Acharya *et al*., 2013; Haddeland *et al*., 2012; Piani *et al*., 2010), in a post-processing stage, is often performed. Ehret *et al*., (2012) present the state-of-the art of bias correction methods as well the assumptions and implications.

The main objectives of this paper are: firstly, to evaluate the quality of the 5 km resolution WRF simulations with annual re-initializations, to predict incident shortwave solar radiation at the surface ($SW\downarrow$) through the comparison with observations and other WRF simulations (continuous and previously validated); secondly, to characterize the solar radiation at the surface with bias correction and the cloud fraction, in the 1950–2010 period over the IP, in order to assess the regions with major solar resource potential. The paper is structured as follows: sections 3.2 to 3.4 describes the methodology used in this study, as well as the data, model setup and study area. The performance of the simulations and bias correction

methodology is discussed in section 3.5. A detailed climatology of $SW\downarrow$ and cloud cover over IP is presented and discussed in section 3.6. Finally, conclusions are presented in section 3.7.

3.2. Datasets and Methods

3.2.1. Model and numerical experiments

WRF mesoscale model V3.3.1. (Skamarock *et al*., 2008) was configured with two domains, using two-way nesting, with horizontal resolutions of 75 km and 25 km, and 30 vertical pressure levels. From the 25 km resolution simulation output, a dynamical downscaling to a 5 km resolution domain was carried out (Figure 3.1), using one way nesting, with hourly output. The results of the 5 km resolution simulation ($WRF5$ hereinafter) are used in the characterization of the IP climatology.

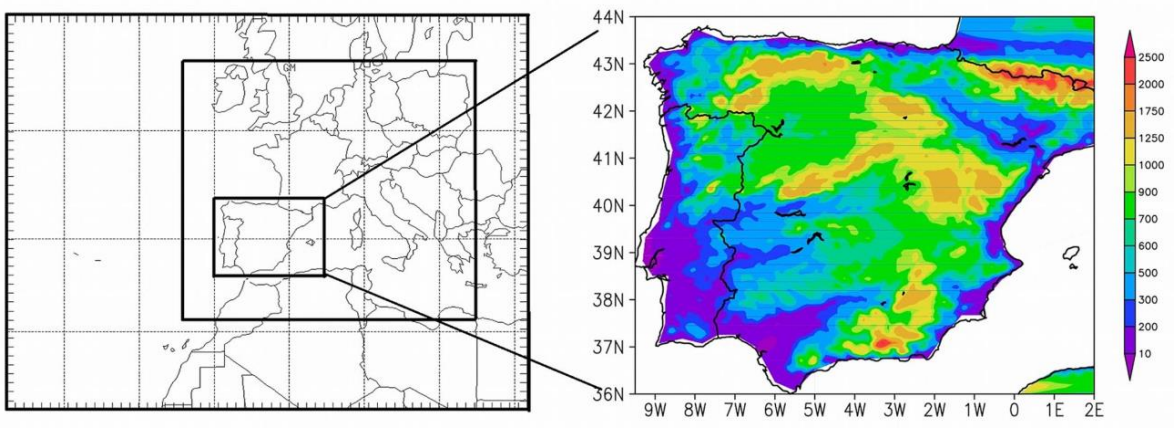

Figure 3.1. 75 km, 25 km and 5 km WRF simulation domains (left) and orography (in meters) used by WRF simulations (right).

In order to reduce the time required to simulate 60 years, the procedure adopted in this work consists in splitting the climate runs into several yearly simulations that are performed simultaneously. $WRF5$ was integrated continuously for 13 months starting from 00 UTC 1 May of each year for six decades (1950–2010). The first month of each simulation was used as model spin up time and was neglected in the analysis. The NCEP/NCAR (National Centers for Environmental Prediction/National Center for Atmospheric Research) reanalysis data at 2.5° latitude/longitude resolution (Kalnay *et al*., 1996), updated every 6 hours, was used as initial and forcing boundary condition. The model setup for these simulations are described

in detail in Dasari *et al*. (2014), where the results were validated for extreme events of heat and cold waves and showing a good agreement with E−OBS V7.0 dataset (Haylock *et al*., 2008).

Since the $WRF5$ simulation followed a less common simulation strategy based on multiple one year time-slices, its performance is also investigated through comparison with results obtained from a continuously integrated WRF simulation ($WRF9$). $WRF9$ simulation was previously validated for temperature and precipitation over Portugal (Soares *et al*., 2012), precipitation over Iberia (Cardoso *et al*., 2013) and offshore wind (Soares *et al*., 2014), with the results showing a good agreement with observations. In $WRF9$, the model simulation ran continuously from $00\ UTC\ 1\ January$ 1989 to the end of 2012 where the first month is used as model spin up. The $WRF9$ simulation was performed using two one-way nested grids (27 and $9\ km$ horizontal resolution) and the results from the finer domain are used for comparison. The outermost domain was designed in a way to reduce spurious boundary effects in the inner region and both grids were centered in the Iberian Peninsula. Additionally, grid nudging (Stauffer and Seaman 1990) was applied to the outermost grid, every $6h$ at all levels above the planetary boundary layer. This WRF simulation was forced by ERA-Interim reanalysis (Berrisford *et al*., 2009). CAM3 was selected to parameterize radiation processes at sub-grid scales for both shortwave and longwave radiation (Collins *et al*., 2004). This scheme takes into account the interactions of the radiation with clouds and with several aerosol types and trace gases. A detailed description of $WRF9$ simulations can be found in Soares *et al*. (2012). Similarities and differences in physical parameterizations, for $WRF5$ and $WRF9$, can be seen in Table 3.1.

Table 3.1. Configurations of the physical parametrizations used in each model.

Model	**NCEP/NCAR WRF−ARW**	
Acronym	$\boldsymbol{WRF5}$	$\boldsymbol{WRF9}$
Resolution	$5km$	$9km$
Vertical Level	30σ	49σ
Microphysics	WSM3 – class simple ice scheme (Hong *et al*., 2004)	WSM6 – Class single moment (Hong and Lim, 2006)
SW	CAM3 (Collins *et al*., 2004)	
LW		
PBL	YSU (Hong *et al*., 2006)	Mellor-Yamada-Janjic (Janjic, 2001)
Convection scheme	Grell-Devenyi ensemble (Grell, G.A. and D. Devenyi, 2002)	Betts-Miller-Janjic (Betts, 1986; Betts and Miller, 1986; Janjic, 1990; 1994,2000)

3.2.2. Observational data

In order to assess the ability of WRF model to simulate the $SW\downarrow$, these results were compared with daily observations obtained from 65 stations of IPMA (Portuguese Weather service) and AEMET (Spanish Weather service).

Global solar irradiance was measured using Kipp & Zonen pyranometers, model CM-11, with a spectral sensitivity in the wavelength range 305–2800 nm and with an uncertainty of $\pm$ 2% (according to the manufacturer). These instruments are classified, in accordance with International Standard ISO 9060/1990, as secondary standards. This classification was adopted by the World Meteorological Organization (WMO, 2008).

In the Spanish network, all radiometers are calibrated every two years. For more information see Ruiz-Arias *et al*. (2015) or García *et al*. (2014). Relatively to IPMA, calibration was performed only at the factory (Kipp & Zonen), and some of the pyranometers in the network were replaced in the period used. The quality control is based mainly on the spatial distribution of records over all observational stations.

The comparison between simulations and observations was made using the nearest neighbour technique, i.e., the closest grid point model values were compared with the correspondent measured ones. The analysis was made for the time periods when observations and simulations were simultaneously available (2000–2009).

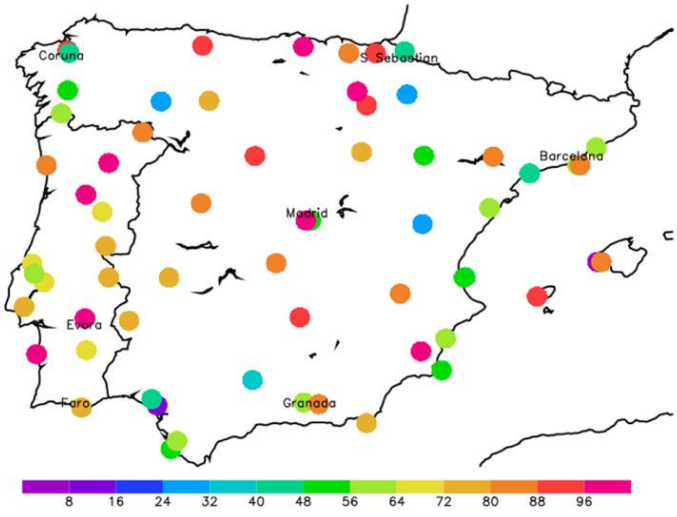

Figure 3.2. Geographical location of the 65 observational stations used to evaluate the WRF simulations and length of the time series.
The scale indicates the percentage of days available at each station for the period 2000−2009.

Figure 3.2 presents the location of the $SW\downarrow$ ground-based stations and the percentage of days with data within the mentioned period. Since the observations have different time periods, for seasonal analysis, it was decided not to compute monthly means for the stations with less than 20 days for each month in the respective observation period, yielding a total of fifteen stations. In turn, a given yearly value is considered valid if at least $2/3$ of valid monthly values are available in that year. IP average errors were computed considering all fifteen stations. Winter (DJF), Spring (MAM), Summer (JJA) and Autumn (SON) were defined according to standard procedures in meteorology.

3.2.3. Cloud Fraction estimation

Clouds have a strong impact in the Earth's radiation budget by modifying the shortwave (SW) and longwave (LW) radiative fluxes. From RCMs it is possible to obtain radiation fluxes considering the presence (all sky) or absence (clear sky) of clouds. In this work, clear sky and all-sky shortwave downward radiation are used in order to estimate the cloud fraction simulated by the WRF model. In this sense, a shortwave radiative cloud fraction ($SWRCLF$) was defined as the ratio of the global solar radiation downward to clear-sky radiation as suggested by Deardorf (1978), Crawford and Duchon (1999), Choi *et al*. (2008) and Gubler *et al*., (2012):

$$SWRCLF = 1 - \frac{SW_{all_{sky}}}{SW_{clear_{sky}}} \tag{3.1}$$

$SW_{all_{sky}}$ is the all-sky shortwave downward radiation at the surface, and $SW_{clear_{sky}}$ is the clear sky shortwave downward radiation that reaches the Earth's surface. The ratio $SW_{all_{sky}}/SW_{clear_{sky}}$ expresses the reduction of solar radiation mainly due to clouds, with values near one representing clear-sky conditions and near zero a total cloud cover. It should be noticed that the $SWRCLF$ is not exactly a cloud fraction, in particular it never attains the value 1. Despite being different from the cloud cover estimated by the meteorological observers, this definition linked to the light attenuation by clouds, may be used as a proxy to cloud fraction, with the advantage of that it is directly applicable in the field of solar energy, as it is an indicator of the cloud effect on its availability at the surface. In this work, the term *clear*

sky days means days without clouds or partially cloudy and refer to $SWRCLF$ values lower than or equal to 0.10 (less than 1 $okta \sim 0.13$).

3.2.4. Statistical error measures and methods

The results of global radiation for each station were compared with the ground-based measurements in order to assess the quality of the simulations. The mean bias ($BIAS$), mean absolute error (MAE), mean absolute percentage error ($MAPE$), root mean square error ($RMSE$) and correlation coefficient (r) were calculated and are defined as:

$$BIAS = \frac{1}{N}\sum_{i=1}^{N}(m_i - o_i) \tag{3.2}$$

$$MAE = \frac{1}{N}\sum_{i=1}^{N}|m_i - o_i| \tag{3.3}$$

$$MAPE = \frac{MAE}{\frac{1}{N}\sum_{i=1}^{N} o_i} \tag{3.4}$$

$$RMSE = \left[\frac{1}{N}\sum_{i=1}^{N}(m_i - o_i)^2\right]^{\frac{1}{2}} \tag{3.5}$$

$$r = \frac{\sum_{i=1}^{N}(o_i - \bar{o})(m_i - \bar{m})}{[\sum_{i=1}^{N}(o_i - \bar{o})^2 \sum_{i=1}^{N}(m_i - \bar{m})^2]^{\frac{1}{2}}} \tag{3.6}$$

where N is the number of data and m and o are respectively the model simulation and observed values. We defined normalized $BIAS$ ($NBIAS$), and normalized root mean square error ($NRMSE$) as respectively $BIAS$ and $RMSE$ divided by the $SW\downarrow$ mean.

3.2.5. Statistical bias correction methodology

In this study a bias correction was applied, based on the methodology proposed by Piani *et al*. (2010) where a detailed description may be found. The implementation described in Hagemann *et al*. (2011) was followed. The methodology is based on the adjustment of a transfer function that "transforms" the original simulated dataset in a corrected set with the same probability distribution function (PDF) as the observed set. In order to adjust the transfer function, the simulated and observed time series, of the same length and for the same period, are sorted in ascending order and plotted one versus another. The transfer function, with a few set of parameters is then the result of a fitting procedure. In general, different kinds of functions can be tested, but Hagemann *et al*. (2011) found that in the majority of the cases a two-parameter linear fit is sufficient.

In this study, data from the Clouds and the Earth's Radiant Energy System (CERES) were used as the observations, in order to correct the $WRF5$ model outputs. The CERES experiment is one of the scientific satellite instruments developed for NASA's Earth Observing System (EOS). The first CERES instrument was launched in December of 1997 aboard NASA's Tropical Rainfall Measurement Mission (TRMM) satellite. CERES instruments are now installed also on three separate satellite missions, including the EOS Terra and Aqua observatories more recently on the Suomi National Polar-orbiting Partnership (S–NPP) observatory. CERES is a set of three co-aligned broadband radiometer detectors whose spectral ranges are $8\ to\ 12\ \mu m$ for infrared, $0.3\ to\ 5\ \mu m$ for shortwave and $0.3\ to\ 100\ \mu m$ for global radiation. CERES products include both solar-reflected and Earth-emitted radiation from the top of the atmosphere to the Earth's surface. The Energy Balanced and Filled (EBAF) surface products (Kato *et al*., 2013) are used in this study corresponding to the Surface Downwelling Shortwave Radiation and Surface Downwelling Clear Sky Shortwave Radiation, for the period March 2000 until December 2009. CERES data were obtained from NASA website (ceres.larc.nasa.gov) and are available on a monthly basis with a $1° \times 1°$ horizontal resolution. Detailed information about CERES origins, instrument calibrations, source of errors among other technical features, can be found in Wielicki *et al*. (1996).

3.3. Regional Climate model simulations: Assessment and bias correction

3.3.1. Comparison of daily and seasonal simulated SW↓ against observations

Figure 3.3a shows the daily bias values of $SW\downarrow$ and it is found that for the majority of the stations the model overestimates the $SW\downarrow$ with values of approximately 30 Wm^{-2}. The highest bias values are mostly located in the north/northeastern part of IP (Asturias, Basque Country and Catalonia) with values between $30-50\,Wm^{-2}$. In the central part of IP, $WRF5$ overestimates the $SW\downarrow$ by $30\,Wm^{-2}$. At southwest and southeast, $WRF5$ tends to underestimate observations exhibiting values in the range of $-20\,Wm^{-2}$ to $0\,Wm^{-2}$.

The mean bias in $WRF5$ is consistent with the one obtained for Spain by Ruiz-Arias *et al.* (2016). These authors found a mean bias of approximately $29\,Wm^{-2}$ over the period 2003–2012, with highest values along the Cantabrian coast and mountains as in the case of present $WRF5$ analysis.

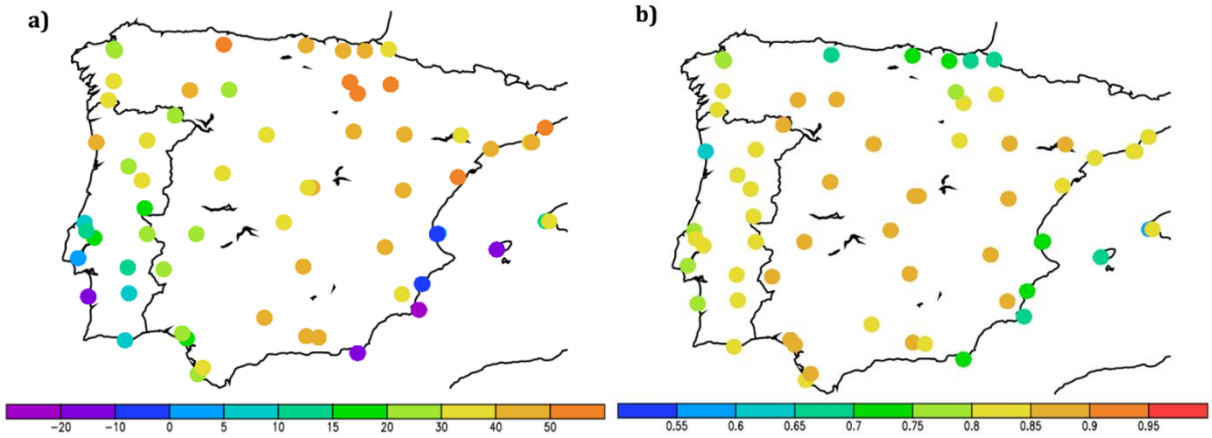

Figure 3.3. Daily *BIAS* (a) and correlation coefficient (b) for the $WRF5$.
BIAS in Wm^{-2}. (In the computation of the correlation, the annual cycle was not suppressed)

$WRF5$ daily simulation shows highest $RMSE$ at the northern regions of IP (not shown here), especially over the Basque country (above 80 Wm^{-2}) and smallest values in central and south regions over IP (65 Wm^{-2}).

Daily correlation coefficients between ground-based observations and $WRF5$ (Figure 3.3b) show that $WRF5$ performs better in the central part of IP, with high correlation coefficients, above 0.80. North/northwestern regions of IP present the smallest r values (above 0.6). It is important to notice that the correlation coefficient is insensitive to biases and thus it only explains the spatial similarities/differences between simulations and observations for the various stations over the figure. Table 3.2 summarizes the errors found for daily values.

Table 3.2. Performance of WRF model for both resolutions in a daily and seasonal basis (spatially averaged values over the IP).

	Resolution	DAILY	DJF	MAM	JJA	SON
$\boldsymbol{BIAS\ (Wm^{-2})}$	$WRF5$	29.9	25.1	43.6	37.1	22.1
	$WRF9$	31.8	17.1	47.6	45.4	21.1
$\boldsymbol{MAE\ (Wm^{-2})}$	$WRF5$	51.7	25.9	46.8	52.4	28.1
	$WRF9$	39.2	18.0	47.6	46.1	21.7
$\boldsymbol{RMSE\ (Wm^{-2})}$	$WRF5$	71.6	29.7	53.9	61.7	33.0
	$WRF9$	55.5	21.6	51.6	52.5	25.5
$\boldsymbol{r}$	$WRF5$	0.8	0.9	0.8	0.6	0.9
	$WRF9$	0.9	0.9	0.9	0.8	0.9

As detailed in section 3.2.2, the seasonal analysis was done considering only fifteen ground-stations. The seasonal bias shows similar spatial patterns to the results obtained for the daily bias analysis. $WRF5$ is able to simulate the seasonal evolution of $SW\downarrow$ (see Figure 3.4), although an overall overestimation can be seen in the majority of the ground-based stations for all seasons, with only two exceptions: Sines (south-west coast of Portugal) and Ibiza (Spanish Mediterranean island).

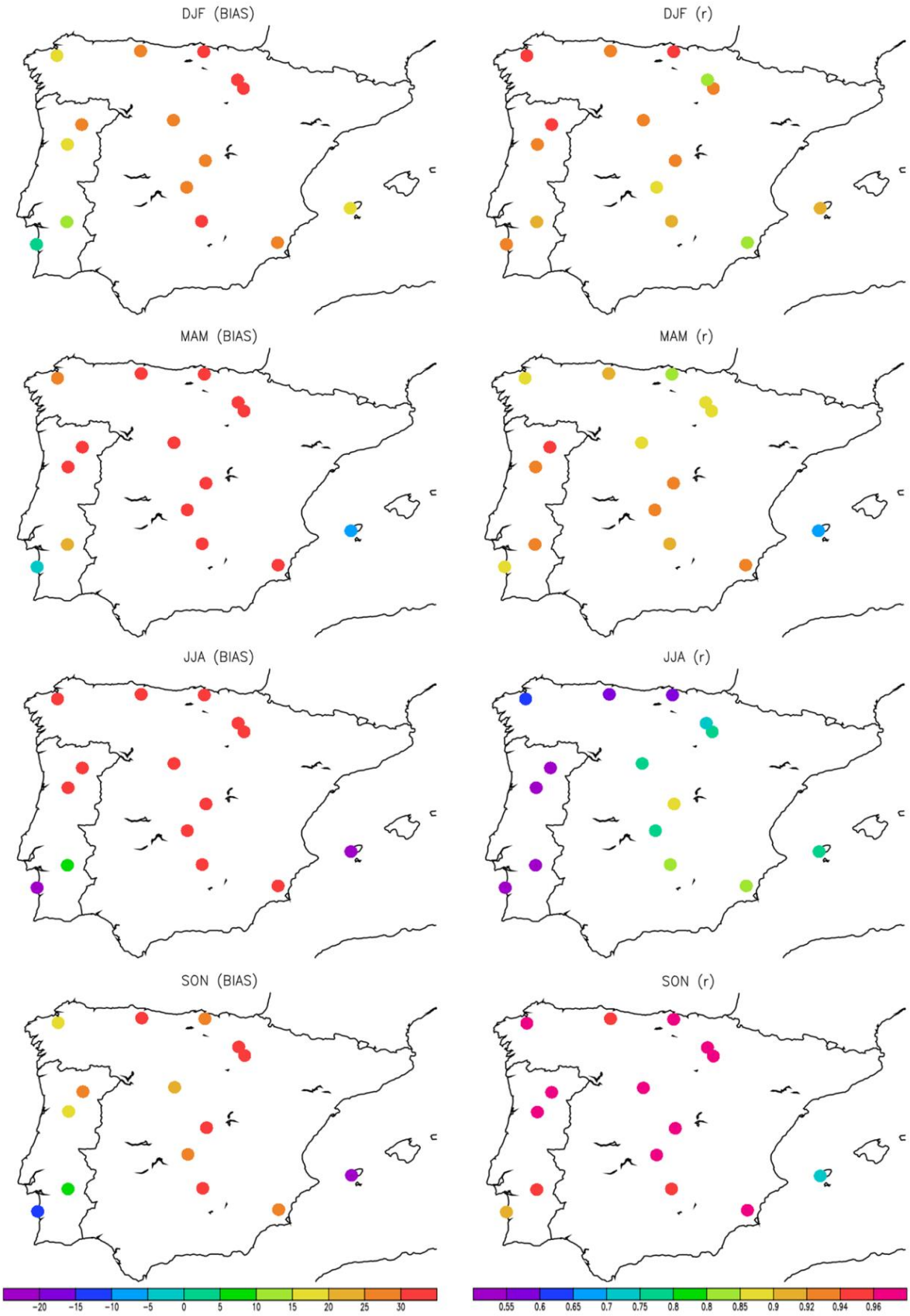

Figure 3.4. Seasonal *BIAS* and correlation coefficient for $SW\downarrow$ compared with ground-based observational data. *BIAS* in Wm^{-2}.

$WRF5$ performance is better in winter and autumn in comparison with spring and summer (see Table 3.2). The smallest mean bias error is found in autumn ($22\ Wm^{-2}$) and the highest value for spring ($44\ Wm^{-2}$), which may be related to the larger variability of cloud conditions over the area in springtime (Salgueiro *et al*., 2014). According to Ramos *et al*. (2014), the cyclonic weather type over IP has a maximum in spring, imposing a considerably large cloud radiative effect as documented in Salgueiro *et al*., 2016. $RMSE$ are relatively high in spring and summer, with values above $50\ Wm^{-2}$ (Table 3.2), and the smallest errors are found in the southwestern region and southeastern coast of Iberian Peninsula (not show here), in line with the spatial distribution obtained for bias analysis (Figure 3.3a).

$WRF5$ seasonal errors are also consistent with the monthly errors found by Ruiz-Arias *et al*. (2016). The worst statistical results obtained in the mountainous regions of Cantabria and the Pyrenees suggest that the model, at this resolution, has limited skill in representing orographic clouds. However, this topic needs further investigation. Ruiz-Arias *et al*. (2016), suggest that the bias found in WRF could be a result of an underestimation of the actual cloud amount, and possibly, a misrepresentation of the radiative impact of low cumulus clouds.

Seasonal correlation coefficient varies between 0.6 in summer and $\sim$0.9 in autumn, with large spatial dispersion in spring and especially in summer. The poor performance of the model in summer was also found by Dasari *et al*. (2014) for temperature, and it may be explained by an incorrect quantification of the aerosol effects, since the model uses a monthly mean distribution of aerosols (Collins *et al*., 2004) and not actual values. Cardoso *et al*. (2013) also found small correlation coefficients in summer precipitation as a result of a combination of strong surface heating, instability and the connected convection over some parts of IP. According to Alapaty *et al*. (2012), NWP models do not consider cumulus cloud feedbacks in radiation at a subgrid-scale, and these effects can cause a bias in shortwave and longwave radiation. This may also explain the relatively high $RMSE$ found in our analysis.

3.3.2. Comparison with other validated WRF simulation

The $WRF5$ performance is additionally investigated by comparison with results obtained from the previously validated $WRF9$ experiment, where continuous model integration was performed.

Table 3.2 and Figure 3.5 show the results of the comparison with the observation, for both models.

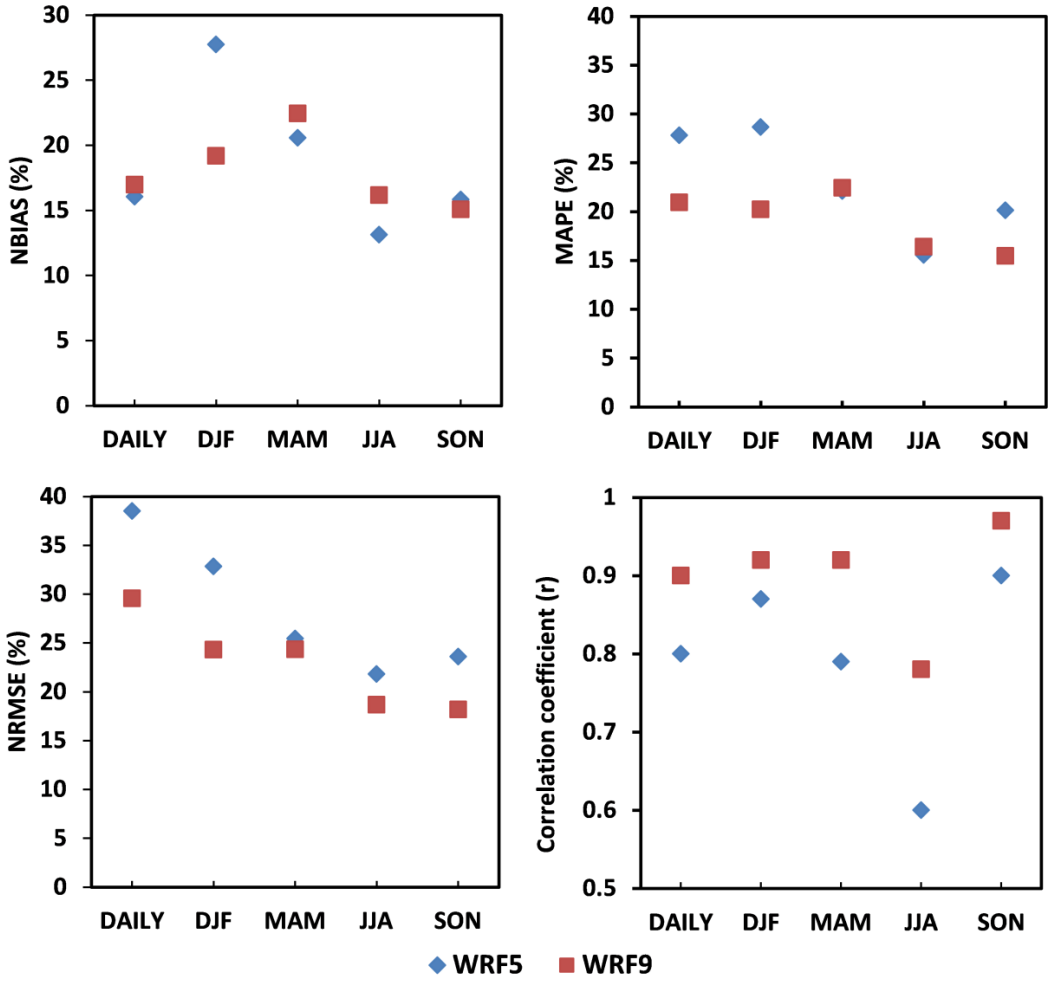

Figure 3.5. Correlation coefficients and statistical errors ($NBIAS$, $NMAE$ and $NRMSE$) over IP, in the 2000−2009 period for $WRF5$ and $WRF9$.

In general, $WRF5$ and $WRF9$ overestimate the observed $SW\downarrow$ either on a daily or on a seasonal basis. Daily $NBIAS$ of $SW\downarrow$ in $WRF5$ is slightly smaller than in $WRF9$, whereas with respect to the $MAPE$, $NRMSE$ and correlation coefficients, $WRF9$ shows a slightly better performance than $WRF5$. Daily $NBIAS$ values show, for both configurations, errors below 17%. $NRMSE$ for $WRF5$ are larger than for $WRF9$, with values of 40% and 30%, respectively. The correlation coefficients between daily simulated and observed $SW\downarrow$, for both experiences during the whole period compared (2000–09) are greater than 0.8, revealing a good model behaviour.

Seasonal $NBIAS$ of $SW\downarrow$ show that the $WRF5$ forecast has a slightly better performance than $WRF9$, with values varying between 13% and 28%. With respect to the $NRMSE$, $WRF5$ ($WRF9$) forecast shows values in the range of 22% (19%) in summer and ~33% (24%) in winter (see Figure 3.5). $MAPE$ shows that $WRF5$ slightly outperforms $WRF9$ in spring with an error of 22%, and in the summer season with an error of 16%. Seasonal correlation coefficients produce very similar results with high correlations, for both experiences, especially in autumn ($r \geq 0.9$). It can be observed in Figure 3.5, that for both experiences, the errors show a clear seasonal dependence.

Our errors present the same magnitude as those of other studies such as Lorenz *et al*. (2009) over the south of Spain, with $NRMSE$ between irradiance forecasts and observations in the range of 20% to 35%.

The use of different parameterizations in numerical models inevitably leads to different results (Cossu and Hocke, 2014; Mercader *et al*., 2010) but, according to this analysis, statistical errors obtained in $WRF5$ and $WRF9$ are in agreement for $SW\downarrow$ and presents comparable errors.

The comparisons of the simulations obtained in both experiments with the observations show that the quality of the prediction of solar radiation by the $WRF5$ simulation, which uses the less conventional technique of annual re-initializations, is not lower than the previously validated $WRF9$ simulation.

3.3.3. Statistical bias correction and comparison against observations

The bias between models and observations may be reduced by applying a bias correction. This methodology was applied to $SW\downarrow$ radiation by Ruiz-Arias *et al*. (2015).

Following the methodology described in Hagemann *et al*. (2011), summarized in section 3.2.5, the shortwave all sky and clear sky shortwave radiative fluxes at the surface were corrected using the CERES dataset. To obtain the transfer function, WRF and CERES data were spatially averaged over IP for the common period. The transfer function, shown in Figure 3.6, was obtained using monthly average values.

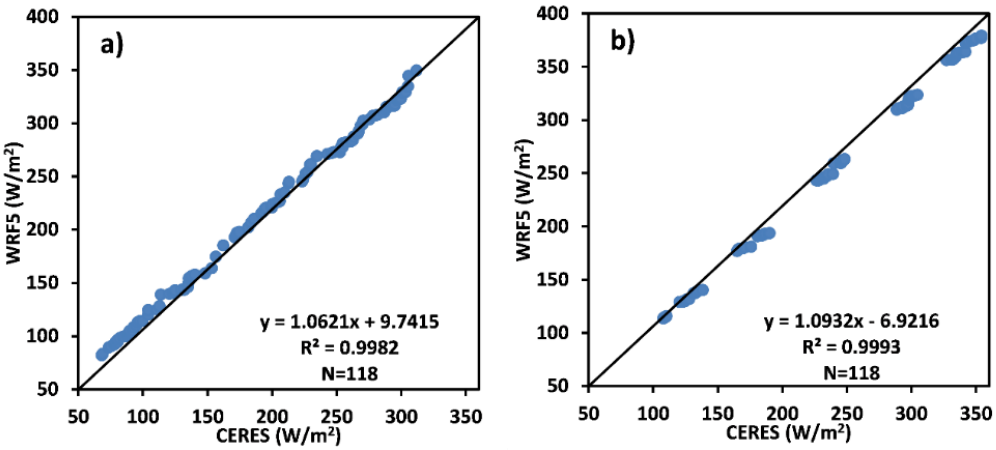

Figure 3.6. Transfer functions obtained from WRF data and CERES data on a monthly basis for $SW\downarrow$ (a) and clear Sky $SW\downarrow$ (b). The functions were obtained from monthly spatial mean values over IP for 2000−2009 period.

Figure 3.6b also reveals that the model produces higher clear sky shortwave radiation than estimated by CERES. The $SWRCLF$ was determined from the bias corrected $WRF5$ clear sky radiation parameter.

The transfer function obtained was applied to all modelled values, at all grid points and time steps. The corrected values were then compared with ground-based observations for the same period. Note that these time series are independent from the CERES data used to compute the transfer function. Figure 3.7 shows the correlation and the $NBIAS$ between $WRF5$ and ground-based observed $SW\downarrow$ fluxes, for the 2000–2009 period, after bias correction.

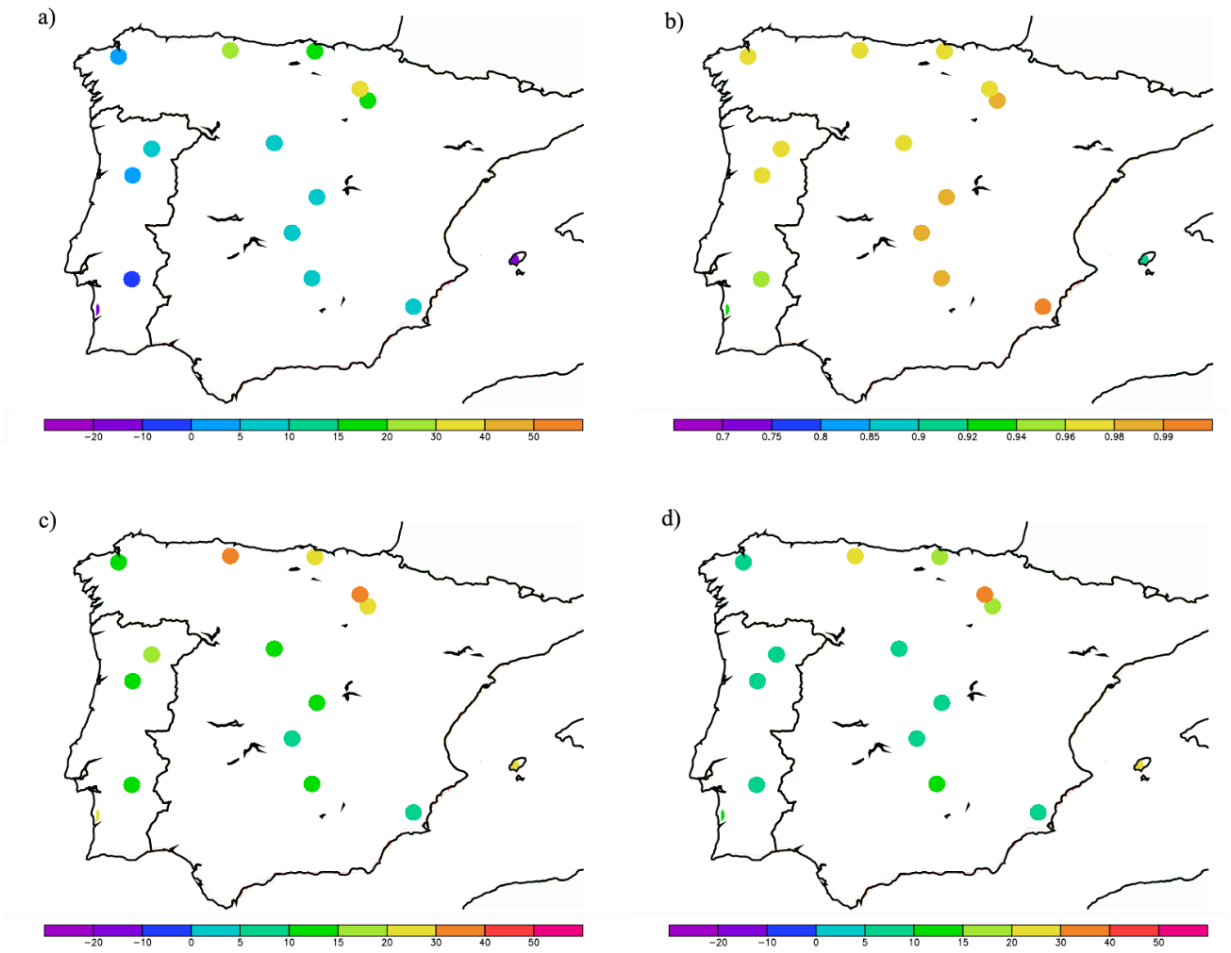

Figure 3.7. (a) $NBIAS$ (in percentage) and (b) correlation coefficient (c) $NRMSE$ and (d) $MAPE$ for $SW\downarrow$ over 2000−2009 period between model and observations for several Iberian ground-based stations.

The analysis of Figure 3.7 shows a strong correlation between $WRF5$ $SW\downarrow$ and observations, with a mean correlation of the order of ~0.97, improving the scores obtained before the bias correction (see section 3.1). The differences between model and observations were significantly reduced after the correction. The mean $NBIAS$ fell from 17% to 7% $(\sim 11\, Wm^{-2})$. The corrected $NBIAS$ are close to those shown in Ruiz-Arias *et al.* (2015). $NRMSE$ (Figure 3.7c) and $MAPE$ (Figure 3.7d) dropped respectively from 39% to 18% and from 28% to 14%.

In general, $WRF5$ simulations show a very similar performance when compared with observational ground-based data, $WRF9$ and CERES data, which increases the confidence in the climatology that will be addressed in the next section.

3.4. SW↓ climatology over the Iberian Peninsula for 1950–2010 period

Figure 3.8 illustrates the climatological 60 year mean $SW\downarrow$ over IP, at a 5 km horizontal resolution, obtained from the $WRF5$ simulations after applying the post-processing bias correction methodology.

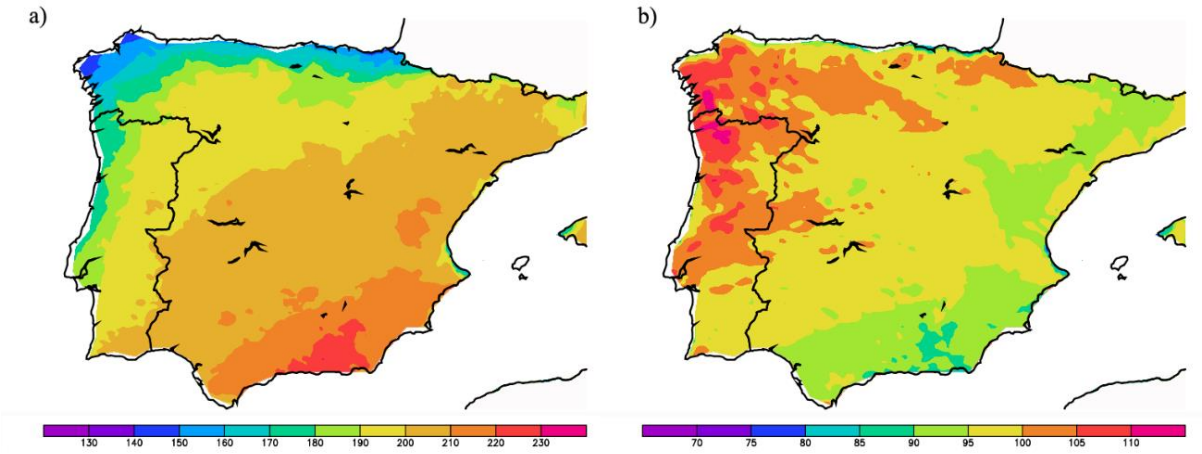

Figure 3.8. Sixty-year annual mean for the 1950−2010 period of, (a) $SW\downarrow$ and (b) standard deviation. Values are in Wm^{-2}.

During this period, the mean $SW\downarrow$ ranged from a minimum of 140 Wm^{-2} in the north of IP to a maximum value above 230 Wm^{-2} at the south corresponding to a spatial average value of 190 Wm^{-2}. The spatial distribution clearly shows a gradient increasing from north to south and from west to east modelled by the effects of the coast and topography. Ruiz-Arias *et al.* (2015) also found this gradient, with lower irradiation values northward.

In Spain, Andalusia and Murcia are the regions with the highest $SW\downarrow$. The greatest mean value of $SW\downarrow$ (230 Wm^{-2}) was found in Granada and Almeria. The lowest mean values are associated with the west and north Atlantic coastal zone and range between 140 Wm^{-2} and 180 Wm^{-2}. The smallest values are found in Coruna (Galicia – Spain). For Portugal, the central and southern parts (Alentejo and Algarve) are those with the highest mean $SW\downarrow$ values (above 200 Wm^{-2}). This pattern is, in general, consistent with the study conducted by Sanchez-

Lorenzo *et al*. (2009) for Spain, over the 1985–2010 period, which used observational sunshine duration data.

The SW variability (annual standard deviation) is relatively high in the northern part of IP, particularly in Galicia (Spain), with an average value of $105\ Wm^{-2}$. For Portugal, Minho and Douro Litoral (at north) are the regions where the $SW\downarrow$ variability is larger, with averages above $100\ Wm^{-2}$. The spatial distribution of $SW\downarrow$ during the four seasons is depicted in Figure 3.9 and reveals values that range from a minimum of $50\ Wm^{-2}$, in winter, to a maximum around $325\ Wm^{-2}$, in the summer season. Maximum $SW\downarrow$ values are found over the south of Portugal and Spain. The lowest $SW\downarrow$ values, independently of the season, are found over north/northeast regions of IP. High variability (standard deviation) is found in spring and summer seasons (Figure 3.9), especially along the Atlantic coastal regions, with values above $80\ Wm^{-2}$. This same high variability was found by Ruiz-Arias *et al*. (2015), with the Cantabrian coast presenting lower values of radiation in comparison with the rest of Spain.

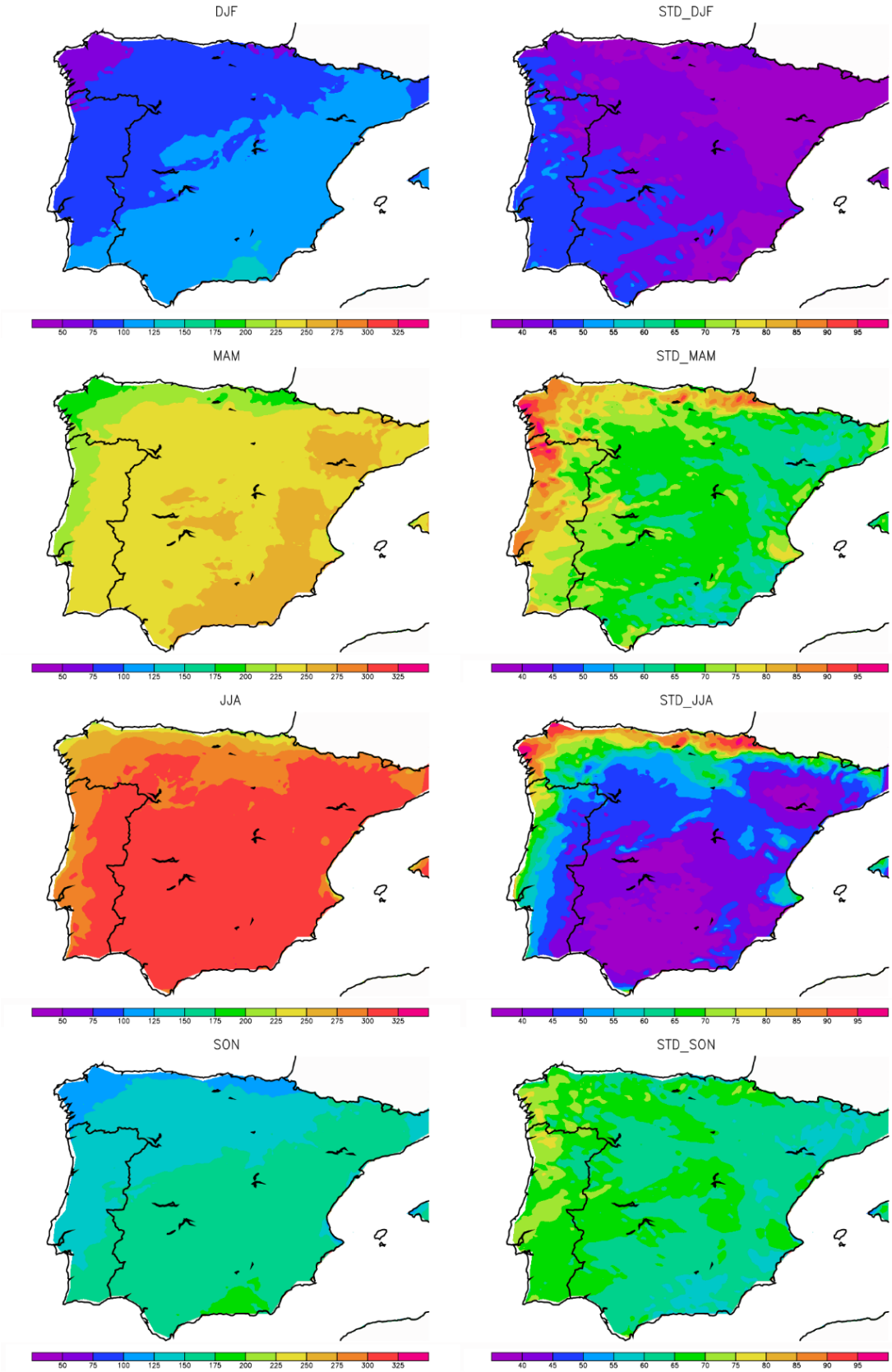

Figure 3.9. Spatial seasonal average in the period 1950-2010 for $SW\downarrow$, Winter (DJF), Spring (MAM), Summer (JJA), Autumn (SON), and standard deviation in Winter (STD_DJF), Spring (STD_MAM), Summer (STD_JJA) and Autumn (STD_SON).

Values are in Wm^{-2}.

Annual cycles of $SW\downarrow$ and $SWRCLF$, obtained from monthly means over land, are plotted in Figure 3.10. These plots show, as expected, an annual pattern for $SW\downarrow$ with maximum values in summer, presenting a peak of 340 Wm^{-2} (median value) in July and an inverse pattern for $SWRCLF$, with a minimum peak in June and July (0.04). It should be noted that $SWRCLF$ is computed using $SW\downarrow$, which reinforces their interdependence.

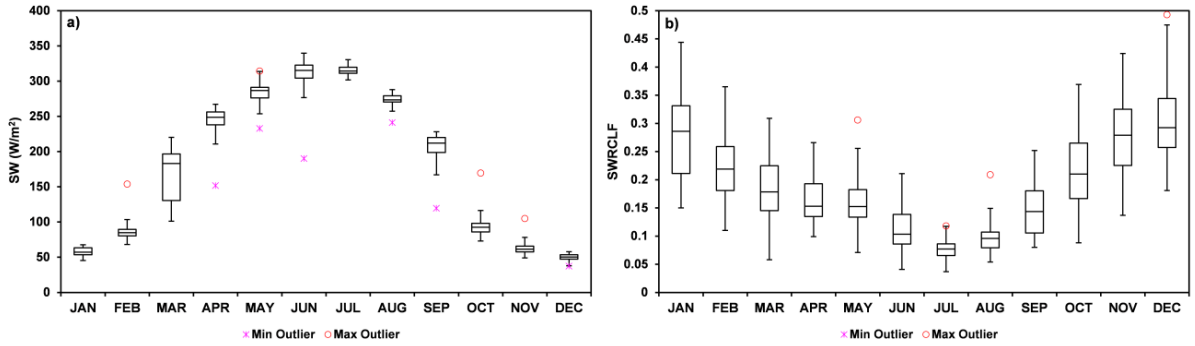

Figure 3.10. Annual cycle of monthly mean area averaged $SW\downarrow$ (a) and $SWRCLF$ (b) over IP for the 1950−2010 period.

The horizontal solid line within the box represents the median. The bottom and top of the boxes indicate the first and third quartiles, respectively. The circles and crosses represent outliers. The lower and upper ends of the whiskers are the minimum and maximum values of the datasets, respectively. $SWRCLF$ varies between 0 (without clouds) and 1 (overcast).

The shape of the boxplots show that the data distributions are generally symmetrical (see box and respective median). The interquartile ranges are relatively small in July and August for $SW\downarrow$ and $SWRCLF$, which suggest a low inter-annual variability (long periods with no clouds) during summer. $SW\downarrow$ variability is higher in March and September. For $SWRCLF$, larger spreads are obtained in the months of autumn and winter (Figure 3.10b). In those months, upper quartiles have values above 0.2 as expected and in accordance with the results obtained by Sanchez-Lorenzo (2009), for total cloud cover in Spain. The boxplots of Figure 3.10 allow for the identification of potential outliers. The existence of outliers may be partially explained by the interannual variability in the frontal system tracks affecting the region (Ramos *et al.*, 2014; Trigo *et al.*, 2002) and by the irregular occurrence of Saharan dust events (Obregón *et al.*, 2015; Wagner *et al.*, 2009; Alados-Arboledas *et al.*, 2003). These events are not taken into account by the numerical model since the concentration and properties of the aerosols are fixed in the WRF simulations (Collins *et al.*, 2004).

Figure 3.11 shows maps of the percentage of clear sky days for the whole period and over two selected months: August and December.

a)

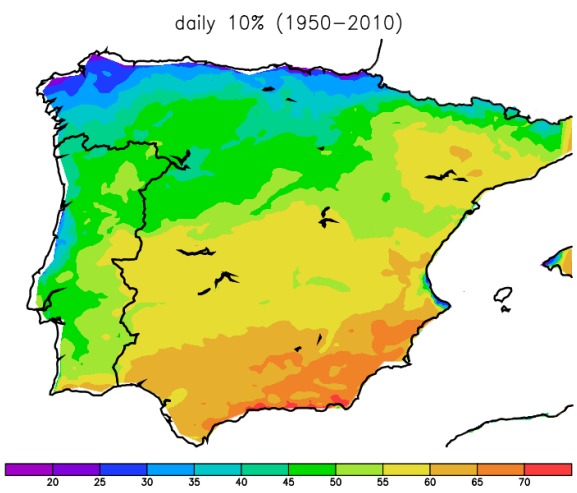

b)

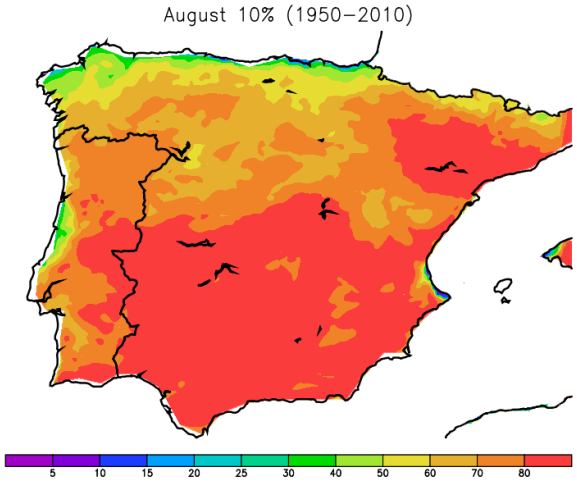

c)

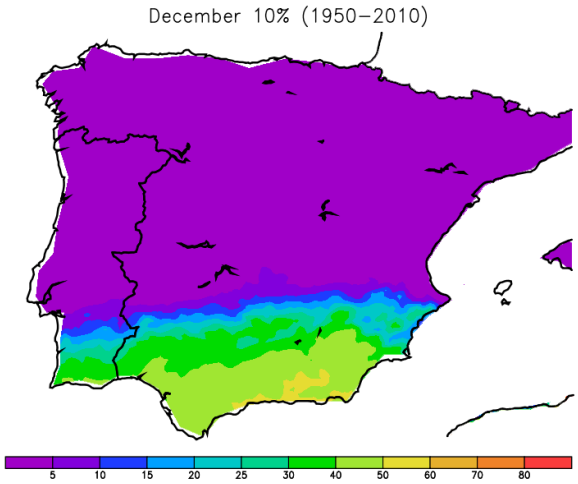

Figure 3.11. Percentage of clear sky days of (a): daily, (b) August and (c) December. Values are in percentage.

The maps show a high percentage of days without clouds, especially over central, south (Andalusia and Algarve) and northeast (Catalonia) parts of IP. Over these regions, more than 30% of the days may be considered as clear sky (less than 1 $okta - SWRCLF$ less or equal to 0.1 for a conservative perspective, since the synoptic scale of WMO considers clear sky days until 2 $oktas$ for the recording of the total cloud cover).

In December, for over $2/3$ of the Iberian Peninsula (north coastal regions of Portugal until Tagus River, Galicia and Basque Country), the percentage of clear sky days is less than 10% of the days in all period. However, areas along Spanish Mediterranean coast (Southeastern part of Andalusia, Murcia, Valencian community and Catalonia) present more than 30% of clear sky days, even in December. On the other hand, in August, the percentage of clear sky days is above 70% in more than half of the Iberian Peninsula (central and south). This result is consistent with Ridao *et al*. (2007), which found that Andalusia (south of Spain) is the region with the greatest potential of all European regions for the implementation of solar energy systems.

3.5. Conclusions

A high resolution climatology of $SW\downarrow$ solar radiation over IP, obtained from simulations performed using the WRF model at 5 km resolution ($WRF5$) is presented in this work. The comparison between $WRF5$ and observations for the downward shortwave radiation at the surface shows a good performance, although with a slight overestimation of radiation. The results indicate that the model simulations were significantly improved after applying a bias correction using CERES data. The daily bias over central IP was approximately 28 Wm^{-2} ($\sim$17%) before bias correction and 7% after. In the northern coastal regions, namely in Galicia, Asturias, Cantabria and Basque Country, daily bias are above 40 Wm^{-2} (before bias correction). Similar results were obtained for the seasonal analysis. Correlation coefficients obtained from the comparisons between the observations and the model results are high, above 0.8 for 70% of the ground-based stations. Seasonal correlation coefficients show a lower correlation in summer and higher values in autumn with values between 0.4 (summer) and 0.9 (autumn).

The $WRF5$ strategy, based on multiple one year time-slices, was found to be a valid alternative to the more computationally time demanding strategy based on continuous model integration, as its results exhibit a similar behaviour and comparable errors to those obtained in a previously validated WRF run simulation at 9 km ($WRF9$). $NRMSE$ for $SW\downarrow$ ranges from 22 Wm^{-2} to 39 Wm^{-2}, for $WRF5$ and 18 Wm^{-2} to 30 Wm^{-2}, for $WRF9$ configuration. Regardless of the season, $WRF9$ always presents smaller $NRMSE$ than $WRF5$.

The errors found in the present work, although mitigated by the application of a bias correction, may be related with a misrepresentation of clouds at higher spatial resolution (see Lara-Fanego *et al.*, 2012b), and first of all, by an incorrect quantification of the aerosol effects, since the run uses a monthly mean distribution of aerosols (Collins *et al.*, 2004) and not actual values. In fact, the main limitation of this work is the failure to take into account the evolution of aerosol distribution over the Iberian Peninsula, which is known to have been very important during the last century (see for example Mateos *et al.*, 2014b; Antón *et al.*, 2017). This misrepresentation of the aerosols may introduce large temporal and spatial deviations and prevents the utilization of the simulated series for trend analysis, as the uncertainties related to the non aerosol inclusion are larger than those resulting from solar radiation changes. Future works should take into account the spatial and temporal evolution of aerosol loads.

The IP climatology of $SW\downarrow$ produced for the 1950–2010 period confirms the existence of two gradients (latitudinal and longitudinal). Regions with higher $SW\downarrow$ values are situated in the southeastern regions of IP (Andalusia and Murcia). The lowest values of mean $SW\downarrow$ were found in the northwestern region of Galicia. The variability of $SW\downarrow$ also increases from south to north and from east to west directions with higher values over Galicia.

The cloud cover was also evaluated following the definition proposed by Crawford and Duchon (1999) namely the shortwave radiative cloud fraction ($SWRCLF$). Results show that the southern half of the Iberian Peninsula has a larger part of its territory with more than 30% of clear sky days during the period under study, and these values are substantially higher in summer months (above 80% for almost all territory).

The $SW\downarrow$ radiation climatology obtained from the WRF 5 km simulations is a solid base in the planning of renewable power plants on solar resources, providing estimates in areas where there are no measurements. It should however be taken into account that aerosols can attenuate on average 10 to 20% of the horizontal irradiance and even more when desert dust aerosols are present. Thus the simulation results presented should be used with some caution since a monthly mean distribution of aerosols was considered.

The presented climatology points out Andalusia (Spain), Murcia (Spain), Alentejo (Portugal) and Algarve (Portugal) as the regions with the greatest $SW\downarrow$ potential to implement solar energy systems, allowing to identify, at a fine scale, the areas that have higher solar potential.

Based on these results, it can be stated that WRF simulations over Iberian Peninsula represent relatively well the downward solar radiation at the surface after a simple bias correction and can be used to study the future distribution of solar radiation over the region, according to different climate change scenarios.

Conflict of Interests

The authors declare there is no conflict of interests with regard to this manuscript.

Acknowledgements

The work is co-funded by the European Union through the European Regional Development Fund, included in the COMPETE 2020 (Operational Program Competitiveness and Internationalization) through the ICT project (UID/GEO/04683/2013) with the reference POCI-01-0145-FEDER-007690 and also through the ALOP project (ALT20-03-0145-FEDER-000004).

Clarisse Magarreiro wishes to acknowledge the Portuguese Science Foundation (FCT) grant SFRH/BD/79544/2011.

Pedro M.M. Soares thanks the Portuguese Science Foundation (FCT) for funding under Project SOLAR - PTDC/GEOMET/7078/2014

The authors are grateful to AEMET (Spanish Weather service) and IPMA (Portuguese Weather service) for providing surface data used in this work and NASA for providing CERES data.

4.

Assessment of Direct Normal Irradiance Forecasts based on IFS/ECMWF data and observations in the south of Portugal

This chapter is a transcription of the paper published with the following reference:

Perdigão, J.; Canhoto, P.; Salgado, R.; Costa, M.J. Assessment of Direct Normal Irradiance Forecasts Based on IFS/ECMWF Data and Observations in the South of Portugal. 2020. Forecasting, 2, 130-150. https://doi.org/10.3390/forecast2020007

Abstract

Direct Normal Irradiance (DNI) predictions obtained from the Integrated Forecasting System of the European Centre for Medium-Range Weather Forecast (IFS/ECMWF) are compared against ground-based observational data for one location at the south of Portugal (Évora). Hourly and daily DNI values are analysed for different temporal forecast horizons (1 to 3 days ahead) and results show that the IFS/ECMWF slightly overestimates DNI for the period of analysis (1 August 2018 until 31 July 2019) with a fairly good agreement between model and observations. Hourly basis evaluation shows a relatively high errors, independently of the forecast day. Root mean square error increases as the forecast time increases with a relative

error of ~45% between the first and the last forecast. Similar patterns are observed in the daily analysis with comparable magnitude errors. The correlation coefficients between forecast and observed data are above 0.7 for both hourly and daily data. A methodology based on a new DNI attenuation Index (DAI) is developed here to estimate cloud fraction from hourly values integrated over a day and, with that, to correlate the forecasts accuracy with sky conditions. This correlation with DAI reveals that in IFS/ECMWF model, the atmosphere as being more transparent than reality since cloud cover is underestimated in the majority of the months of the year, taking the ground-based measurements as reference. The use of DAI estimator confirms that the errors in IFS/ECMWF are larger under cloudy skies than under clear sky. The development and application of a post-processing methodology improves the DNI predictions from the IFS/ECMWF outputs, with a decrease of error of the order of ~ 30%, when compared with raw data.

Keywords: Direct Normal Irradiance (DNI); IFS/ECMWF; Forecast; Evaluation; DNI Attenuation Index (DAI); Bias correction

4.1. Introduction

Solar energy is becoming a crucial renewable resource in modern societies, contributing to the sustainability of the planet with the mitigation of greenhouse gases emissions by reducing the consumption of coal or fuel oil for electricity production. However, the availability of solar resource over time at a given region of interest determines the cost/benefit of solar power plants implementation. Since the temporal series of solar radiation measurements are spatially limited, and thus scarce and sometimes inexistent, the prediction and validation of solar resource is a key factor for such enterprises.

Several researchers have estimated the potential of renewable energies like wind or solar radiation for electricity or thermal energy production around the world; for example, in Europe and Africa (Gaetani el al., 2014), in Chile (Escobar *et al*., 2015), in Iberian Peninsula (Santos *et al*., 2015), in United Kingdom (Du *et al*., 2016), and in Spain (Ruiz-Arias *et al*., 2012). Solar power is a very promising energy source in Iberian Peninsula (IP) and a strong growth is expected in this area. In the IP there are multiple options for using renewable energy (solar, wind, hydro) to generate electricity, however the solar resource is high throughout the year (Perdigão *et al*., 2017; Ruiz-Arias *et al*., 2015; Šúri *et al*., 2007).

Concerning solar energy, there are two main ways of converting solar energy into electricity: photovoltaic (PV) and concentrating solar power (CSP). The PV panels convert either direct and diffuse solar irradiance, while the CSP technology only concentrate the Direct Normal Irradiance (DNI). The focus of this work is on the prediction of DNI, in view of its use in CSP plant management. The forecast of global solar radiation (direct + diffuse) for the same region was addressed, for example, in Perdigão *et al*. (2017) and Pereira *et al*. (2019).

There are several approaches to predict solar irradiance such as Numerical Weather Prediction (NWP), Cloud Motion Vector (CMV), statistical time series analysis and other methods (Ruiz-arias *et al*., 2016; Martín *et al*., 2010; Alsamamra *et al*.,2009). In the last years, one of the major research challenges for the use of NWP in solar energy applications is the DNI forecast, aiming at the development and increase of CSP installed capacity and operation management. These CSP needs the knowledge of DNI for specific sites (Kraas *et al*., 2013; Law *et al*., 2014), and one of the difficulties is the need to forecast the DNI with several days ahead to increase efficiency and minimize the operational costs of the power plants (Nonnenmacher *et al*., 2016; Gomez-Gil *et al*., 2012). For instance, Casado-Rubio *et al*. (2017) proposed a simple

methodology to obtained DNI forecast, based on Weather Research and Forecasting model (WRF model) and a radiative transfer simulation (for 1-day forecast) and found that this procedure can be used as diagnostic tool for operational power plants.

Until the most recent years, DNI measurements are not available in many places or with long series, and this variable was not a direct output of NWP models. Currently, the Integrated Forecast System of the European Centre for Medium-Range Weather Forecasts (IFS/ECMWF) provides the direct normal irradiance as an output. However, the use of NWP models in DNI forecast is still not perfect and requires Multiple Output Statistic (MOS) methodologies (Law *et al.*, 2014). Lopes *et al*. (2018) used the IFS global model of ECMWF to assess DNI for short-term (24 hours) in south of Portugal and (2018) found relative differences in the range ~7% to ~12% on an annual basis between predictions and observations at ground-based stations. Lara-Fanego *et al*. (2012a) found a relative root mean square error of 60% for hourly DNI forecasts in Spain for all sky conditions, using the Advanced Research Weather Research and Forecasting model (WRF). Troccoli and Morcrette (2014) analysed the direct solar radiation data using two different radiation schemes of the IFS/ECMWF for four ground-based measuring stations in Australia and found mean absolute errors between 18% and 45% and correlation coefficients between 0.25 and 0.85. In that work, the usage of a post-processing bias correction improved results, resulting in mean absolute errors between 10% and 15% and correlation coefficients of about 0.9. Ruiz-Arias *et al*. (2015) also found better results for DNI forecasts from WRF model by using a post-processing algorithm. Law *et al*. (2014) presents a comprehensive review on DNI forecast obtained from several methods and some examples of DNI forecast accuracies are presented. According to Vick *et al*. (2012), most studies on DNI models have assessed the annual and hourly mean bias and root mean square errors between measured and DNI models. However, according to the same authors, the accuracy of monthly and daily direct normal irradiation forecasts should also be assessed to detect gaps in DNI modelling that may be improved and correlated with sky conditions, time of the year or location.

Since there are a number of on-going projects in Portugal to explore the solar resource, it is imperative to carry out studies that help understand the errors associated with direct normal irradiance predictions over several days ahead.

The Portuguese Institute for Sea and Atmosphere (IPMA), the meteorological Portuguese authority, uses the ECMWF global model predictions as a main forecast tool. Comparisons between operational global NWP models show that the ECMWF skills over Europe are the best (Haiden *et al.*, 2012). Good numerical predictions of the near surface weather conditions

presuppose a good representation of the surface radiative balance. However, a correct forecast of the global irradiance does not necessarily mean an accurate partition between direct and diffuse components, as this partition is not essential in order to solve the surface balance. In response to a growing demand from the solar energy market, the ECMWF has recently (2015) started to include DNI among the available predicted variables. These forecasts are likely to be used by solar plants in southern Portugal.

Therefore, the main objective of this study is to assess the performance of the IFS/ECMWF global model (CY45R1 cycle – released at 5 June /2018) to predict DNI in south of Portugal, by comparing its results with observational data of Évora station, on an hourly and daily basis and for various forecasting horizons (up to four days ahead). This publication also presents a method to predict sky conditions based on observational DNI data. A post-processing methodology is also tested in order to minimize the bias in the IFS/ECMWF model.

4.2. Datasets and Methods

4.2.1. DNI observational data

The measurements used in this study are obtained from the observatory of Atmospheric Sciences located at the University of Évora ($38.57° N$, $7.9° W$, 293 m a.m.s.l.). DNI was measured using a first-class pyrheliometer (Kipp & Zonen, model CHP01), following the World Meteorological Organization (WMO) and the International Standard ISO 9060:1990. This model of pyrheliometer was designed to measure the solar irradiance with an opening half-angle of 2.5°.

A period of one year of DNI measurements is used in this study, from 1 August 2018 until 31 July 2019. The sensor output is sampled every 5 seconds and one-minute mean, minimum, maximum and standard deviation values are recorded. Hourly values are then computed by averaging one-minute values when the number of records for that hour corresponds to at least fifty minutes. The data for solar zenith angles above 89° (twilight and nighttime) were not considered and thus removed from the analysis. The daily mean was computed using a similar methodology of that used by Troccoli and Morcrette (2014), i.e. if one or more hourly values are not present on a given day, then that day is not used in the analysis.

All instruments of this measuring station are subject to maintenance and cleaning procedures following the recommendations of the World Meteorological Organization and data was subject to BSRN (Baseline Surface Radiation Network) quality filters (Long *et al*., 2010) based on physically possible and extremely rare values.

In this chapter, the seasons are defined according to the WMO nomenclature i.e., winter (December–January–February: DJF), spring (March–April–May: MAM), summer (June–July–August: JJA) and autumn (September–October–November: SON).

4.2.2. DNI forecast data

Predicted DNI from IFS/ECMWF, from 1 August 2018 until 31 July 2019, was obtained with a resolution of $0.125^{\circ} \times 0.125^{\circ}$ (lat×lon grid). The forecast data are provided with an hourly

time step for the first three days and with a three-hour time step for the 4th day. In this work, forecasts were separated into four intervals: day_0 (1st day); day_1 (2nd day); day_2 (3rd day); and day_3 (4th day). The predicted accumulated solar irradiation in hour time steps for the entire forecast horizon is converted into hourly mean irradiance values of DNI.

The shortwave radiation scheme of the IFS/ECMWF used in this study is the new radiation scheme implemented at 11 July/2017, called ecRad (Hogan and Bozzo, 2016). This scheme is faster than the previously McRad scheme (Morcrette *et al*., 2008) and, can be executed more times during the forecast. This scheme computes the profiles of shortwave and longwave irradiances at half levels, and these are interpolated horizontally back onto the model grid using cubic interpolation (Hogan and Bozzo, 2016). The aerosol distribution was adapted from Tegen *et al*. (1997), using a climatology of six hydrophobic aerosol species as well as the newer climatology obtained from a reanalysis of atmospheric composition produced by the Copernicus Atmosphere Monitoring Services (CAMS), with 11 hydrophilic and hydrophobic species (Flemming *et al*., 2017).

According with Hogan and Bozzo (2016), ecRad incorporates a method to represent longwave scattering of clouds which leads to an improvement in forecast skills. The default ice optical properties are computed using the Fu scheme (Fu, 1996), but two additional schemes are available.

In the work by Hogan and Bozzo (2016), it is possible to find the evolution of the ECMWF Radiation Scheme after 2000 and the options available. More details on the physical processes (and the options available) are reported in the IFS documentation in the ECMWF web page (www.ecmwf.int).

The nearest neighbour technique was used to select the forecast data for comparison with measurements. To assess forecasting accuracy, the observational data was compared with the forecasts for the nearest model grid point. Wild and Schmucki (2011), made several statistical tests surrounding a grid point to analyse trends and the results showed that different grid points surrounding a given grid point (selected by a Lat/Lon value) do not differ significantly from each other in the majority of the cases.

4.2.3. Statistical indicators for model assessment

The quality of the DNI forecasts is evaluated against observational data using common statistical parameters as the mean bias error (MBE), mean absolute error (MAE), root mean square error ($RMSE$) and correlation coefficient (r). In this work, errors are calculated based on hourly, daily and monthly mean values. Similar to the analysis presented by Nonnenmacher *et al*. (2016) and Perez *et al*. (2013), night-time values (zero solar irradiance) are excluded from the model assessment. The ratio (RSR) between the root mean square error and the observations standard deviation (σ_{obs}) is also determined.

These statistical parameters are defined as follows:

$$MBE = \frac{1}{n}\sum_{i=1}^{N}(m_i - o_i) \tag{4.1}$$

$$MAE = \frac{1}{N}\sum_{i=1}^{N}|m_i - o_i| \tag{4.2}$$

$$RMSE = \left[\frac{1}{N}\sum_{i=1}^{N}(m_i - o_i)^2\right]^{\frac{1}{2}} \tag{4.3}$$

$$r = \frac{\sum_{i=1}^{N}(o_i - \bar{o})(m_i - \bar{m})}{[\sum_{i=1}^{N}(o_i - \bar{o})^2 \sum_{i=1}^{N}(m_i - \bar{m})^2]^{\frac{1}{2}}} \tag{4.4}$$

$$RSR = \frac{RMSE}{\sigma_{obs}} = \frac{\left[\frac{1}{N}\sum_{i=1}^{N}(m_i - o_i)^2\right]^{\frac{1}{2}}}{[\sum_{i=1}^{n}(o_i - \bar{o})^2]^{\frac{1}{2}}} \tag{4.5}$$

where N is the number of data points and m and o are the forecast and observed values, respectively. The MBE represents a systematic error between predicted and observational

values, while the $RMSE$ quantifies the spread in the distribution of errors. The MBE provides information on the underestimation (negative values) or overestimation (positive values) of forecasts using the measured values as reference. On the other hand, the $RMSE$ is very sensitive to high magnitudes errors due to the higher statistical weight of large errors. The MAE represents the average magnitude of errors in a set of forecasts without considering their direction (bias) and gives the same weight to all errors (see as an example, Chai and Draxler, 2014), i.e., it is less sensitive to large deviations. $RMSE$ is one of the most relevant statistical parameters for solar power plants analysis (e.g. Landelius *et al*., 2018). For all statistical parameters, the best results are obtained when values are equal or near zero, except for the correlation coefficient when values closer to one correspond to better performances. According with Moriasi *et al*. (2007), RSR incorporates the benefits of error index statistics and includes a scaling/normalization factor, so that the resulting statistic and reported values can apply to various constituents. The RSR parameter varies between zero and a positive value with the values close to zero representing a better forecast simulation Moriasi *et al*. (2007). The same thresholds performance ratings as shown in Table 4 of Moriasi *et al*. (2007) are used here, i.e., values of $RSR < 0.5$ indicate the optimal performance rating while $RSR > 0.7$ represent unsatisfactory model performance rating.

4.2.4. Cloud Area Fraction and DNI Attenuation Index (DAI)

In most of solar radiation studies, an index known as clearness index is used to quantify the bulk atmosphere transmittance (see Iqbal, 1975; Lopes *et al.*, 2018, among others). This clearness index is defined as the ratio of global horizontal irradiance to extraterrestrial horizontal irradiance.

In this section, a new methodology is proposed to estimate the clearness of the atmosphere (termed DNI attenuation index– DAI) based exclusively on the observed direct normal irradiance. DNI varies during the day due to Sun-Earth geometry and atmospheric constituents, though the main factor of DNI variation is the cloud coverage, which can drastically reduce this component of solar radiation when the direct beam from the sun is intercepted, sometimes reaching a value of zero depending on the type of clouds. The DAI is therefore an indicator of the cloud attenuation of DNI.

This method is based on the integration of the measured hourly mean values of DNI (see Figure 4.1a) obtained every day, for a given month, and it constitutes a measure of sky conditions for a particular month. This has the advantage of not relying on reanalyses, satellite data or other products that could also be a source of bias.

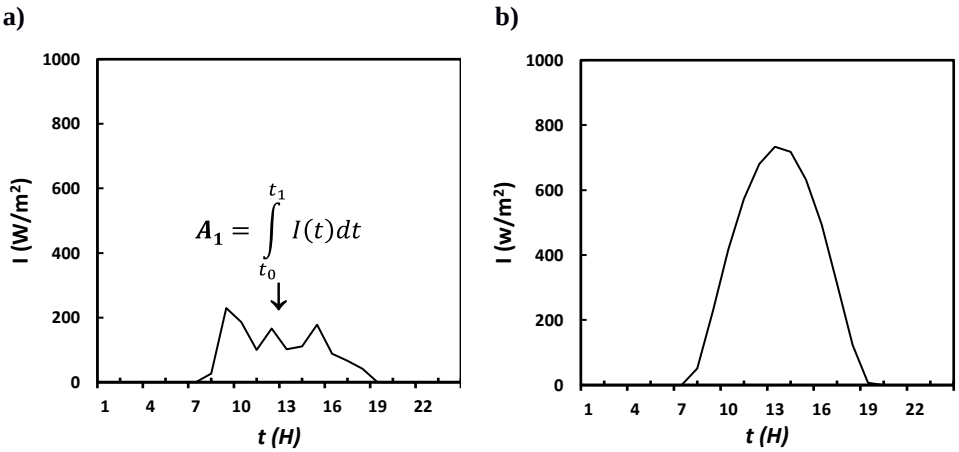

Figure 4.1. Curves of hourly mean DNI projected on the horizontal plane for two different days: (a) partially cloudy sky and (b) clear sky day.

A is the area under the curve corresponding to the measured DNI (energy per unit area) and is obtained by numerical integration using the trapezoid rule.

In this way, a dimensionless quantity (in percentage) called DNI attenuation index (DAI) is defined as

$$DAI_i = \left(1 - \frac{A_i}{NF}\right) \times 100\% \tag{4.6}$$

where

$$A_i = \int_{t0}^{t1} I(t)dt \sim \frac{\Delta t}{2} \sum_{k=1}^{24} (I_{k-1} + I_k) \tag{4.7}$$

with $\Delta t = 3600\ s$ because a time step of one hour is used and NF is the normalization factor calculated as

$$NF = \max_{1 \le i \le n}(A_i) \tag{4.8}$$

in which i is the number of day of the month.

To obtain the DAI it is assumed that the maximum value of daily energy per unit area (integral) in a given month is interpreted as a clear sky day in that month and the DAI will take the value of zero for that particular day. Different normalization factors will be expected for different months, with higher values during the summer. Although DAI does not allow to effectively distinguish the contribution of aerosols or cloud cover to DNI variations, it provides a clear idea of the transparence of the atmosphere for a specific day and it hints at the identification of a clear day (or clearness of atmosphere) from an overcast day or extreme aerosol event. The DAI varies between zero (clear sky day) and one (overcast sky).

The relation between DAI and oktas was established through three classes of days (WMO, 2008): class I – clear sky day ($0-2\ oktas$; $DAI < 31.25\%$); class II – partially cloudy skies ($3-5\ oktas$; $31.25 \leq DAI \leq 68.75\%$) and class III as cloudy skies ($6-8\ oktas$; $68.75\% \leq DAI \leq 100\%$), in the same way as presented in Table 1 of the article of Jafariserajehlou *et al*. (2019).

The total cloud area fraction obtained from the Clouds and the Earth's Radiant Energy System (CERES) radiometer combined with the Moderate Resolution Imaging Spectroradiometer (MODIS), both on board the Terra and Aqua satellites, is also considered in this work for assessment of DAI estimates. The CERES-MODIS cloud mask data were obtained on a monthly basis (CERES_SYN1deg_Ed4.1) for the period available for this study (08/2017 until 05/2019) and from CERES portal (see ceres.larc.nasa.gov). The cloud area fraction consists of the percentage of cloudy pixels identified in areas of 1°×1° (Wielicki *et al*., 1996).

4.2.5. Post-processing correction

A linear least square statistical method for bias correction in order to correct daily direct solar radiation values obtained from IFS/ECMWF was tested. This method is the simplest post-processing technique and has been applied in several studies over the past years (see for example Polo *et al*., 2015). Mejia *et al*. (2018) found that MOS linear fit procedure outperformed the quantile-quantile mapping (Q-Q).

The linear regression parameters were computed for each month using forecast and observed daily values for the period of $01/08/2017$ until $31/07/2018$.

The correction parameters are obtained, for each month, using the linear equation

$$y^{i}_{model,j} = m_j \times x^{i}_{obs,j} \quad + b_j \tag{4.9}$$

$$i = 1, \dots 28/30/31\,;\; j = 1, \dots 12$$

where x_{obs}, m_j and b_j are, respectively, the observed DNI values, the slope of the fitted line and the intercept.

The regression parameters were used to correct the IFS/ECMWF forecasts for the following year – the period of analysis (01/08/2018 until 31/07/2019) – using the following equation (Polo *et al*., 2016)

$$y^{i}{}_{BC_{model,j}} = y^{i}{}_{model,j} - \left[\left(m_j - 1\right)x^{i}{}_{obs,j} + b_j\right] \tag{4.10}$$

$$i = 1, \dots 28/30/31\,;\; j = 1, \dots 12$$

4.3. Results and discussion

4.3.1. Assessment of hourly and daily DNI forecasts

As an example, Figure 4.2 shows the time series of predicted hourly mean DNI during four consecutive days and the corresponding observed values for two selected cases, one in JJA, other in SON: forecasts issued on 1st August 2017 00:00 and on 27th November 2017 00:00.

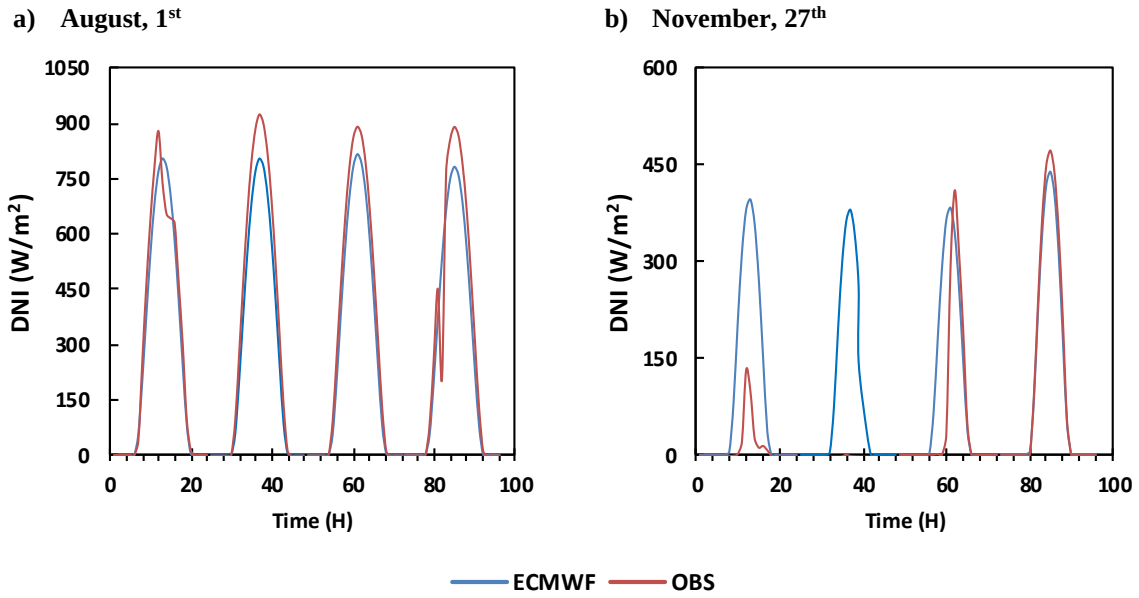

Figure 4.2. Example of four consecutive days of observed (red line) and simulated (blue line) hourly mean DNI in Évora starting at (a) 1st August 2017 00:00 and (b) 27th November 2017 00:00.

The IFS/ECMWF forecasts have a similar behavior to that of observational DNI for the two selected cases, with a fairly good agreement, especially in the case of August (Figure 4.2a). Figure 4.2b show a partially cloudy day (day_0) and a cloudy day (day_1), making evident that the model did not predict clouds correctly on November 28 since observational data clearly shows an overcast day. Another interesting feature in Figure 4.2 is that the IFS/ECMWF scheme slightly underestimated the DNI in the Summer case (Figure 4.2a) and overestimated it in the Autumn case (Figure 4.2b) in the case of partly cloudy day. It is important to note that the example presented in Figure 4.2 is simply a selected example.

Figure 4.3 shows the comparison between ground-based measurements of hourly mean DNI and forecast data obtained from IFS/ECMWF for the entire period of study and for the four forecasted days.

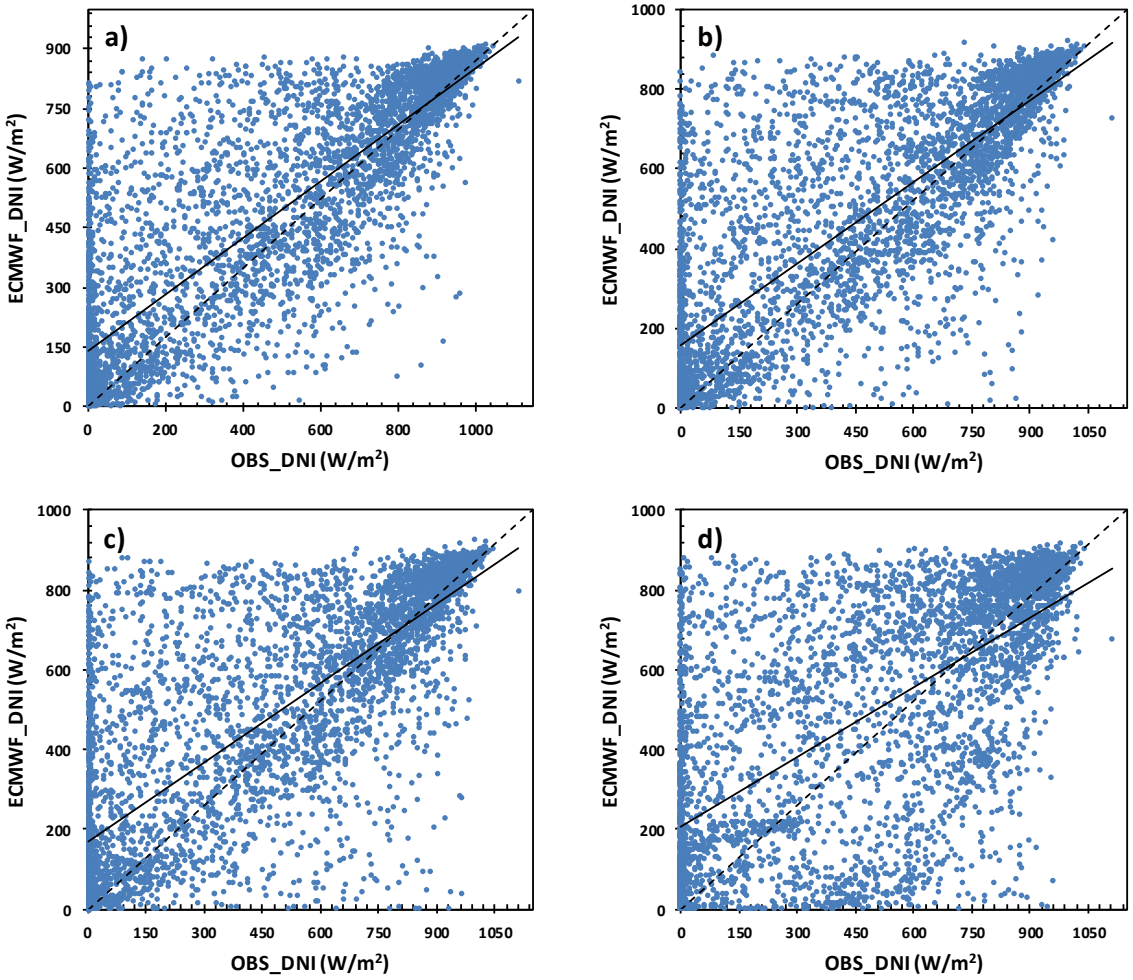

Figure 4.3. Scatter plots of predicted vs. measured hourly mean DNI for: (a) day_0, (b) day_1, (c) day_2 and (d) day_3, during the entire period considered.

The dashed line represents the $y = x$ line and the solid line is the least squares regression fit.

As expected, the errors associated to the hourly DNI forecast are quite significant with a strong scatter around $y = x$ line (dashed line). The slope of the regression line gives an indication of the quality of the forecasts and it is possible to conclude that the DNI IFS/ECMWF forecast are reasonable for the first three days ahead since the density of points is higher around the $y = x$ line (dashed line in Figure 4.3). The worst forecast is for day_3. From the Figure 4.3 it is also possible to verify that IFS overestimates DNI for lower values and underestimates DNI for higher irradiance values. This underestimation can be explained by the use of a constant

monthly aerosol climatology in the IFS/ECMWF as argued by Lopes *et al*. (2018), concluding that the model tends to underestimate DNI under very clear sky atmospheric conditions, when the actual aerosol concentrations are below mean values.

The statistical errors, on an hourly basis, are presented in Table 4.1.

Table 4.1. Statistical indicators of comparison between observed and predicted hourly mean DNI for the entire period (01/08/2018 – 31/07/2019).
Bold values mean best score.

Day	MBE (Wm^{-2})	MAE (Wm^{-2})	$RMSE$ (Wm^{-2})	r
0	13.54	**136.80**	**195.41**	**0.84**
1	15.03	146.35	210.60	0.81
2	17.273	154.97	224.02	0.78
3	**1.048**	197.88	267.25	0.70

The assessment between datasets shows that errors increase from the first day of forecast to the last day; day_0 exhibited the best performance with the lowest errors. MBE between calculated and measured DNI is smaller than $18\,Wm^{-2}$. Regarding the MAE and $RMSE$, their values increases from day_0 to day_3 (fourth day of forecast) with a difference between them of $\sim 61 Wm^{-2}$ $(\sim 45\%)$ and $72\,Wm^{-2}$ $(\sim 37\%)$, respectively. High correlation coefficients $(r \geq 0.70)$ are obtained between the observations and forecasts for all forecast horizons (see Table 4.1).

The boxplots of Figure 4.4 show the MBE, MAE, $RMSE$ and correlation coefficient based on hourly values for each forecast day and for the entire period of data (365 days).

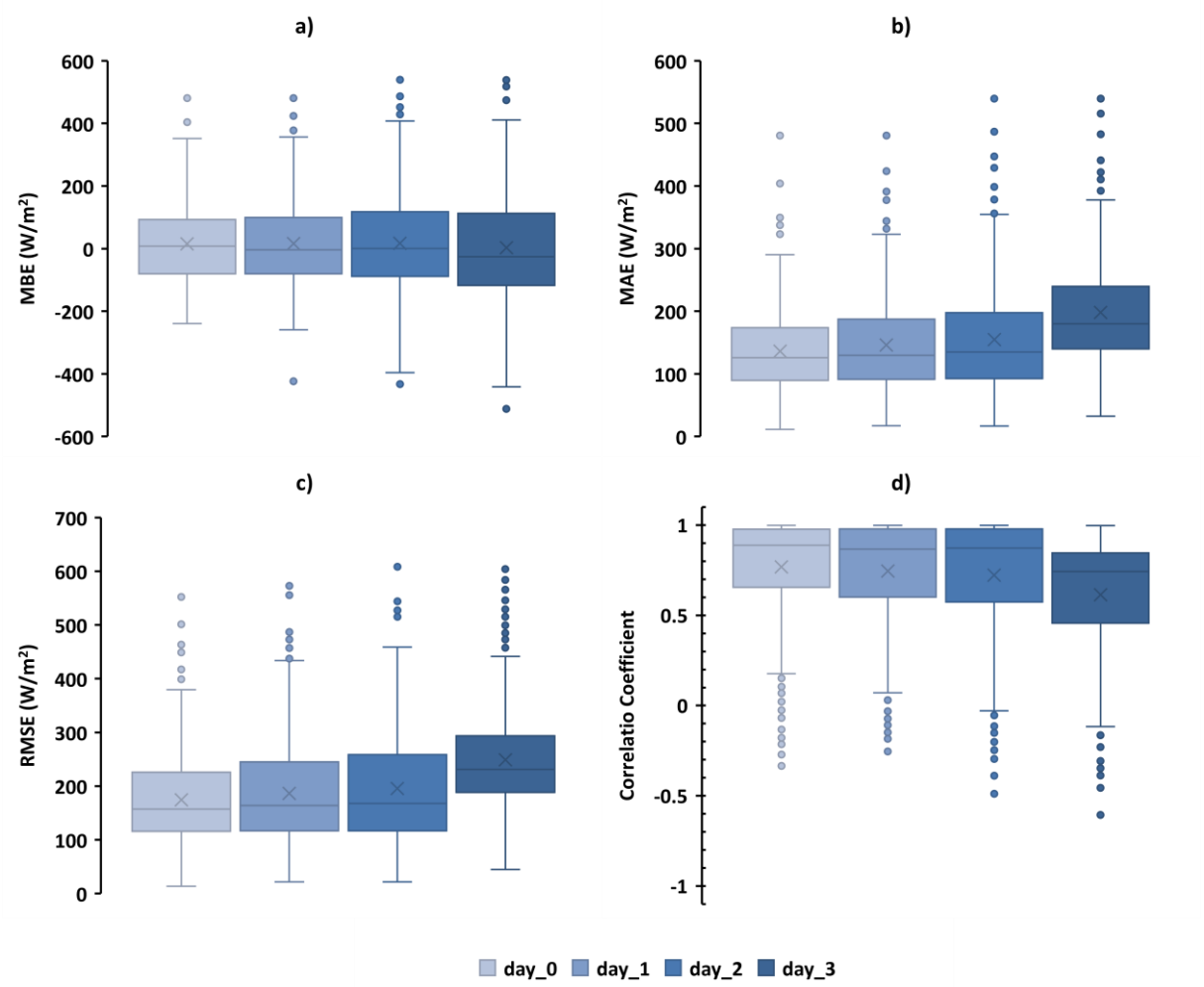

Figure 4.4. Boxplots of statistical indicators based on hourly values for (a) MBE, (b) MAE, (c) $RMSE$ and (d) correlation coefficient, for different days ahead of forecast.

The crosses represent the mean value of the sample, the horizontal solid line within the box represents the median, and the bottom and top of the boxes indicate the first and third quartiles, respectively. Boxes correspond to the interquartile range (IQR) where fifty per cent of the data is located. The circles represent the outliers, and the lower and upper ends of the whiskers are the minimum and maximum values of the datasets, respectively.

MBE indicates a slightly overestimation of hourly mean DNI for the majority of the forecasts days ($> 50\%$) in the period. The length of the IQR is a measure of the relative dispersion of a dataset and Figure 4a show similar length, in IQR, for the first two days of forecasts with values in $[-80; 100\ ]\ Wm^{-2}$. On the other hand, the difference between the IQR of first forecast day and the last one (day_4) in the same plot is about 24%. In what concerns to MAE and $RMSE$, as expected, a similar pattern like MBE was found, with errors increasing as the lead time of the forecast increases, and a relative percentage error, relatively to the mean, between day_0 and day_3, for both parameters, of the order of 30%. It is worth noting that a significant number

of outliers exist after the second day of forecasting. As for the correlation coefficients, these values indicate a good forecast performance with the best results obtained for day_0 with the highest median value of ~0.98 (Figure 4.4d). The correlation coefficient (r) presents a good performance for all forecast days in the analysis.

Considering now the daily mean values, Figure 4.5 shows the comparison between measured and predicted DNI for the entire period.

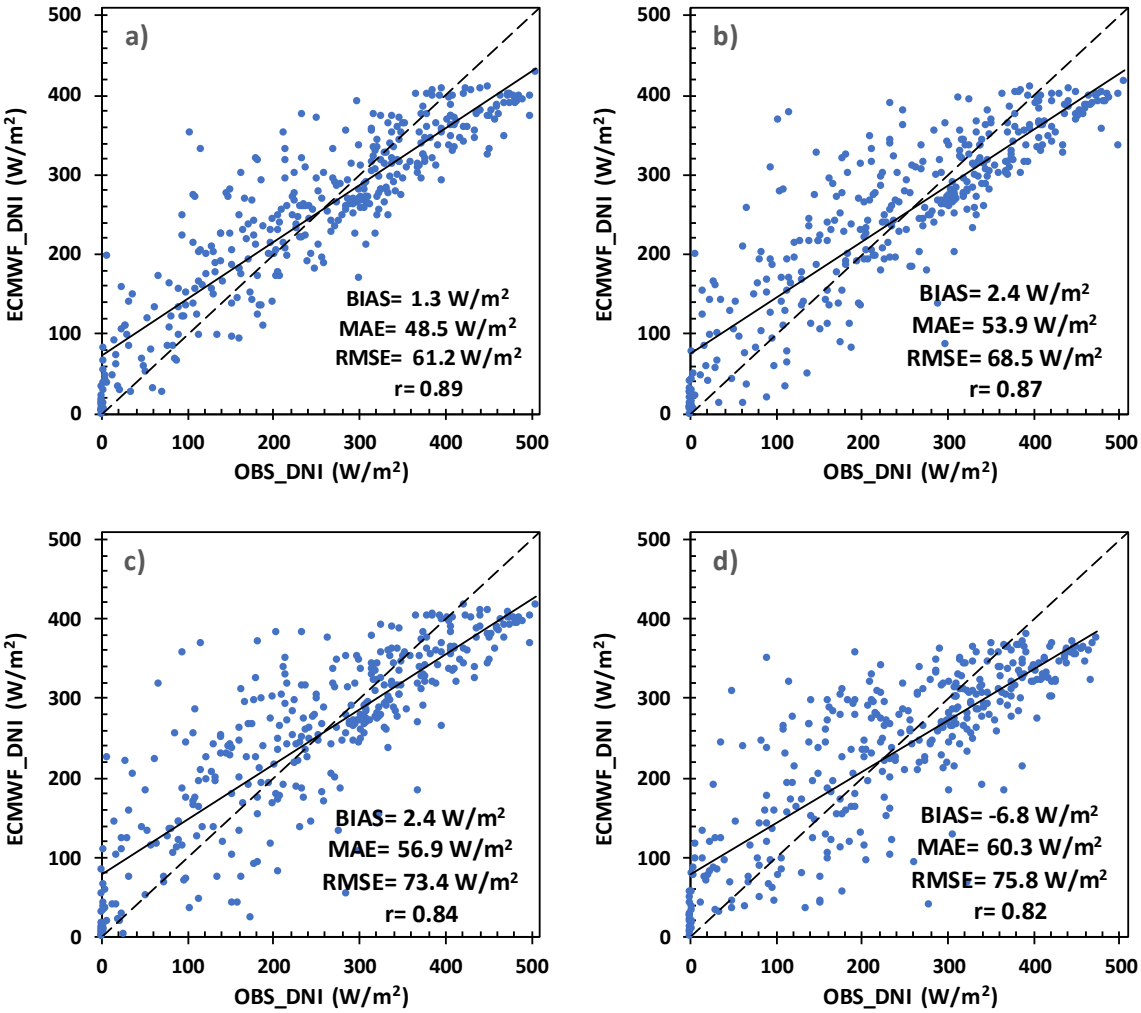

Figure 4.5. Comparison between predicted and measured daily mean DNI for the four prediction days: (a) day_0, (b) day_1; (c) day_2 and (d) day_3.
MBE, MAE, $RMSE$ and r are also presented in each plot. The solid lines are the linear fits and the dashed line represents the $y = x$ line.

As observed in the case of hourly values, the differences between observed and predicted DNI increases from the first day of forecast to the last one. Another common feature observed is the

DNI overestimation for lower values of direct normal irradiance as it can be seen through the trend lines. The statistical indicators obtained are comparable to the analysis made for the hourly values, showing a low forecast bias, with MBE values below 7 Wm^{-2} for all forecast days. Regarding $RMSE$, an increase of 35% percent (from ~61 Wm^{-2} to 76 Wm^{-2} between the first and the last day of forecast. It is evident from the scatter plots of Figure 4.5 that between roughly 250 Wm^{-2} and 350 Wm^{-2} the distribution of data points is closer to the $y = x$ line (ratio 1:1), which reveals a good agreement between observations and predictions. The overestimation occurs for observational DNI values below 200 Wm^{-2}, with a larger dispersion, which may reflect inaccuracies in IFS cloud representation.

Figure 4.6 shows the monthly mean of daily values of simulated and measured DNI for the period between 1 August/2018 and 31 July/2019, thus allowing to analyze the similarity between datasets throughout the year for the different forecast days.

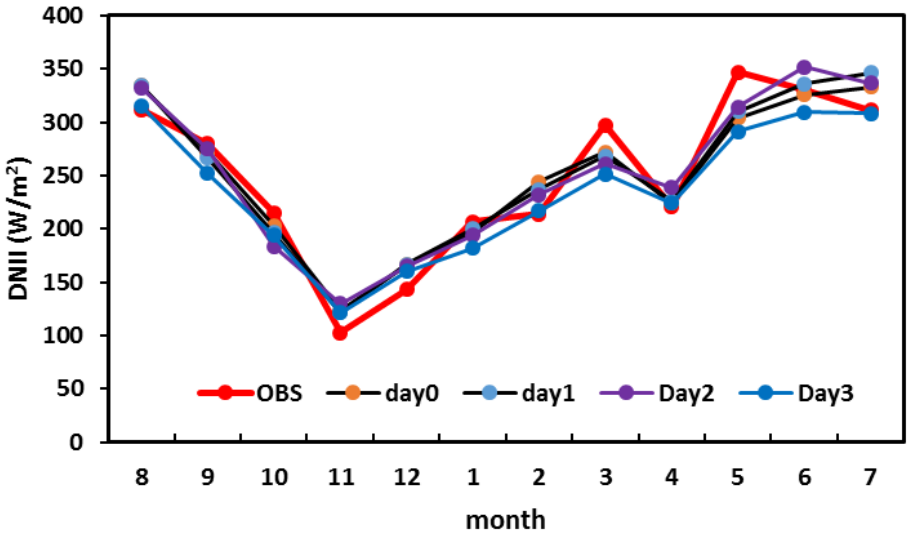

Figure 4.6. Monthly mean of predicted and observed daily mean DNI in Évora for the four different forecast days in the period from August/2018 to July/2019.

As shown in Figure 4.6, IFS/ECMWF model overestimates the radiation in more ~50% of the days throughout the year, independently of forecast day, although with small differences datasets.

The variation of statistical indicators between datasets (on a daily basis) grouped by months is presented in Figure 4.7.

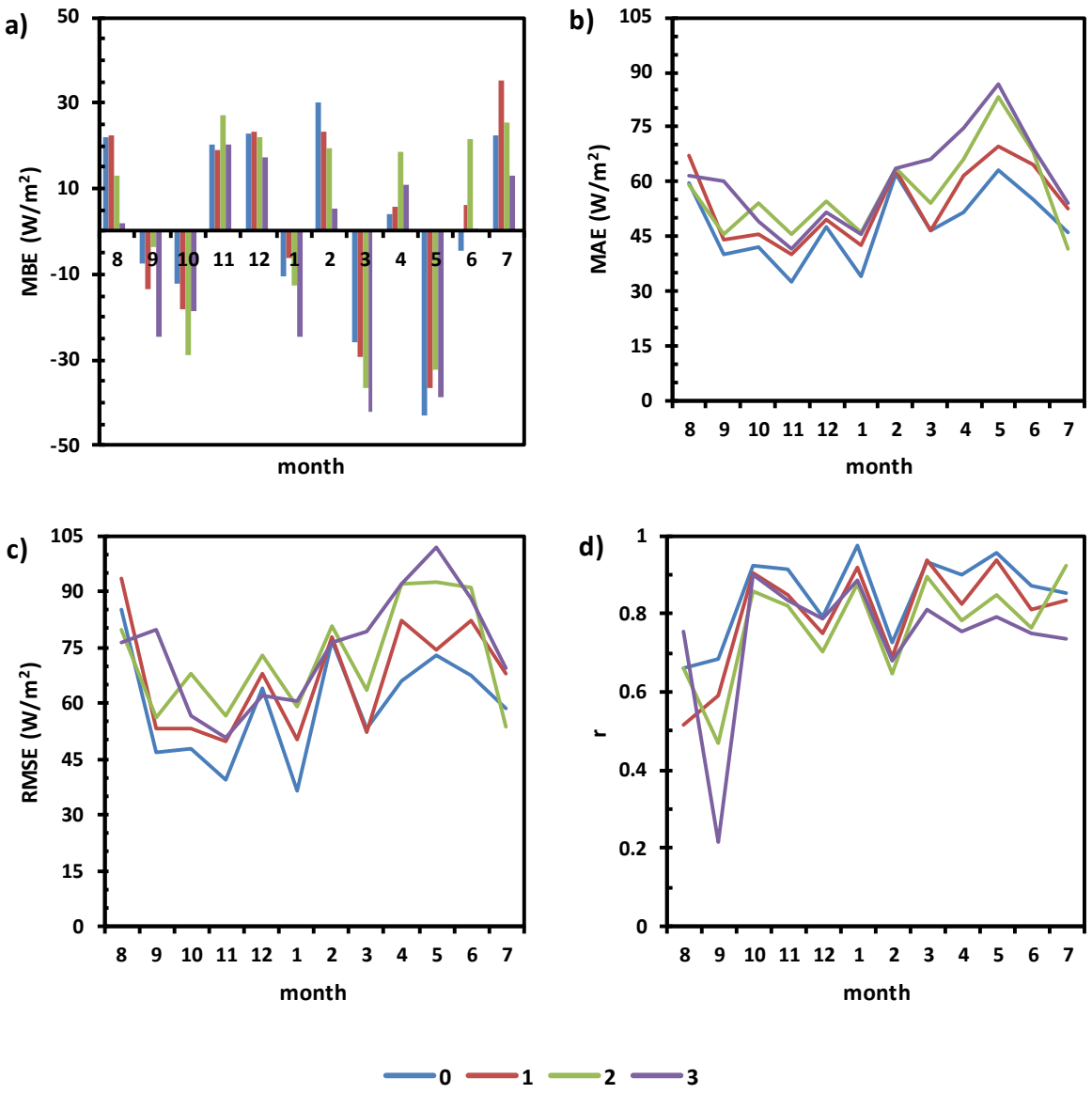

Figure 4.7. Statistical indicators obtained from the comparison between measurements and predictions of daily mean DNI values of. (a) MBE; (b) MAE; (c) $RMSE$; (d) correlation coefficient. 0, 1, 2 and 3 represent day_0, day_1, day_2 and day_3, respectively.

Overall, MBE, MAE and $RMSE$ present better results for the first day of forecast (day_0). The highest values of statistical errors correspond to the forecasts obtained for day_3.

From Figure 4.7a, MBE values ranges from about $-42\ Wm^{-2}$ to $35\ Wm^{-2}$, and show ~60% of the months with positive MBE values (independently of forecast days). According with the same figure, the underestimation occurs in two thirds of the months belonging to the MAM and SON seasons, probably as a consequence of a less accurate representation of the clouds (or aerosols) at short time scales in the radiative scheme of IFS/ECMWF.

According with Lopes *et al*. (2018), the IFS global model from ECMWF tends to underestimate DNI in clear sky conditions due to the use of a monthly mean profile of aerosols. Perdigão *et al*. (2017) also used the same argument in the assessment and characterization of the shortwave downward radiation incident at the Earth's surface over Iberian Peninsula using the mesoscale Weather Research and Forecasting (WRF) model.

Figure 4.7b and 4.7c show that MAE and $RMSE$ present lower values, independently of forecast day, in JJA and SON seasons. MAE and $RMSE$ present a similar variation that as found for MBE (Figure 4.7b and 4.7c) with values ranging from $33\,Wm^{-2}$ to $87\,Wm^{-2}$ and $36\,Wm^{-2}$ to $102\,Wm^{-2}$, respectively. As mentioned above, results show high correlation coefficients for all forecast days, although with the IFS/ECMWF model performing better in the first day of forecast.

The majority of statistical errors found in this work are in line with values obtained in the forecast of DNI by Nonnenmacher *et al*. (2016) and Lara-Fanego *et al*. (2012a) using WRF model, and Gala *et al*. (2013) using a clear sky model, among other studies. Table 2 of Law *et al*. (2014), show a summary of the state of art of DNI accuracy obtained from NWP and other methodologies.

4.3.2. Relation between the DNI attenuation index (DAI) and DNI forecasts

Inaccurate representation of clouds in the radiative transfer scheme of global numerical weather prediction models is the primary cause of errors in the prediction of solar radiation. In this section, the DNI attenuation index (DAI) is proposed to assess and analyze the impact of cloud representation in DNI forecast from the IFS/ECMWF model, as defined in Section 4.2.4 (Equation 4.6).

Before analyzing the relationship between the DAI index, computed using data from the Évora radiometric station (section 4.2.1) and the quality of the DNI forecast errors, the reliability of *DAI* is assessed, on a monthly basis, using the Total Cloud Area Fraction from CERES (section 4.2.4) for the same local. According to Almorox *et al*. (2017), global solar irradiation obtained from CERES, at monthly basis, provide a very good accuracy for solar radiation studies since their results shows a good fit between CERES data and solar radiation data from different meteorological stations over Spain.

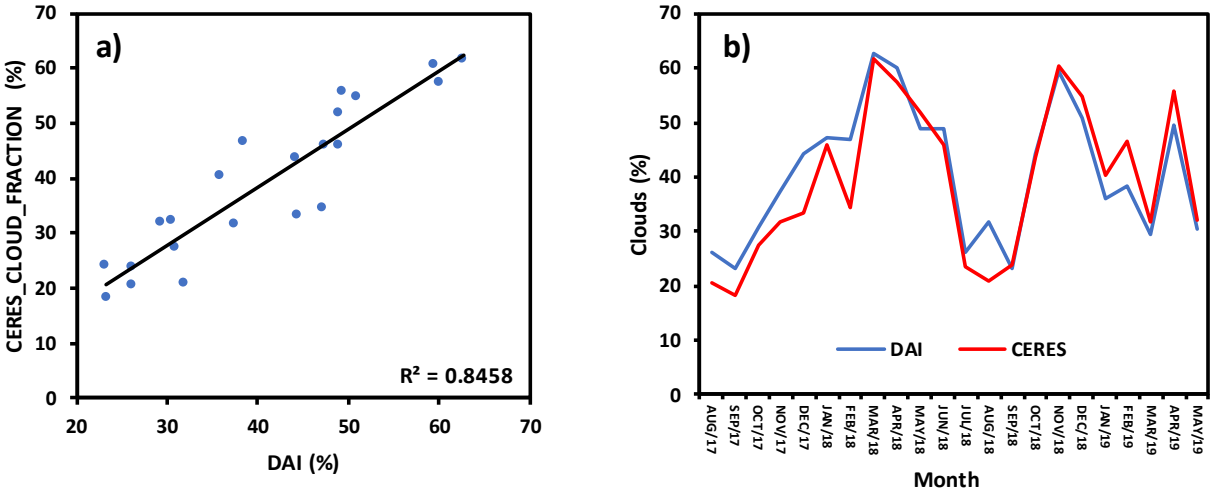

Figure 4.8. (a) Monthly mean cloud cover from CERES versus *DAI* in Evora, and (b)Temporal evolution of CERES cloud Fraction (red line) and *DAI* (blue line) in the period between Aug/2017 and Jul/2019 (twenty-two months).

Black solid line represents the linear fit.

The linear regression between CERES cloud fraction and *DAI* shows a good agreement between these two indexes (Figure 4.8a), with a correlation coefficient of $r \sim 0.92$. When comparing the temporal evolution of *DAI* and cloud area fraction (CERES) on a monthly basis, both time series exhibits a similar pattern (Figure 4.8b), and shows, as expected, a decrease of cloud cover in JJA season in contrast with an increase of the cloud cover in the DJF season. The major discrepancies between datasets occur in February/2018, February/2019 and in August/2018, corresponding to periods in which the region was affected by aerosol events (Saharan dust particles, in February, and forest fires in August).

The results suggest that *DAI* may be used as a proxy to cloud cover, particularly suitable to estimate the impact of clouds on the DNI forecast.

As for the observations, the *DAI* of model predictions was also calculated and hereafter is referred as *DAI* (IFS). Figure 4.9 shows a boxplot comparison between *DAI* and *DAI* (IFS) index.

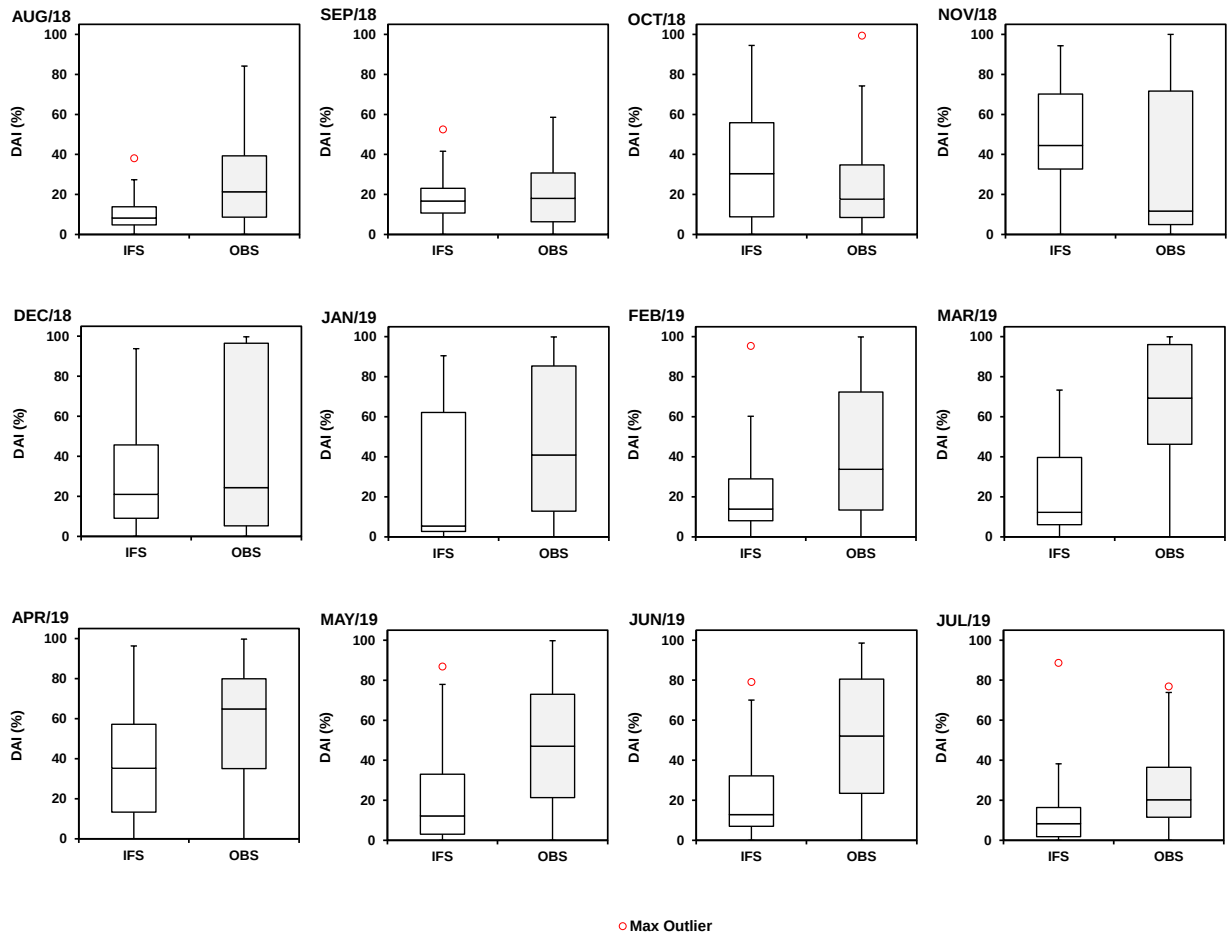

Figure 4.9. Monthly boxplots of daily mean values of *DAI* based on observations (OBS) and IFS/ECMWF forecasts (IFS), for Évora.
The red circles represent outliers (maximum value).

From Figure 4.9 it can be seen that in the majority of analyzed months, the *DAI* (IFS) is lower than *DAI*, meaning that cloud scheme in IFS/ECMWF model underestimates the clouds and aerosols events when compared with the *DAI* index. *DAI* are characterized by a lower variability in summer with more than 50% of the days with values lower than 31.25% (clear sky days) and a higher variability during spring season (higher IQR values with more than 50% of days with values higher than 31.25%). These results are in line with the study by Royé *et al.* (2018), in which low levels of cloudiness (clear skies days) over Iberian Peninsula were found for the case of summer months, using satellite data from the MODIS and for the period 2001–2017, with the exception of the Cantabrian coast. On the other hand, the variability of observed *DAI* is higher, mainly due to a higher variability on actual cloud cover and aerosol concentrations values. This variability also explains the relative high errors reported in

previously section. Perdigão *et al*. (2017) also found a high variability in downward shortwave radiation during March.

Figure 4.10 shows the relation between the cloud class, grouped according to cloud coverage (in $oktas$), estimated on the basis of DAI, as indicated in Section 4.2.4, and the statistical indicator $RMSE$ (in three ranges of values), obtained for each day, from hourly raw values. Day type class (I-clear, II-partially cloudy and III-overcast) is obtained following the WMO guidelines.

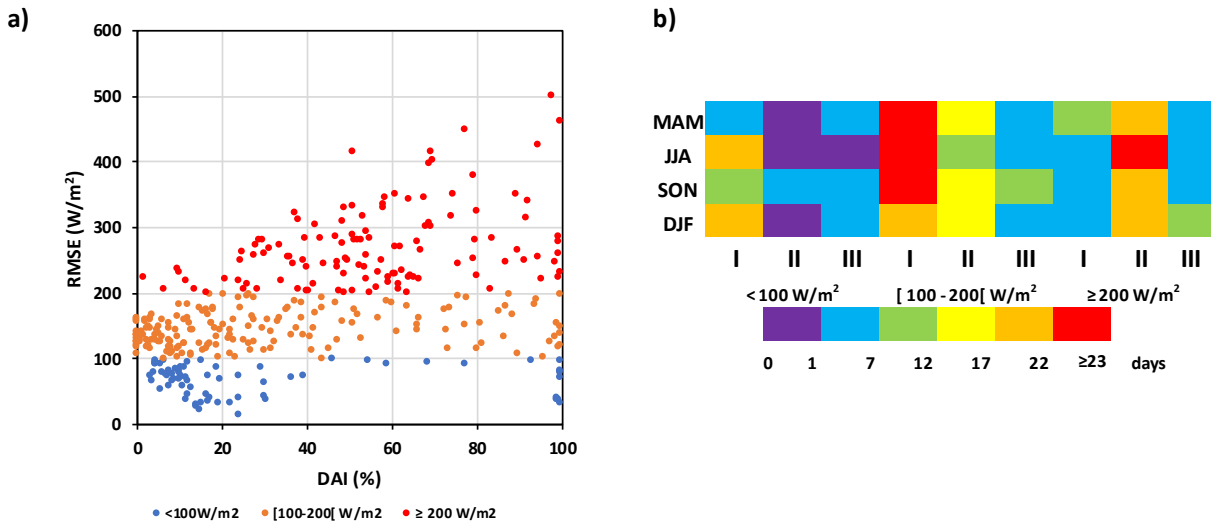

Figure 4.10. (a) Scatter plot of DAI versus Root Mean Square Error ($RMSE$) for day_0 and (b) Number of days in a seasonal basis within different ranges of forecast errors grouped in classes, according to the cloud coverage – class I ($0-2$ $oktas$), class II ($3-5$ $oktas$) or class III ($6-8$ $oktas$) for $RMSE$.

From both plots of Figure 4.10, it becomes evident that $RMSE$ strongly depends on the sky conditions, and its possible verify that:

(i) Approximately $\sim$19% of the days presents $RMSE$ values lower than 100 Wm^{-2} (blue dots in Figure 10a). This percentage corresponds mostly to a cloud coverage lower than or equal to two $oktas$ – clear skies days;

(ii) $\sim$47% of the days presents a cloud coverage of class II type, in the range $[100-200]$ Wm^{-2};

(iii) $RMSE$ values above 200 Wm^{-2} occur for $\sim$34% of the days (red dots in Figure 10a). For this value, the majority of days are found in the cloud coverage type II category, suggesting that the model gives worst results in partially cloudy days, due to an inaccurate cloud representation

or of their effects on the solar irradiance at the surface. For instance, Lopes (2015) found that thin clouds (like cirrus) may cause a decrease in DNI of around 20%;

(iv) the errors found in summer months can be explained by the monthly constant aerosol climatology used in IFS/ECMWF as argued by Lopes *et al*. (2018).

The analysis of the climatology of cloud cover at Évora based on DAI for the period from 1 August/2018 to 31 July/2019 (Figure 4.10b), shows that circa 45% of the days are in the class I, considering only $RMSE$ errors below 200 Wm^{-2}, and these days are mainly in the MAM and JJA seasons, when more clear skies days occur over Évora city. These values are consistent with those found by Sanchez-Lorenzo *et al*. (2009) and by Perdigão *et al*. (2017) for the same sky conditions over the Iberian Peninsula.

Concerning the cloud coverage of class II and III, for the period in analysis and independently of the $RMSE$ values, there are ~37% and ~13% of days, respectively. Cloud coverage of type III are mostly found in DJF season.

It's important to mention that the quality and reliability of the forecast of solar radiation is directly related to the accuracy of cloud representation as well as of aerosols. For instance, Lara-Fanego *et al*. (2012a) found that $RMSE$ values ranged from 20% to 100% for clear and cloudy skies, respectively, using WRF model over Andalusia.

Another feature can be seen in Figure 4.11 where it is possible to observe a relation between the RSR and the DAI for the first day of forecast (day_0).

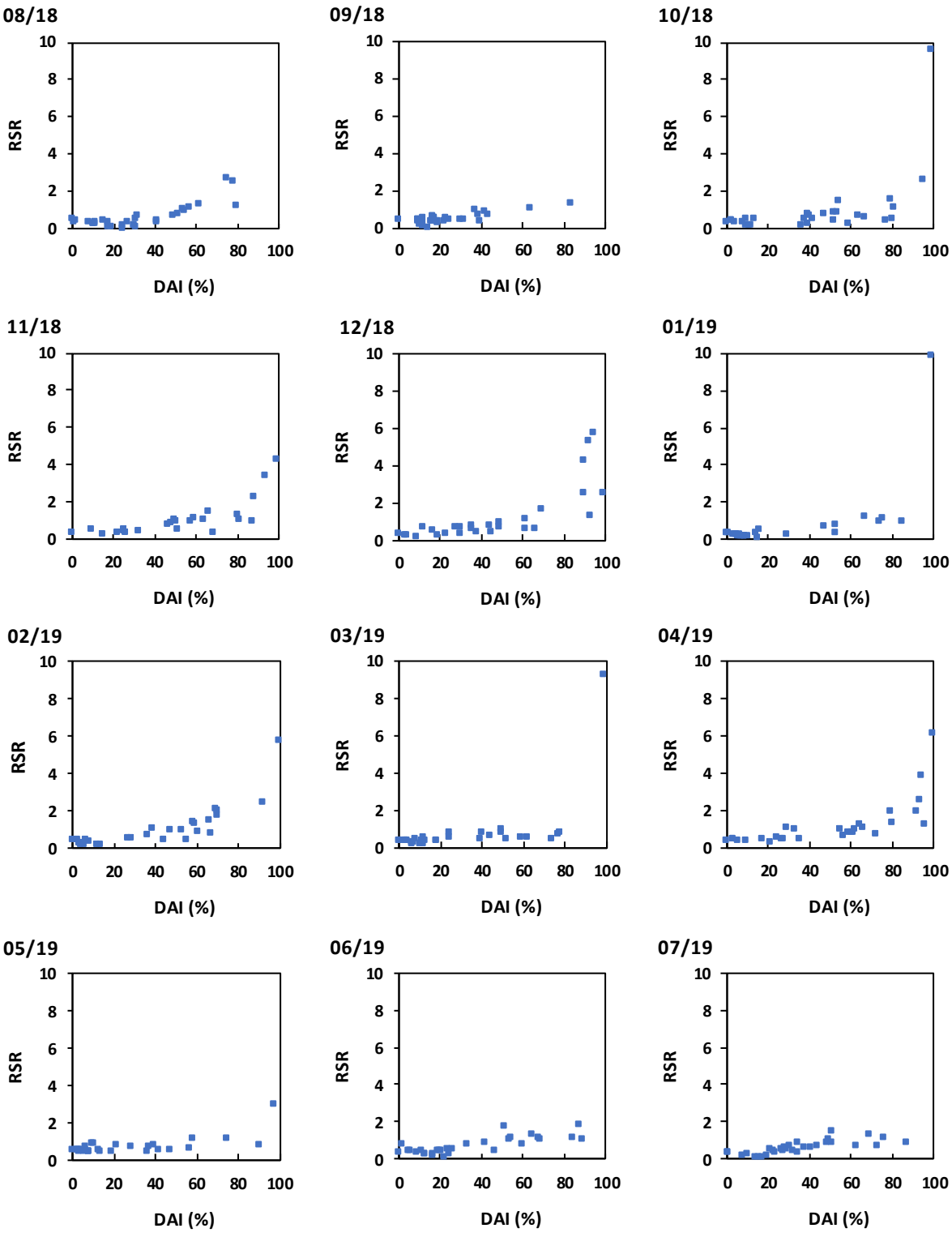

Figure 4.11. Relation between *DAI* and *RSR* based on hourly mean DNI forecasts and measurements for the first day of predictions between 01/08/2018 and 31/07/2019 (one year). *RSR* is dimensionless varying between zero and a large positive number.

As expected, from Figure 4.11, as the DAI increases the RSR increase. The forecast obtained from IFS/ECMWF presents a better performance for clear sky days. In general, the DNI forecast tends to be more accurate ($RSR < 0.5$) for lower values of DAI, which represents $\sim 50\%$ of the days in Évora. This value of clear sky days is of the same order of the study of Freile-Aranda *et al*. (2017), who found, for a climatic region which includes Évora, a minimum cloud cover (at an annual average) around 43%. The best performance (of IFS/ECMWF) are found for summer months (smaller values of $RSR \leq 0.5$ and $DAI \leq 2$oktas). For instance, Kraas *et al*. (2013), also found that during summer season the forecasts are generally more reliable than in other seasons.

4.3.3. Statistical bias correction analysis of daily DNI forecasts

The bias between solar radiation forecasts from Numerical Weather Prediction models and observations can be decreased by applying a bias post-processing correction. This bias correction methodology have been used in solar radiation studies by several authors, such as Ruiz-Arias *et al*. (2015), Polo *et al*. (2015, 2016), Perdigão *et al*. (2017), Mejia *et al*. (2018), among other authors.

The forecast values of DNI are corrected following the methodology described in section 4.2.5. In Figure 4.12, we show the result of the application of the MOS method for the various forecast horizons.

Error metrics are also presented in graphs using the new corrected predictions.

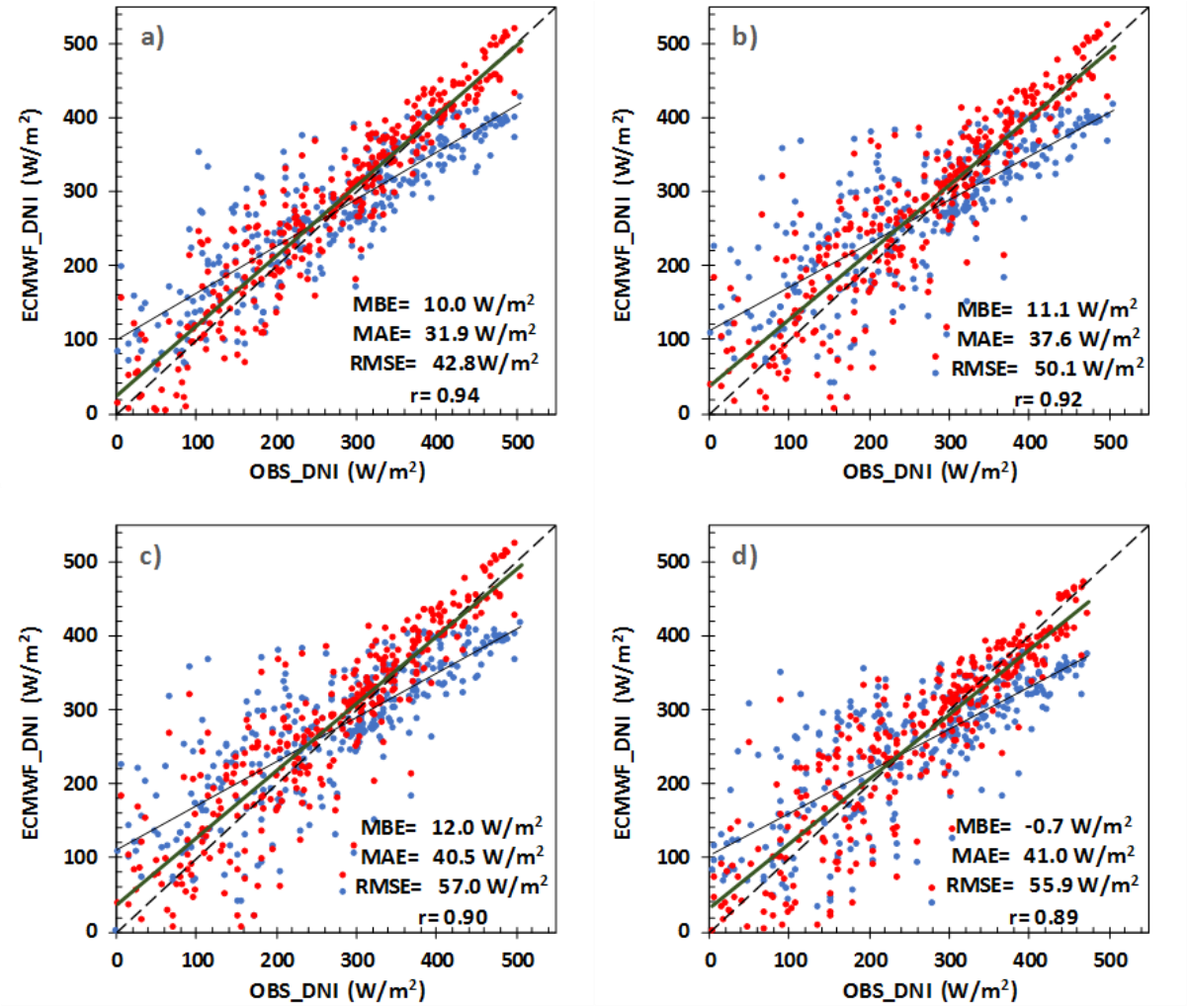

Figure 4.12. Comparison between predicted and measured daily mean DNI for the four prediction days: (a) day_0, (b) day_1; (c) day_2 and (d) day_3 before (blue dots) and after bias correction (red dots). MBE, MAE, $RMSE$ and r, after BC, are also presented in each plot.

The solid lines are the linear fits - green for BC procedure and black for IFS/ECMWF raw data - and the dashed line represents the $y = x$ line.

Overall, the MOS correction significantly improve the results. The corrected data exhibited (now) less dispersion around $y = x$ line. Statistical errors decrease in the order of about 30%, when compared with initial IFS predictions and independently of the forecast day. For example, MAE values decrease from the interval $[49 - 60]\ Wm^{-2}$ to $[32 - 41]\ Wm^{-2}$, while $RMSE$ values decrease from $[61 - 76]\ Wm^{-2}$ to $[43 - 57]\ Wm^{-2}$. Correlation coefficient are in line with previously values, i.e., all r values were improved with values ≥ 0.89.

To a better comparison, Figure 4.13 shows the cumulative distribution functions (CDF) of daily DNI, for each day of forecast, before and after correction procedure.

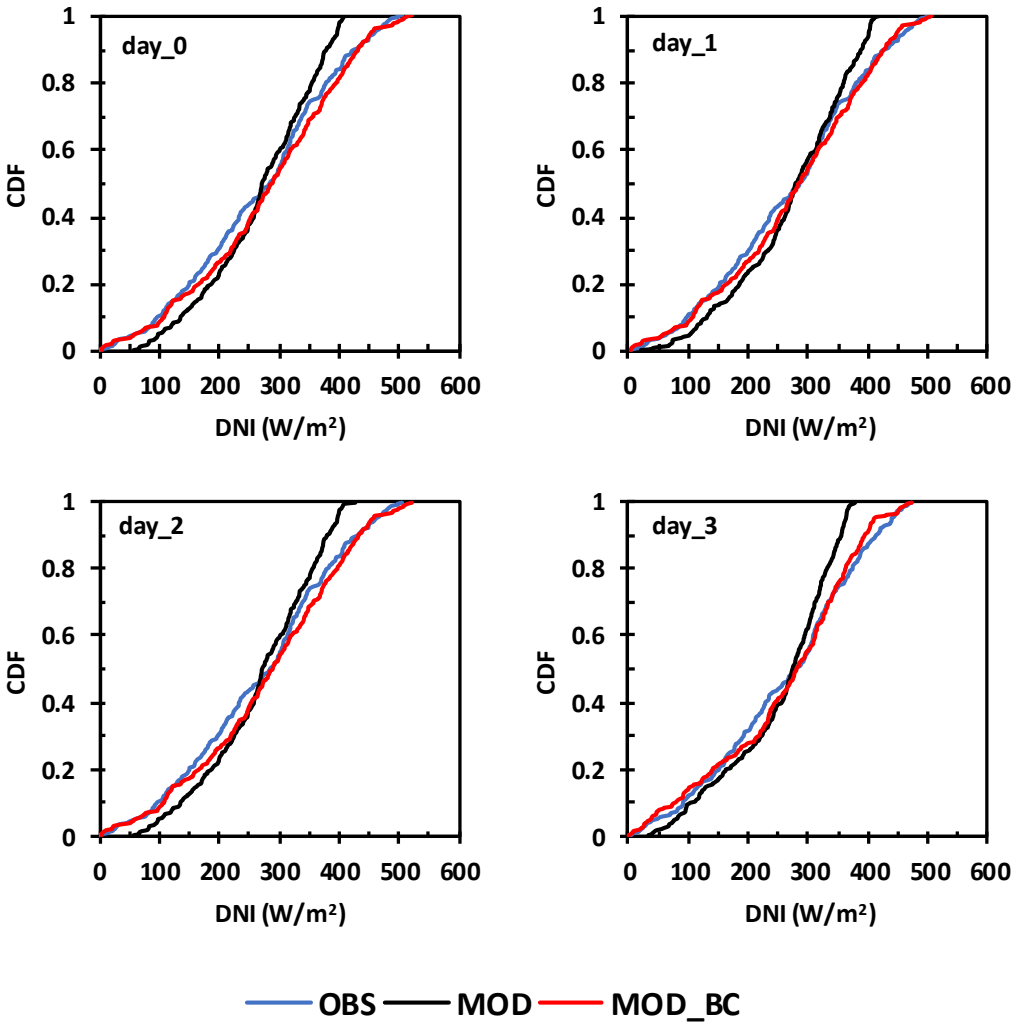

Figure 4.13. Cumulative distribution functions (CDF) of daily mean DNI grouped by day of forecast, (a) Day_0; (b) day_1; (c) day_2 and (d) day_3, from 1/08/2018 to 31/07/2019, original forecasts (black line), forecasts after bias correction (red line) and observations (blue line).

Results in Figure 4.13 show the similarity of the CDF between observational and IFS/ECMWF outputs before and after the bias correction. In general, and independently of the forecast day, as said before, the linear regression method successfully improved the DNI outputs with the new corrected cumulative distribution function plots closer to the observed DNI.

4.4. Conclusions

Given the importance that alternative energies have in a sustainable economic, social and environmental perspective, it is important to know in advance how solar, wind or other renewable energy resource change on an hourly, daily or monthly basis. In this work, DNI from Integrated Forecasting System of European Centre for Medium-Range Weather Forecasts (IFS/ECMWF) dataset was evaluated over one year (1/08/2018 to 31/07/2019) against observed DNI, at hourly time scales, for one station located at Evora (south of Portugal) for different days ahead of forecast (until three days ahead).

Statistical $BIAS$, MAE, $RMSE$, RSR and correlation coefficient were used to assess the relation between IFS/ECMWF and observational DNI. Additionally, this paper, also describes a new methodology based on DNI observations (we called of DNI attenuation index – DAI) to estimate the transparency of the atmosphere in a particular region. The DAI was evaluated with total cloud cover parameter obtained from CERES product data and results showed high correlation coefficients between datasets, suggesting that DAI can be used as proxy to classify the cloud coverage in direct solar radiation studies. This index was used to analyze the relation between the cloud coverage and the predicted DNI, as well as the respective associated error.

The IFS/ECMWF DNI forecasts present similar magnitudes and pattern relatively to observational data but the errors increase with the forecast lead time (from 1 to 3 days ahead). Discrepancies between modelled and measured radiation are relatively small mainly for the first three days of forecasts. The analysis of hourly data showed that the DNI is overestimated by IFS/ECMWF. Regarding the correlation coefficient, values are found above ≥ 0.7, independently of the forecast day. This work also shows that the first day ahead forecast (day_1) has similar error magnitudes in relation to the first 24 hours forecast (day_0).

Hourly analysis also shows values of MBE, lower than $20\ Wm^{-2}$. Regarding the MAE and $RMSE$ values, an increase from day_0 to day_3 was observed, with a difference between the first and the third day of forecast $\sim 45\%$ and $\sim 37\%$, respectively. High correlation coefficients ($r \geq 0.7$) are found for all forecast days.

Daily analysis shows better results, with MBE values lower than $7\ Wm^{-2}$ for all forecast days. In the case of $RMSE$, values increase about 35% percent from the first day of forecast to the

last one. The correlation coefficients of daily data are higher than in the case of hourly data, ranging between 0.82 (day_3) and 0.89 (day_0).

The mean-monthly cloud coverage is well captured by DAI along the year. As expected, the observed DNI is higher in spring and summer months with the lowest values in DAI for the same seasons. The underestimation of cloud cover by the IFS/ECMWF seems to be evident since comparison between observed and predicted DAI reveals that model tends to underestimate the effects of clouds on DNI. This relation was also found for Andalusia (located in Iberian Peninsula) using WRF model by Lara-Fanego *et al*. (2012a) in the case of three days ahead DNI forecasts.

The accuracy of IFS/ECMWF to forecast DNI is higher for clear or partially cloudy sky days. DAI index confirms that the performance of the IFS/model decrease with an increasing of clouds/aerosols effects.

A bias correction post-processing through a linear regression was used to correct the IFS/ECMWF predictions, which has shown to significantly improve the forecast for Évora with a decrease in the order of 30% for all statistical error metrics, except for the correlation coefficient, independently of the days ahead in consideration.

The results obtained in this work are consistent with those obtained by Lopes *et al*. (2018) for the same location, and by Nonnenmacher *et al*. (2016), Troccoli and Morcrette (2014), among others, where it was found that errors increase with the lead time forecast. Overall, ECMWF DNI forecasts provide valuable information for the management and operation of CSP plants, especially after the usage of the post-processing bias correction.

5

Conclusion

"Discovery follows discovery,

each both raising and answering questions,

each ending a long search,

and each providing the new instruments for a new search."

Robert Oppenheimer

Solar radiation is a primary energy source and a crucial component of the global energy balance, which drives different systems, such as the hydrologic or the climate systems.

In the Iberian Peninsula many commercial and research power plant systems are in place in order to use solar energy for the production of electricity. In this context, the knowledge of the flux of solar radiation that affects the Earth's surface and its evolution, becomes extremely important and is critical as an assessment for a strategic planning of projects related to the production of solar energy.

The present work aimed to contribute to the evaluation of the solar resource in two main frames: evolution and analysis of the trends of solar radiation at the surface over the Iberian Peninsula using ERA–40 and NCEP/NCAR reanalysis products, and in the prediction of solar radiation (global and direct) at the surface based on numerical weather prediction models.

This thesis is the compilation of three publications (each forming a chapter), and the research main findings of this work are presented by chapter.

In **chapter two**, *Variability and trends of downward surface global solar radiation over the Iberian Peninsula from ERA–40 reanalysis*, the variability and trends of surface radiation over the Iberian Peninsula using ground based, ERA–40 reanalysis from ECMWF and NCEP/NCAR

reanalysis data were examined. An extensive analysis is also made for five Portuguese ground based stations.

Due to the lack of reference series, these annual $SW\downarrow$ series were tested by means of four (absolute) homogeneity tests in order to test the quality of the data. After this, reanalysis products were validated with these series and with thirteen previously validated series obtained from Sanchez-Lorenzo *et al*. (2013a), over Spain. Monthly means of $SW\downarrow$ for 40 years were carried out and analyzed. Deviations from the temporal mean for each month and for each year were computed and variations discussed. The relation between the interannual variability of solar radiation over Iberian Peninsula and the cloud cover were analyzed. The trends of surface radiation for each month during the past decades was computed and discussed. The main ideas to take out of this work are:

- ***SW↓ mean values over Portugal ground based stations show two periods,*** in line with literature – ***dimming and brightening periods*** (e.g., Ohmura and Lang, 1989; Stanhill and Cohen , 2001; Wild, 2009, 2012, among others), although ***with an earlier turning year*** as compared to other regions of Europe (e.g., Wild, 2009; Sanchez-Lorenzo *et al*., 2013b; Sanchez-Lorenzo *et al*., 2015). ***This reversal and partial recovery were found around mid-70s***. The comparison was restricted to the period when observations were available (~1960-1990).

- ***The turning year from dimming to brightening was found around five years before in the observational stations located in the south as compared to the stations in the north***. ***Ground based stations located in areas with high industrial and population density are those where the reversal from dimming to brightening arises later.*** This behavior was explained with local causes associated to industry presence over the region and the dominant circulations patterns over north Atlantic Ocean that influence the interannual variability of clouds.

- ***ERA–40 reanalysis product reveals a reasonable capability to reproduce solar radiation over IP***, specially in a monthly basis, considering the uncertainty in the observational data, the monthly ERA–40 mean aerosol profile (fixed), and its spatial resolution.

- ***ERA–40*** (NCEP/NCAR) ***annual and monthly averaged of SW↓ values are always lower*** (higher) ***than the corresponding ground-based measurement values***. The inaccurate representation of clouds, especially the convective systems, as well as the non-inclusion of the actual concentration of aerosols in the reanalysis process can be considered as causes for this disagreement.

• ***ERA–40 captures better the dimming period than NCEP/NCAR,*** but both ***with a transition in the dimming period to brightening in the early 1970s*** and in line with observational stations (special in the south). ***The magnitude of the trends presents slight differences between observational series and reanalysis*** products.

• ***At a regional scale*** *(IP divided in areas of 1°×1°)****, ERA–40 reveal a dimming period that finished in 1970 in the south and center of IP and a few years later*** *(~4/5 years)* ***in the north regions***.

• The ***dimming/brightening phenomena in the Iberian Peninsula from ERA–40 must be*** primary related with decadal changes in the cloud radiative effects and also to changes in the aerosol loading , especially over south regions where brightening arise five to ten years earlier than shown in literature (e.g, Ohmura and Lang, 1989; Liepert, 2002; Wild *et al.*, 2005).

• ***$SW\downarrow$ climatology obtained from ERA–40***, over IP, ***shows a latitudinal gradient with higher values at lower latitudes and lower values at higher latitudes***. ***TCC negatively correlates to $SW\downarrow$, revealing a strong dependence of clouds on radiation*** scheme of reanalysis products, since the annual aerosol field is fixed, and so only the clouds and the water vapor may have a direct impact on the $SW\downarrow$.

In chapter three, *Climatology and variability of solar radiation obtained from WRF regional climate simulations in Iberian Peninsula (1950-2010),* the mesoscale $WRF-ARW$ was evaluated to predict the incident shortwave radiation at the surface. The model was configured using three nested domains with a horizontal resolution of 75, 25 and $5\ km$ (this last one centered over the region of study), with 30 vertical hydrostatic pressure levels for a 60 year period between 1950–2010, and was initiated with NCEP reanalysis data available at 2.5° resolution for each year starting from the 1st May and each simulation run for 13 months. The first month of each simulation was neglected and the model boundary conditions were updated at every 6 hour interval also from NCEP reanalysis data. After validations using ten years of data (2000–2009 period) over 65 ground-based stations and a post-processing bias correction methodology, WRF outputs were used to create a detailed climatology of $SW\downarrow$ (and clouds) in order to improve the characterization of this important resource over this region. Main findings of this chapter were:

• ***The dynamical downscaling used in this thesis*** started from a single set of initial conditions, ***with re-initialization time slices integrations*** of thirteen months. This methodology ***revealed***

to be a valid alternative to the more computationally time demanding strategy based on continuous model integration (without interruption for re-initialization). Results obtained with ***this methodology were compared with another WRF model configuration and errors were comparable***.

- ***WRF model overestimates the SW↓ in the majority of the stations located in the north/northeastern of IP and*** *tends to* ***underestimate SW↓ over the southwest and southeast regions***.

- ***Daily correlation coefficients reveal that WRF performs better in the central part of IP than over the North/North-Western regions***.

- ***Incorrect quantification of the aerosol*** effects in radiative scheme of the model ***explain mean bias*** whose values are in agreement with Ruiz-Arias *et al*. (2016).

- ***Errors were significantly reduced after application of a BC post-processing methodology*** (in approximately 41%).

- ***SW↓ climatological for 60 years,*** over IP, ***showed a spatial distribution*** with a gradient ***that increases from north to south and from west*** to east modelled by the effects of the coast and topography.

- ***The highest SW↓ variability is major in the northern part of IP***, particularly in Galicia (Spain).

- ***SWRCLF show that the percentage of clear sky days*** (less than $okta$), *for the whole period,* ***are more than*** 30% ***of the days*** (include all seasons) ***at south of IP*** (Andalusia, Murcia and Algarve). ***In the summer*** *months* ***this value rises for more than*** **70**%.

- ***The climatology obtained*** with *WRF* model ***points out Andalusia*** (Spain), ***Murcia*** (Spain), ***Alentejo*** (Portugal) ***and Algarve*** (Portugal) ***as the regions with the greatest SW↓ potential to implement solar energy systems***.

In the last chapter, *Assessment of Direct Normal Irradiance Forecasts based on IFS/ECMWF data and observations in the south of Portugal*, the direct solar irradiance forecasts provided by IFS/ECWMF are evaluated for Évora ground-based station. The errors associated with these forecasts were quantified at very short (1 hour) and short term (1 to 3 days), for one year of data. The quality of the forecast and error quantification were assessed by using a set of statistical error metrics. It was also proposed a method for modelling sky conditions using the

in situ observational data of the measured DNI. To improve IFS/ECMWF predictions, a *post-processing* BC methodology, based on a linear regression, was tested. Major findings were:

- **IFS/ECMWF overestimates DNI for lower values of radiation and underestimates DNI** under clear sky atmospheric conditions **for higher irradiance values.** This underestimation can be explained by the use of a constant monthly aerosol climatology in the IFS/ECMWF.

- IFS/ECMWF model **overestimates** the radiation in $\sim 50\%$ **of the days throughout the year**, independently of forecast day horizon, although with small differences datasets.

- The ***underestimation occurs in the majority of the days belonging to Spring and Summer months***, probably as a consequence of a less accurate representation of the clouds (or aerosols) at short time scales in the radiative scheme of IFS/ECMWF.

- ***The assessment between datasets show that the statistical errors are comparable*** (in hourly and daily basis). Overall, ***statistical analysis shows better results for the first day*** of forecast, with errors ***increasing from the first day*** of forecast ***to the last one.*** The majority of statistical errors found in this work are in line with values obtained by Nonnenmacher *et al*. (2014) and Lara-Fanego *et al.* (2012a), both studies using WRF model or by Gala *et al.* (2013) using a clear sky model, among other studies.

- ***A new proxy (DAI*** *– DNI Attenuation Index****) was developed to provides a clear idea of the transparency of the atmosphere*** for a specific day since it allows the identification of a clear day from an overcast day or extreme aerosol event. ***Results turned out to be promising***. This method has the advantage of not relying on reanalyses, satellite data or other products that could also be a source of bias.

- The ***annual cycle of monthly clouds is well captured*** by DNI attenuation index (DAI).

- Results obtained using DAI proxy show that ***cloud scheme in IFS/ECMWF underestimates the clouds and aerosols*** events.

- The analysis of the **climatology of cloud cover at Évora based on *DAI***, for the analyzed period, ***shows that*** 45% ***of the days are in the cloud coverage class I*** (below to 2 $oktas$). ***DAI are characterized by a lower variability in summer*** with more than 50% of the days with values lower than 31.25% (clear sky days) ***and a higher variability during spring season***. The values are consistent with those found by Sanchez-Lorenzo *et al*. (2009) and by Perdigão *et al*. (2017) for the same sky conditions over the Iberian Peninsula.

• **DNI forecast tends to be more accurate for lower values of *DAI*** which represents ~50% of the days in Évora. This value is consistent with the study of Freile-Aranda *et al*. (2017).

• ***The*** application of a ***post-processing methodology*** (in a daily basis) ***improves the estimation of DNI***. The ***simulated values were significantly closer of to the ground-based observations and*** errors ***where reduced in some cases*** more than **30**%.

6.

References

- Acharya, N., Chattopadhyay, S., Mohanty, U. C., Dash, S. K., Sahoo, L. N., 2013. On the BIAS correction of general circulation model output for Indian summer monsoon. Meteorological Applications 20 (3), 349-356, doi: 10.1002/met.1294.
- Alados-Arboledas, L., H. Lyamani, and F. J. Olmo., 2003. Aerosol size properties at Armilla, Granada (Spain). Quarterly Journal of the Royal Meteorological Society 129.590, 1395-1414, doi: 10.1256/qj.01.207.
- Alapaty, K., Herwehe, J. A., Otte, T. L, C Nolte, G., Bullock, O. R., Mallard, M. S., Kain, J. S., Dudhia, J., 2012. Introducing subgrid-scale cloud feedbacks to radiation for regional meteorological and climate modelling. Geophys. Res. Lett. 39, L24809, doi:10.1029/2012GL054031.
- Albrecht, B.,1989. Aerosols, cloud microphysics, and fractional cloudiness. Science 245, 1227 – 1230, doi:10.1126/science.245.4923.1227.
- Alexandersson H., 1986. A homogeneity test applied to precipitation data. Journal of Climatology 6, 661–675.
- Alexandru, A., de Elia, R., Laprise, R., Separovic, L., Biner, S., 2008. Sensitivity study of regional climate model simulations to largescale nudging parameters. Mon Wea Rev 137, 1666–1686, doi:10.1175/2008MWR2620.1.
- Almorox, J., Ovando, G., Sayago, S., Bocco, M.,. 2017. Assessment of surface solar irradiance retrieved by CERES. International Journal of Remote Sensing 38, 12, 3669-3683. http://dx.doi.org/10.1080/01431161.2017.1302111.
- Alpert, P, Kishcha P, Kaufman YJ, Schwarzbard R., 2005. Global dimming or local dimming?: Effect of urbanization on sunlight availability. Geophys. Res. Lett. 32, L17802: doi:10.1029/2005GL023320.

- Alpert, P, Kishcha P., 2008. Quantification of the effect of urbanization on solar dimming. Geophys. Res. Lett. 35, L08801: doi:10.1029/2007GL033012.
- Alsamamra, H., Ruiz-Arias, J. A., Pozo-Vázquez, D., Tovar-Pescador, J., 2009. A comparative study of ordinary and residual kriging techniques for mapping global solar radiation over southern Spain. Agricultural and Forest meteorology 149 (8), 1343-1357, https://doi.org/10.1016/j.agrformet.2009.03.005.
- Angstrom, A. K., 1924. Solar and terrestrial radiation. Q. J. Roy. Meteorol. Soc. 50, 121–126. http://dx.doi.org/10.1002/qj.49705021008.
- Antón, M., *et al*., 2012. Global and diffuse shortwave irradiance during a strong desert dust episode at Granada (Spain). Atmospheric Research 118: 232-239, doi:10.1016/j.atmosres.2012.07.007.
- Antón, M., R. Román, A. Sanchez-Lorenzo, J. Calbó, J.M. Vaquero, 2017. Variability analysis of the reconstructed daily global solar radiation under all-sky and cloud-free conditions in Madrid during the period 1887-1950. Atmospheric Research 191, 94-100, http://dx.doi.org/10.1016/j.atmosres.2017.03.013.
- Argüeso, D., J. M. Hidalgo-Muñoz, S. R. Gámiz-Fortis, M. J. Esteban-Parra and Y. Castro-Díez, 2012. Evaluation of WRF mean and extreme precipitation over Spain: Present climate (1970–99). J. Climate 25, 4883–4897, doi:10.1175/JCLI-D-11-00276.1.
- Arrillaga, J.A., Yagüe, C., Sastre, M. and Román-Cascón, C.,2016. A characterization of sea-breeze events in the eastern Cantabrian coast (Spain) from observational data and WRF simulations. Atmospheric Research 181, 265–280,doi.org/10.1016/j.atmosres.2016.06.021.
- Asplund, M., Grevesse, N., Sauval, A.J., Scott, P., 2009.The chemical composition of the Sun. Annu. Rev. Astron. Astrophys. 47, 481
- Augustine, J. A., and E. G. Dutton. 2013. Variability of the surface radiation budget over the United States from 1996 through 2011 from high-quality measurements. J. Geophys. Res. Atmos. 118, 43–53, doi:10.1029/2012JD018551.
- Avolio, E., Torcasio, R. C., Lo Feudo, T., Calidonna, C. R., Contini, D., and Federico, S., 2016. Improvement of Solar and Wind forecasting in southern Italy through a multi-model approach: preliminary results. Adv. Sci. Res. 13, 69-73, https://doi.org/10.5194/asr-13-69-2016.
- Ayeta, A., Tandeo, P., 2018. Nowcasting solar irradiance using an analog method and geostationary satellite images. Solar Energy, Volume 164, Pages 301-315, https://doi.org/10.1016/j.solener.2018.02.068.

- Banks, R. F. and Baldasano, J. M., 2016. Impact of WRF model PBL schemes on air quality simulations over Catalonia Spain. Sci. Total Environ. 572, 98–113, https://doi.org/10.1016/j.scitotenv.2016.07.167.
- Berger, A., Loutre, M.F., 1991. Insolation values for the climate of the last 10 million years. Quaternary Science Reviews, Volume 10, Issue 4, Pages 297-317, https://doi.org/10.1016/0277-3791(91)90033-Q.
- Berrisford, P., Dee, D., Fielding, K., Fuentes, M., Kallberg, P., Kobayashi, S., Uppala, S., 2009. The ERA-Interim Archive. ERA Report Series. 1. Technical Report. European Centre for Medium-Range Weather Forecasts, Shinfield Park, Reading, pp16.
- Betts A.K., 1986. A new convective adjustment scheme. Part I: Observational and theoretical basis. Quart. J. Roy. Meteor. Soc. 112, 677–691.
- Betts, A.K., Miller, M.J., 1986. A new convective adjustment scheme. Part II: Single column tests using GATE wave, BOMEX, and arctic air-mass data sets. Quart. J. Roy. Meteor. Soc. 112, 693–709.
- Betts, AK, Zhao M., Dirmeyer PA, Beljaars ACM., 2006. Comparison of ERA–40 and NCEP/DOE near-surface data sets with other ISLSCP-II data sets. J. Geophys. Res. 111, D22S04, doi:10.1029/2006JD007174.
- Bijarniya JP, Sudhakar K, Baredar P., 2016. Concentrated solar power technology in India: A review. Renew Sustain Energy Rev 63, 593–603, https://doi.org/10.1016/j.rser.2016.05.064
- Bromwich, D. H., R. L. Fogt, K. I. Hodges, and J. E. Walsh, 2007. A tropospheric assessment of the ERA–40, NCEP, and JRA-25 global reanalyses in the polar regions. J. Geophys. Res. 112, D10111, doi:10.1029/2006JD007859.
- Buishand, T., 1982. Some methods for testing the homogeneity of rainfall records, J. Hydrol. 58, 11–27.
- Cardoso, R. M., Soares, P. M. M., Miranda, P. M. A., Belo-Pereira, M., 2013. WRF high resolution simulation of Iberian mean and extreme precipitation climate. International Journal of Climatology 33 (11), 2591-2608, DOI: 10.1002/joc.3616.
- Cardoso Pereira, S.; Marta Almeida, M.; Carvalho, A.C.; Rocha, A., 2019. Extreme precipitation events under climate change in the Iberian Peninsula. Int. J. Climatol., Volume 40, Issue 2 , https://doi.org/10.1002/joc.6269.
- Carrol, B. and Ostlie, D., An Introduction to Modern Astrophysics, Addison-Wesley publishing company, 1996. ISBN: 0201547309

- Casado-Rubio, J., Revuelta, M., Postigo, M., Martínez-Marco, I., and Yagüe, C. A., 2017. Post-processing Methodology for Direct Normal Irradiance Forecasting Using Cloud Information and Aerosol Load Forecasts, J. Appl. Meteorol. Clim. 56, 1595–1608, https://doi.org/10.1175/JAMC-D-16-0297.1.
- Caselles, V., Estrela,M.J., Miró, JJ, 2018. Comparative assessment of RAMS and WRF short-term forecasts over Eastern Iberian Peninsula using various in-situ observations, remote sensing products and uncoupled land surface model datasets. Atmospheric Research, Volume 213,, Pages 476-491, https://doi.org/10.1016/j.atmosres.2018.06.022.
- Chai, T. and Draxler, R. R., 2014. Root mean square error (RMSE) or mean absolute error (MAE)? – Arguments against avoiding RMSE in the literature, Geosci. Model Dev. 7, 1247-1250, https://doi.org/10.5194/gmd-7-1247-2014.
- Chan, N. L. A., 2013. Solar Electricity from Concentrator Photovoltaic System (Doctoral dissertation). Retrieved from https://spiral.imperial.ac.uk/bitstream/10044/1/14206/1/Chan-NLA-2013-PhD-Thesis.pdf
- Chen, Wei-Dong , Cui, Fang, Zhou, Hai, Ding, Huang, Li, Deng-Xuan, 2017. Impacts of different radiation schemes on the prediction of solar radiation and photovoltaic power. Atmospheric and Oceanic Science Letters 10:6, 446-451, DOI: 10.1080/16742834.2017.1394780.
- Chiacchio M, Ewen T, Wild M, Arabini E., 2010. Influence of climate shifts on decadal variations of surface solar radiation in Alaska. Climate and Dynamics, Volume 115, Issue D10, doi: 10.1029/2009JD012533.
- Chiacchio, M., and M. Wild., 2010. Influence of NAO and clouds on long-term seasonal variations of surface solar radiation in Europe. J. Geophys. Res. 115, D00D22, doi:10.1029/2009JD012182.
- Chineke, T., 2008. Equations for estimating global solar radiation in data sparse regions. Renewable Energy 33(4), 827-831, DOI: 10.1016/j.renene.2007.01.018.
- Choi, M., Jacobs, J. M., Kustas, W. P., 2008. Assessment of clear and cloudy sky parameterizations for daily downwelling longwave radiation over different land surfaces in Florida. USA. Geophys. Res. Lett. 35, L20402, doi:10.1029/2008GL035731.
- Cislaghi M, De Michele C, Ghezzi A, Rosso, R., 2005. Statistical assessment of trends and oscillations in rainfall dynamics. Analysis of long daily Italian series. Atmospheric Research, Volume 77, Issues 1-4, Pages 188-202, doi:10.1016/j.atmosres.2004.12.014.

- Coakley, James A. and Yang, Ping. Atmospheric Radiation: A Primer with Illustrative Solutions, 1st Edition, Wiley Series in Atmospheric Physics and Remote Sensing, 2014. ISBN: 9783527410989
- Collins, W. D., Rasch, P. J., Boville, B. A., Hack, J. J., McCaa, J. R., Williamson, D. L., and Zhang, M., 2004. Description of the NCAR community atmosphere model (CAM 3.0). NCAR Tech. Note NCAR/TN-464+ STR, 226.
- Cossu, F., Hocke, K., 2014. Influence of microphysical schemes on atmospheric water in the Weather Research and Forecasting model. Geoscientific Model Development 7(1), 147-160.
- Cravidão F, Matos, MA. 1990. A população portuguesa dos anos 60 ao final do século xx: o envelhecimento acelerado. in Cadernos de Geografia, n. 9, Coimbra, pp. 35-48.
- Crawford, T. M., Duchon, C. E.,1999. An improved parameterization for estimating effective atmospheric emissivity for use in calculating daytime downwelling longwave radiation. J. Appl. Meteorol. 38, 474–480.
- Cusworth, D. H., Mickley, L. J., Leibensperger, E. M., and Iacono, M. J., 2017. Aerosol trends as a potential driver of regional climate in the central United States: evidence from observations. Atmos. Chem. Phys. 17, 13559-13572, https://doi.org/10.5194/acp-17-13559-2017.
- Dasari, H. P., Salgado, R., Perdigao, J., Challa, V. S., 2014. A Regional Climate Simulation Study Using WRF-ARW Model over Europe and Evaluation for Extreme Temperature Weather Events. International Journal of Atmospheric Sciences, Article ID: 704079, 22 p.
- Deardorff, J. W., 1978. Efficient prediction of ground surface temperature and moisture, with inclusion of a layer of vegetation. Journal of Geophysical Research: Oceans 83 (C4), 1889-1903.
- Diagne, M., David, M., Boland, J., Schmutz, N., Lauret, P., 2014. Post-processing of solar irradiance forecasts from WRF model at Reunion Island. Solar Energy 105, 99–108.
- Dorvlo, A. S.S., Jervase, J. A., Al-Lawatib, A., 2002. Solar radiation estimation using artificial neural networks, Applied Energy, Volume 71, Issue 4, Pages 307-319, https://doi.org/10.1016/S0306-2619(02)00016-8.
- Du, Hu, Jones, Phillip John and Lannon, Simon Charles. Creating localised near future weather data for predicting the performance of buildings in the UK. Presented at: The 12th REHVA World Congress CLIMA 2016, Aalborg, Denmark, 22-25 May 2016. Published

in: Heiselberg, P. K. ed. CLIMA 2016 - 12th REHVA World Congress, 22-25 May 2016, Aalborg, Denmark. Aalborg: Aalborg University, Department of Civil Engineering, p. 537.

- Dudhia, J., 2014. A history of mesoscale model development. Asia-Pacific Journal of Atmospheric Sciences 50 (1), 121-131, DOI:10.1007/s13143-014-0031-8.
- Eddy, J. 1976. The Maunder Minimum. Science 192, 1189-1202. http://dx.doi.org/10.1126/science.192.4245.1189.
- Ehnberg, J. S., Bollen, M. H., 2005. Simulation of global solar radiation based on cloud observations. Solar Energy 78 (2), 157-162, DOI: 10.1016/j.solener.2004.08.016.
- Ehret, U., Zehe, E., Wulfmeyer, V., Warrach-Sagi, K., Liebert, J., 2012. Should we apply BIAS correction to global and regional climate model data?. Hydrology and Earth System Sciences 16 (9), 3391-3404, doi: 10.5194/hess-16-3391-2012.
- Enriquez-Alonso, A., Sanchez-Lorenzo, A., Calbó, J., González, J.A., Norris, J. R., 2015. Cloud cover climatologies in the Mediterranean obtained from satellites, surface observations, reanalyses, and CMIP5 simulations: validation and future scenarios. Climate Dynamics, p1-21, doi: 10.1007/s00382-015-2834-4.
- Escobar, R. A., Cortés, C., Pino, A., Salgado, M., Pereira, E. B., Martins, F. R., Boland, J., Cardemil, J. M., 2015. Estimating the potential for solar energy utilization in Chile by satellite-derived data and ground station measurements. Solar Energy 121, 139-151. http://doi.org/10.1016/j.solener.2015.08.034.
- Feser, F., Rockel, B., Von Storch, H., Winterfeldt, J., Zahn, M., 2011. Regional climate models add value to global model data: a review and selected examples. Bulletin of the American Meteorological Society 92 (9), 1181, https://doi.org/10.1175/2011BAMS3061.1.
- Flemming, J., Benedetti, A., Inness, A., Engelen, R. J., Jones, L., Huijnen, V., *et al*., 2017. The CAMS interim reanalysis of carbon monoxide, ozone and aerosol for 2003–2015. Atmospheric Chemistry and Physics 17, 1945–1983.
- Folini, D., and Wild, M., 2011. Aerosol emissions and dimming/brightening in Europe: Sensitvity studies with ECHAM5-HAM. J. Geophys. Res. 116, D21104, doi:10.1029/2011JD016227.
- Fonseca, D., Carvalho, M. J., Marta-Almeida, M., Melo-Gonçalves, P. & Rocha, A., 2016. Recent Trends of Extreme Temperature Indices for the Iberian Peninsula. Physics and Chemistry of the Earth, Parts A/B/C, 94, 66-76, https://doi.org/10.1016/j.pce.2015.12.005.
- Fouquart, Y., and Bonnel, B., 1980. Computation of solar heating of the Earth's atmosphere: A new parameterization. Beitr. Phys. Atmos., 53, 35–62.

- Fragoso, Marcelo, *et al*., 2010. The exceptional rainfall event in Lisbon on 18 February 2008. Weather 65.2: 31-35.
- Freile-Aranda, M. D., Gomez-Amo, J. L., Utrillas, M. P., Pedros R. and Martínez-Lozano. J. A., 2017. Seasonal analysis of cloud characteristics and radiative effect over the Iberian Peninsula using MODIS-CERES observations. Tethys, 14, 3–9. DOI:10.3369/tethys.2017.14.01.
- Fu, Q., 1996. An accurate parameterization of the solar radiative properties of cirrus clouds. Journal of Climate 9, 2058–2082.
- Gaetani, M., Huld, T., Vignati, E., Monforti-Ferrario, F., Dosio, A., & Raes, F., 2014. The near future availability of photovoltaic energy in Europe and Africa in climate-aerosol modeling experiments. Renewable and Sustainable Energy Reviews 38, 706-716. http://doi.org/10.1016/j.rser.2014.07.041.
- Gala, Y., Fernandez, A., Dıaz, J., Dorronsoro, J., 2013. Support vector forecasting of solar radiation values. In: Pan, J.-S., Polycarpou, M., Wozniak, M., Carvalho, A.P.L.F., Quintian, H., Corchado, E. (Eds.), Hybrid Artificial Intelligent Systems. Springer, Berlin Heidelberg, pp. 51–60.
- García, R. D., Cuevas, E., García, O. E., Cachorro, V. E., Pallé, P., Bustos, J. J., Romero-Campos, P. M., de Frutos, A. M., 2014. Reconstruction of global solar radiation time series from 1933 to 2013 at the Izaña Atmospheric Observatory. Atmos. Meas. Tech. 7, 3139-3150, doi:10.5194/amt-7-3139-2014.
- Gil, Victoria, *et al*., 2015. Analysis of interannual variability of sunshine hours and precipitation over Peninsular Spain. Renewable Energy 83, 680-689, doi:10.1016/j.renene.2015.05.001.
- Gilgen, H., Wild, M. and Ohmura, A. ,1998. Means and trends of shortwave irradiance at the surface estimated from Global Energy Balance Archive Data. J. Clim. 11, 2042 – 2061, doi:10.1175/1520-0442-11.8.2042.
- Giorgi, F., Mearns, L. O., 1999. Introduction to special section: Regional Climate Modeling Revisited. J. Geophys. Res. 104 (D6), 6335–6352, doi:10.1029/98JD02072.
- Gomez-Gil, F. J., Wang, X., & Barnett, A., 2012. Analysis and prediction of energy production in concentrating photovoltaic (CPV) installations. Energies 5(3), 770-789. doi:10.3390/en5030770.

- González-Rojí, S., J., Sáenz, J., Argandoña, J. Díaz, 2020. Moisture Recycling over the Iberian Peninsula: The Impact of 3DVAR Data Assimilation. Atmosphere 11(1), 19; https://doi.org/10.3390/atmos11010019.
- Grell, G.A., Devenyi, D., 2002. A generalized approach to parameterizing convection combining ensemble and data assimilation techniques. Geoph. Res. Let. 29 (14), doi: 10.1029/2002GL015311
- Gubler, S., Gruber, S., Purves, R. S., 2012. Uncertainties of parameterized surface downward clear-sky shortwave and all-sky longwave radiation. Atmospheric Chemistry and Physics 12 (11), 5077-5098.
- Haddeland, I., Heinke, J., Voß, F., Eisner, S., Chen, C., Hagemann, S., Ludwig, F., 2012. Effects of climate model radiation, humidity and wind estimates on hydrological simulations. Hydrology and Earth System Sciences 16 (2), 305-318, doi:10.5194/hess-16-305-2012.
- Hagemann, S., Chen, C., Haerter, J. O., Heinke, J., Gerten, D., Piani, C., 2011. Impact of a statistical BIAS correction on the projected hydrological changes obtained from three GCMs and two hydrology models. Journal of Hydrometeorology 12 (4), 556-578, http://dx.doi.org/10.1175/2011JHM1336.1.
- Haiden, T., M. J. Rodwell, D. S. Richardson, A. Okagaki, T. Robinson, and T. Hewson. 2012. Intercomparison of global model precipitation forecast skill in 2010/11 using the SEEPS score. Mon. Wea. Rev., 140, 2720–2733, https://doi.org/10.1175/MWR-D-11-00301.1.
- Hakuba, M. Z., D. Folini, A. Sanchez-Lorenzo, and M. Wild. 2014. Spatial representativeness of ground-based solar radiation measurements—Extension to the full Meteosat disk, J. Geophys. Res. Atmos., 119, doi:10.1002/2014JD021946.
- Hammer, A., *et al*., 2003. Solar energy assessment using remote sensing technologies. Remote Sensing of Environment, 86, 423–432.
- Hansen, J., M. Sato, and R. Ruedy, 1997: Radiative forcing and climate response. J. Geophys. Res., 102, 6831-6864, doi:10.1029/96JD03436.
- Haylock, M.R., Hofstra, N., Tank A.M.G. K., Klok E.J., Jones P.D., New, M., 2008. A European daily high-resolution gridded dataset of surface temperature and precipitation. J. Geophys. Res. Atmospheres 113, D20119, doi:10.1029/2008JD10201.

- Haywood, J., and Boucher, O. 2000. Estimates of the direct and indirect radiative forcing due to tropospheric aerosols: A review, Rev. Geophys. 38(4), 513–543, doi:10.1029/1999RG000078.
- He, Y., Wang, K., Zhou, C., & Wild, M., 2018. A revisit of global dimming and brightening based on the sunshine duration. Geophysical Research Letters, 45, 4281–4289. https://doi.org/10.1029/2018GL077424.
- Hinrichsen, K., 1994. The Ångström formula with coefficients having a physical meaning. Solar Energy 52, Pages 491-495, https://doi.org/10.1016/0038-092X(94)90656-4.
- Hogan, R. J., and Bozzo, A., 2016. ECRAD: A new radiation scheme for the IFS. ECMWF Technical Memorandum 787, 33 pp.
- Hong, S-Y., J. Dudhia, and S.H. Chen, 2004. A revised approach to ice microphysical processes for the bulk parameterization of clouds and precipitation. Mon. Weather Rev. 132, 103 – 120.
- Hong S-Y., Lim J-OJ, 2006. The WRF single-moment 6-class microphysics scheme (WSM6). J. Korean Meteorol. Soc. 42, 129–151.
- Hong, S-Y. Noh, Dudhia, J., 2006. A new vertical diffusion package with an explicit treatment of entrainment processes. Mon. Wea. Rev. 134, 2318–2341, doi:10.1175/MWR3199.1.
- Hong, S-Y., Chang, E-C., 2012. Asia-Pacific J. Atmos. Sci. 48, 345-355 doi:10.1007/s13143-012-0033-3.
- Hong, S-Y. and Kanamitsu, M., 2014. Asia-Pacific J, Atmos, Sci, 50: 83, doi:10.1007/s13143-014-0029-2
- Hurrell, JW., 1995. Decadal Trends in the North Atlantic Oscillation: Regional Temperatures and Precipitation. Science, Vol. 269, pp.676-679.
- Hurrell, JW., 1996. Influence of Variations in Extratropical Wintertime Teleconnections on Northern Hemisphere Temperatures. Geophysical Research Letters, Vol. 23, No. 6, pp.665-668.
- Imbrie, J., Imbrie, J.Z. 1980. Modeling the climatic response to orbital variations. Science, v. 207, p.943-953. https://www.jstor.org/stable/1683550.
- Inman, Rich H., Pedro, H., Coimbra F.M., 2013. Solar forecasting methods for renewable energy integration. Progress in Energy and Combustion Science Volume 39, Issue 6, 535-576, https://doi.org/10.1016/j.pecs.2013.06.002.

- IPCC, 2014: Summary for Policymakers. In: Climate Change 2014: Mitigation of Climate Change. Contribution of Working Group III to the Fifth Assessment Report of the Intergovernmental Panel on Climate Change [Edenhofer, O., R.Pichs-Madruga, Y. Sokona, E. Farahani, S. Kadner, K. Seyboth, A. Adler, I. Baum, S. Brunner, P. Eickemeier, B. Kriemann, J.Savolainen, S. Schlömer, C. Von Stechow, T. Zwickel and J.C. Minx (eds.)]. Cambridge University Press, Cambridge, United Kingdom and New York, NY, USA.
- Iqbal, M. An Introduction to Solar Radiation. Academic Press, 1975. New York.
- Islam, Shahid, Dincer, Ibrahim, Yilbas Bekir Sami, 2018. Development, analysis and assessment of solar energy-based multigeneration system with thermoelectric generator. Energy Conversion and Management, Volume 156, Pages 746-756, https://doi.org/10.1016/j.enconman.2017.09.039.
- ISO. (1990). ISO 9060:1990: Specification and Classification of Instruments for Measuring Hemispherical Solar and Direct Solar Radiation. Geneva, Switzerland.
- Jafariserajehlou, S., Mei, L., Vountas, M., Rozanov, V., Burrows, J. P., and Hollmann, R., 2019. A cloud identification algorithm over the Arctic for use with AATSR–SLSTR measurements. Atmos. Meas. Tech. 12, 1059-1076, https://doi.org/10.5194/amt-12-1059-2019.
- Jahani, B., Dinpashoh, Y., Wild, M., 2017. Dimming in Iran since the 2000s and the potential underlying causes. International Journal of Climatology, Volume38, Issue3, Pages 1543-1559, https://doi.org/10.1002/joc.5265.
- Janjic ZI, 2001. Nonsingular implementation of the Mellor–Yamada level 2.5 scheme in the NCEP meso model. NCEP office note 437, 61 pp
- Janjic ZI., 1990. The step-mountain coordinate: physical package. Mon. Weather Rev. 118, 1429–1443.
- Janjic ZI., 1994. The step-mountain eta coordinate model: further developments of the convection, viscous sublayer and turbulence closure schemes. Mon. Weather Rev. 122, 927–945.
- Janjic ZI., 2000. Comments on development and evaluation of a convection scheme for use in climate models. J. Atmos. Sci. 57, 3686.
- Janjic, Z. I., 2003. A nonhydrostatic model based on a new approach. Meteorol. Atmos. Phys. 82, 271-–285.

- Jerez, S., Trigo, R. M., Sarsa, A., Lorente-Plazas, R., Pozo-Vázquez, D., Montávez, J. P., 2013. Spatio-temporal complementarity between solar and wind power in the Iberian Peninsula. Energy Procedia 40, 48-57.
- Jiménez, P. A. and Dudhia, J., 2013. On the Ability of the WRF Model to Reproduce the Surface Wind Direction over Complex Terrain. J. Appl. Meteorol. Clim., 52, 1610–1617, doi:10.1175/JAMC-D12-0266.1, 2013.
- Jimenez, P. A., Hacker, J. P., Dudhia, J., Ellen Haupt, S., Ruiz-Arias, J. A., Gueymard, C. A., Thompson, G., Eidhammer, T., and Deng, A. 2016. WRF-Solar: An augmented NWP model for solar power prediction - Model description and clear sky assessment, Bulletin of the American Meteorological Society, 97, 1249–1264, https://doi.org/10.1175/BAMS-D-14-00279.1.
- Jones R.G., Murphy, J.M., Noguer, M., 1995. Simulation of climate change over Europe using a nested regional-climate model. I: Assessment of control climate, including sensitivity to location of lateral boundaries. Quart. J. Roy. Meteor. Soc. 121, 1413–1449.
- Kalnay, E., Kanamitsu, M., Kistler, R., Collins, W., Deaven, D., Gandin, L., Iredell, M., Saha, S., White, G., Woollen, J., Zhu, Y., Chelliah, M., Ebisuzaki, W., Higgins, W., Janowiak, J., Mo, K.C., Ropelewski, C., Wang, J., Leetmaa, A., Reynolds, R., Jenne, R., Joseph, D., 1996. The NCEP/NCAR 40-year reanalyses projects. Bull. Am. Meteorol. Soc. 77, 437–471.
- Kato, S., Loeb, N. G., Rose, F. G., Doelling, D. R., D., Rutan, A., Caldwell, T. E., Yu, L., Weller, R. A., 2013. Surface irradiances consistent with CERES-derived top-of-atmosphere shortwave and longwave irradiances. J. Climate 26, 2719–2740.
- Kaurola, J, Lindfors A, Lakkala K, Hansen G, Josefsson W, Vuilleumier L, Feister U, Slaper H. 2010. On the usability of the ERA–40 reanalysis in the estimation of past surface UV radiation over Europe. J. Geophys. Res., 115, D24107, doi:10.1029/2010JD013810.
- Khaliq, M. N., and T. B. M. J. Ouarda. 2007. Short communication on the critical values of the standard normal homogeneity test (SNHT). Int J Climatol. 27.5: 681-687.
- Kiehl, J. T., and K. E. Trenberth, 1997. Earth's Annual Global mean energy budget, BAMS 78(2), 197–208.
- Kraas, B.; Schroedter-Homscheidt, M.; Madlener, R., 2013. Economic Merits of a State-ofthe-Art Concentrating Solar Power Forecasting System for Participation in the Spanish Electricity Market. Solar Energy (93), pp. 244–255.

- Landelius, T., Lindskog, M., Körnich, H., & Andersson, S., 2018. Short-range solar radiation forecasts over Sweden. Advances in Science and Research 15, 39-44. https://www.adv-sci-res.net/15/39/2018/asr-15-39-2018.pdf.
- Laprise, René, 2008. Regional climate modelling. Journal of Computational Physics 227 (7), 3641-3666.
- Lara-Fanego, V., Ruiz-Arias, J.A., Pozo-Vázquez., A. D., Gueymard, C. A., Tovar-Pescador, J., 2012a. Evaluation of DNI forecast based on the WRF mesoscale atmospheric model for CPV applications. In AIP Conference Proceedings-American Institute of Physics, vol. 1477, no. 1, p. 317, http://dx.doi.org/10.1063/1.4753895.
- Lara-Fanego, V., Ruiz-Arias, J. A., Pozo-Vázquez, D., Santos-Alamillos, F. J., Tovar-Pescador, J., 2012b. Evaluation of the WRF model solar irradiance forecasts in Andalusia (southern Spain). Solar Energy 86 (8), 2200-2217, doi:10.1016/j.solener.2011.02.014.
- Law, E. W., Prasad, A. A., Kay, M., & Taylor, R. A. 2014. Direct normal irradiance forecasting and its application to concentrated solar thermal output forecasting–A review. Solar Energy 108, 287-307. http://doi.org/10.1016/j.solener.2014.07.008.
- Lee, Hyun-Jin; Kim, Shin-Young; Yun, Chang-Yeol. 2017. Comparison of Solar Radiation Models to Estimate Direct Normal Irradiance for Korea. Energies 10, no. 5: 594. doi:10.3390/en10050594.
- Leite, F., Gonçalves, A., Lourenço, L. 2014. Grandes Indêndios na Década de 60 do Século XX, em Portugal Continental, Territorium, 21, ISBN: 0872-8941.
- Liepert BG. 2002. Observed reductions of surface solar radiation at sites in the United States and worldwide from 1961 to 1990. Geophysical Research Letters, 29, NO 10, 1421, doi: 10.1029/2002GL014910.
- Liepert, B, Tegen I. 2002. Multi-decadal solar radiation trends in the United States and Germany and direct tropospheric aerosol forcing. Journal of Geophysical Research, 107 (12), 4153. doi:10.1029/2001JD000760.
- Liley, JB. 2009. New Zealand dimming and brightening, Journal of Geophys. Res., 114, D00D10, doi:10.1029/2008JD01140.
- Lima, Francisco J.L. & Martins, Fernando R. & Pereira, Enio B. & Lorenz, Elke & Heinemann, Detlev, 2016. Forecast for surface solar irradiance at the Brazilian Northeastern region using NWP model and artificial neural networks. Renewable Energy, Elsevier, vol. 87(P1), pages 807-818.

- Liou, K. N. An Introduction to Atmospheric Radiation, 2nd Edition. Academic Press. 2002, ISBN: 9780124514515
- Liu C, Liu X, Zheng H, Zeng Y. 2010. Change of the solar radiation and its causes in the Haihe River Basin and surrounding areas. Journal of Geographical Sciences, 20, Issue 4, 569-580, doi: 10.1007/s11442-010-0569-z.
- Lo, J. C. F., Yang, Z. L., Pielke Sr., R. A., 2008. Assessment of three dynamical climate downscaling methods using the Weather Research and Forecasting (WRF) model. J. Geophys. Res. 113, D09112, doi:10.1029/2007JD009216.
- Lohmann, U. and Feichter, J., 2005. Global indirect aerosol effects: a review. Atmos. Chem. Phys., 5, 715-737, doi:10.5194/acp-5-715-2005.
- Long, C.N., Dutton, E.G., 2010. BSRN Global Network recommended QC tests, V2. J. Clim., 25, 8542–8567. https://doi.org/10.1175/JCLI-D-11-00618.1
- Lopes, F., Silva, H., Salgado, R., Cavaco, A., Canhoto, P., Colarres-Pereira, M., 2018. Short-term forecasts of GHI and DNI for solar energy systems operation: assessment of the ECMWF integrated forecasting system in southern Portugal. Solar Energy 170, 14-30. https://doi.org/10.1016/j.solener.2018.05.039
- Lopes, M., 2015. Desenvolvimento de um sistema de baixo custo para a previsão da irradiância solar a curto prazo (Master thesis dissertation. Retrieved from http: https://fenix.tecnico.ulisboa.pt/downloadFile/281870113702447/Dissertacao_67932.pdf
- Lorenz, E., Remund, J., Müller, S. C., Traunmüller, W., Steinmaurer, G., Pozo, D., and Kurz, C., 2009. Benchmarking of different approaches to forecast solar irradiance. In 24th European photovoltaic solar energy conference, Hamburg, Germany (Vol. 21, p. 25).
- Magarreiro C., Brito, M.C. and Soares, P.M.M., 2014. Assessment of diffuse radiation models for cloudy atmospheric conditions in the Azores region. Solar Energy 108, 538-547.
- Magarreiro, C., 2016. Solar Energy Potential in a Changing Climate: Iberia and Azores Assessment Combining Dynamical and Statistical Downscaling Methods (Doctoral dissertation). Retrieved from http: // repositorio.ul.pt/bitstream/10451/25379/1/ulsd730076_td_Clarisse_Magarreiro.pdf
- Manara, V., M. C. Beltrano, M. Brunetti, M. Maugeri, A. Sanchez-Lorenzo, C. Simolo, and S. Sorrenti, 2015. Sunshine duration variability and trends in Italy from homogenized instrumental time series (1936–2013). J. Geophys. Res. Atmos. 120, 3622–3641. doi:10.1002/2014JD022560.
- Mann, H. B., Econometrica 1945.The Econometric Society, v.13, n.3, p.245-259.

- Mao, F., Pan, Z., Wang, W., Lu, X., and Gong, W., 2017. Estimating the effects of aerosol, cloud, and water vapor on the recent brightening in India during the monsoon season. Atmos. Chem. Phys. Discuss., https://doi.org/10.5194/acp-2017-429.
- Marteau, R., Richard, Y., Pohl, B., Smith, C. C., Castel, T., 2015. High-resolution rainfall variability simulated by the WRF RCM: application to eastern France. Climate Dynamics 44 (3-4), 1093-1107.
- Martín, L., Zarzalejo, L. F., Polo, J., Navarro, A., Marchante, R., Cony, M., 2010. Prediction of global solar irradiance based on time series analysis: Application to solar thermal power plants energy production planning. Solar Energy 84 (10), 1772-1781, doi: 10.1016/j.solener.2010.07.002.
- Mateos, D, Sanchez-Lorenzo A, Antón M, Cachorro VE, Calbó J, Costa MJ, Torres B, Wild M. 2014a. Quantifying the respective roles of aerosols and clouds in the strong brightening since the early 2000s over the Iberian Peninsula. J. Geophys. Res. Atmos., 119, 10, 382–10,393, doi:10.1002/2014JD022076.
- Mateos, D., Antón, M., Toledano, C., Cachorro, V. E., Alados-Arboledas, L., Sorribas, M., Costa, M. J., Baldasano, J. M., 2014b. Aerosol radiative effects in the ultraviolet, visible, and near-infrared spectral ranges using long-term aerosol data series over the Iberian Peninsula. Atmos. Chem. Phys. 14, 13497-13514, https://doi.org/10.5194/acp-14-13497-2014.
- Mejia, J. F., Giordano, M., and Wilcox, E., 2018. Conditional summertime day-ahead solar irradiance forecast. Solar Energy 163, 276 610–622, doi.org/10.1016/j.solener.2018.01.094.
- Mellit, Adel; Pavan, Alessandro Massi, 2010. A 24-h forecast of solar irradiance using artificial neural network: Application for performance prediction of a grid-connected PV plant at Trieste, Italy. Solar Energy, vol. 84, issue 5, pp. 807-821, DOI: 10.1016/j.solener.2010.02.006.
- Mercader, J., Codina, B., Sairouni, A., Cunillera, J., 2010. Results of the Meteorological Model WRF-ARW over Catalonia using different parameterizations of convection and cloud microphysics. Tethys 7, 75-86, http://dx.doi.org/10.3369/tethys.2010.7.07.
- Miguez-Macho G., Stenchikov, GL, Robock, A., 2004. Spectral nudging to eliminate the effects of domain position and geometry in regional climate model simulations. J. Geophys. Res. 109, D13104, doi:10.1029/2003JD004495..

- Miranda PMA., Valente MA, Tomé AR, Trigo R, Coelho MF, Aguiar A, Azevedo EB, O clima de Portugal nos séculos XX e XXI 2006. in Santos e Miranda (eds), 47-113, Gradiva.
- Morcrette, J.-J.; Barker, H.; Cole, J.; Iacono, M.; Pincus, R., 2008.Impact of a new radiation package, mcrad, in the ecmwf integrated forecasting system. Mon. Weather Rev 2008, 136, 4773–4798.
- Moriasi, D. N., Arnold, J. G., Van Liew, M. W., Binger, R. L., Harmel, R. D., and Veith, T., 2007. Model evaluation guidelines for systematic quantification of accuracy in watershed simulations. Trans. ASABE 50 (3): 885-900.
- Morozova, Anna L., Valente, Maria Antónia, 2012. Homogenization of Portuguese long-term temperature data series: Lisbon, Coimbra and Porto. Earth System Science Data, 4, 187-213, doi:10.5194/essd-4-187-2012.
- Nabat P, Somot S, Mallet M, Sanchez-Lorenzo A, Wild M., 2014. Contribution of anthropogenic sulfate aerosols to the changing Euro-Mediterranean climate since 1980. Geophys Res Lett, 41:5605–5611.
- Nonnenmacher, L., Kaur, A., Coimbra, C.F.M., 2014. Verification of the SUNY direct normal irradiance model with ground measurements. Sol. Energy 99, 246–258. https://doi.org/10.1016/j.solener.2013.11.010.
- Nonnenmacher, L., Kaur, A., Coimbra, Coimbra, C., 2016. Day-ahead resource forecasting for concentrated solar power integration. Renew. Energy 86, 866–876. http://dx.doi.org/10.1016/j.renene.2015.08.068.URL:http://www.sciencedirect.com/science/article/pii/S0960148115302688>.
- Noorian, Ali Mohammad, Isaac Moradi, and Gholam Ali Kamali. 2008. Evaluation of 12 models to estimate hourly diffuse irradiation on inclined surfaces. Renewable energy, 33, 1406-1412, doi:10.1016/j.renene.2007.06.027.
- Norris J.R., Wild M. Trends in aerosol radiative effects over China and Japan inferred from observed cloud cover, solar ‘dimming’, and solar ‘brightening’. 2009. Journal of Geophysical Research;114: D00D15, doi:10.1029/2008JD011378.
- Norris, JR, Wild, M., 2007. Trends in aerosol radiative effects over Europe inferred from observed cloud cover, solar ‘‘dimming,’’ and solar ‘‘brightening’’. J. Geophys. Res., 112, D08214, doi:10.1029/2006JD007794.
- Obot NI, Chendo MAC, Udo SO, Ewona IO., 2010. Evaluation of rainfall trends in Nigeria for 30 years (1978-2007). International Journal of the Physical Sciences, Vol. 5 (14), pp. 2217-2222.

- Obregón, M.A., *et al*., 2012. Regional differences of column aerosol parameters in western Iberian Peninsula. Atmospheric Environment 62, 208-219, doi:10.1016/j.atmosenv.2012.08.016.
- Obregón, M.A., Pereira, S., Salguero, V., Costa, M. J., Silva, A. M., Serrano, A., Bortoli, D., 2015. Aerosol radiative effects during two desert dust events in August 2012 over the Southwestern Iberian Peninsula. Atmospheric Research 153, 404–415., doi:10.1016/j.atmosres.2014.10.007.
- Ohmura A. and H. Lang. 1989. Secular variation of global radiation over Europe. In: Current problems in atmospheric radiation (J. Lenoble and J. F. Geleyn, Eds.) Deepak, Hampton, VA 298-301.
- Ohmura, A. 2009. Observed decadal variations in surface solar radiation and their causes. J. Geophys. Res., 114, D00D05, doi:10.1029/2008JD011290. 31135.
- Padma, K. B., Londhe, A. L., Daniel, S., and Jadhav, D. B., 2007. Observational evidence of solar dimming: Offsetting surface warming over India. Geophysical Research Letters, 34, 377-390.
- Perdigão J, Salgado R, Magarreiro C, Soares PMM, Costa MJ., Dasari, H., 2017. An Iberian climatology of solar radiation obtained from WRF regional climate simulations for 1950–2010 period. Atmospheric Research. Available: http://dx.doi.org/10.1016/j.atmosres.2017.08.016.
- Perdigão, J. C., R. Salgado, M. J. Costa, H. P. Dasari, and A. Sanchez-Lorenzo, 2016: Variability and trends of downward surface global solar radiation over the Iberian Peninsula based on ERA-40 reanalysis. Int. J. Climatol. 36, 3917–3933, https://doi.org/10.1002/joc.4603.
- Pereira, S., Canhoto, P., Salgado, R., Costa, M.J., 2019. Development of an ANN based corrective algorithm of the operational ECMWF global horizontal irradiation forecasts. Solar Energy 185, 387–405, https://doi.org/10.1016/j.solener.2019.04.070.
- Perez, R., Elke Lorenz, Sophie Pelland, Mark Beauharnois, Glenn Van Knowe, Karl Hemker, Detlev Heinemann, Jan Remund, Stefan C. Müller, Wolfgang Traunmüller, Gerald Steinmauer, David Pozo, Jose A. Ruiz-Arias, Vicente Lara-Fanego, Lourdes Ramirez-Santigosa, Martin Gaston-Romero, Luis M. Pomares, 2013. Comparison of numerical weather prediction solar irradiance forecasts in the US, Canada and Europe. Solar Energy, Volume 94, Pages 305-326, ISSN 0038-092X, https://doi.org/10.1016/j.solener.2013.05.005.

- Persad GG, Ming Y, Ramaswamy V., 2014. The role of aerosol absorption in driving clear-sky solar dimming over East Asia. J Geophys Res-Atmos, 119:10,410–10,424.
- Pettitt, A. N. 1979. A Non-Parametric Approach to the Change-Point Problem. Appl. Stat.-J. Roy. St. C., 28, 126–135.
- Pfeifroth, U., Bojanowski, J. S., Clerbaux, N., Manara, V., Sanchez-Lorenzo, A., Trentmann, J., Walawender, J. P., and Hollmann, R. 2018a. Satellite-based trends of solar radiation and cloud parameters in Europe. Adv. Sci. Res., 15, 31-37, https://doi.org/10.5194/asr-15-31-2018.
- Pfeifroth, U., Sanchez-Lorenzo, A., Manara, V., Trentmann, J., & HollmannR., 2018b. Trends and variability of surface solar radiation in Europe based on surface- and satellite-based data records. Journal of Geophysical Research:Atmospheres, 123, 1735–1754.https://doi.org/10.1002/2017JD027418.
- Piani, C., Weedon, G. P., Best, M., Gomes, S. M., Viterbo, P., Hagemann, S., Haerter, J. O., 2010. Statistical BIAS correction of global simulated daily precipitation and temperature for the application of hydrological models. Journal of Hydrology 395, 199-215, doi:10.1016/j.jhydrol.2010.10.024.
- Pinto, L., Costa, M., Diniz, L., Sediyama, G., Pruski, E., 2010. Comparação de produtos de radiação solar incidente à superfície para a América do Sul. Revista Brasileira de Meteorologia, v.25, n.4, 469 – 478.
- Polo, J., Martin, L., Vindel, J.M., 2015. Correcting satellite derived DNI with systematic and seasonal deviations: application to India. Renewable Energy 2015, 80, 238–243. http://dx.doi.org/10.1016/j.renene.2015.02.031.
- Polo, J.; Wilbert, S.; Ruiz-Arias, J.A.; Meyer, R.; Gueymard, C.; Súri, M.; Martín, L.; Mieslinger, T.; Blanc, P.; Grant, I.; *et al*., 2016. Preliminary survey on site-adaptation techniques for satellite-derived and reanalysis solar radiation datasets. Sol. Energy 132, 25–37, https://doi.org/10.1016/j.solener.2016.03.001.
- Powers, J. G., and Coauthors, 2017. The Weather Research and Forecasting Model: Overview, system efforts, and future directions. Bull. Amer. Meteor. Soc., 98, 1717–1737, https://doi.org/10.1175/BAMS-D-15-00308.1.
- Pozo-Vázquez, D, Tovar-Pescador J, Gámiz-Fortis SR, Esteban-Parra MJ., Castro-Díez Y., 2004. NAO and solar radiation variability in the European North Atlantic region, Geophys. Res. Lett., 31, L05201, doi:10.1029/2003GL018502.

- Prescott, A., 1940. Evaporation from water surface in relation to solar radiation. Transactions of The Royal Society of South Australia, vol. 40, pp. 114–118
- Qazi, Atika, Fayaz, H., Wadi, A., Raj R. G., Rahim, N.A., Khan, W., 2015. The artificial neural network for solar radiation prediction and designing solar systems: a systematic literature review. Journal of Cleaner Production, Volume 104, Pages 1-12, https://doi.org/10.1016/j.jclepro.2015.04.041Get rights and content.
- Qian, Y, Wang W, Leung LR, Kaiser DP., 2007. Variability of solar radiation under cloud-free skies in China: The role of aerosols, Geophys. Res. Lett. 34, L12804, doi:10.1029/2006GL028800.
- Rahimzadeh, F., Sanchez-Lorenzo, A. , Hamedi, M. , Kruk, M. C. and Wild, M., 2015. New evidence on the dimming/brightening phenomenon and decreasing diurnal temperature range in Iran (1961–2009). Int. J. Climatol. 35, 2065-2079. doi:10.1002/joc.4107,
- Raju, A., Parekh, A., Chowdary, J. S., Gnanaseelan, C., 2015. Assessment of the Indian summer monsoon in the WRF regional climate model. Climate Dynamics 44 (11-12), 3077-3100, Doi 10.1007/s00382-014-2295-1.
- Ramanathan, V., 1987. The role of earth radiation budget studies in climate and general circulation research. J. Geophys. Res. 92(D4), 4075–4095, doi:10.1029/JD092iD04p04075.
- Ramos, A. M., Cortesi, N., Trigo, R. M., 2014. Circulation weather types and spatial variability of the daily precipitation in the Iberian Peninsula. Frontiers in Earth Science 2, 1-17, doi: 10.3389/feart. 00025.
- Reikard, G., 2009. Predicting solar radiation at high resolutions: A comparison of time series forecasts. Solar Energy, 83 (3), 342-349. https://doi.org/10.1016/j.solener.2008.08.007.
- Ridao, A. R., Garca, E. H., Escobar, B. M., Toro, M. Z., 2007. Solar energy in Andalusia (Spain): present state and prospects for the future. Renewable and Sustainable Energy Reviews 11 (1), 148-161.
- Rincón, Angel, Jorba, Oriol, Frutos, Miguel, Alvarez, Leopoldo, Barrios Fernando P., González, Juan A., 2018. BIAS correction of global irradiance modelled with weather and research forecasting model over Paraguay, Solar Energy 170, 201-211, https://doi.org/10.1016/j.solener.2018.05.061.
- Rios-Entenza, A., Soares, P. M., Trigo, R. M., Cardoso, R. M., Miguez-Macho, G., 2014. Moisture recycling in the Iberian Peninsula from a regional climate simulation:

Spatiotemporal analysis and impact on the precipitation regime. Journal of Geophysical Research. Atmospheres 119 (10), 5895-5912, doi: 10.1002/2013JD021274.

- Royé, D., Lorenzo, N., Rasilla, D., Martí, A., 2018. Spatio-temporal variations of cloud fraction based on circulation types in the Iberian Peninsula. International Journal of Climatology, 39, 1716-1732, DOI: 10.1002/joc.5914.
- Ruckstuhl, C., *et al*., 2008. Aerosol and cloud effects on solar brightening and the recent rapid warming, Geophys. Res. Lett. 35, L12708, doi:10.1029/2008GL034228.
- Ruiz-Arias, J. A., Terrados, J., Pérez-Higueras, P., Pozo-Vázquez, D., Almonacid, G., 2012. Assessment of the renewable energies potential for intensive electricity production in the province of Jaén, southern Spain. Renewable and Sustainable Energy Reviews 16 (5), 2994-3001, doi: 10.1016/j.rser.2012.02.006.
- Ruiz-Arias, J. A., Quesada-Ruiz, S., Fernández, E. F., Gueymard, C. A., 2015. Optimal combination of gridded and ground-observed solar radiation data for regional solar resource assessment. Solar Energy 112, 411-424, http://dx.doi.org/10.1016/j.solener.2014.12.011.
- Ruiz-Arias, J. A., Arbizu-Barrena, C., Santos-Alamillos, F. J., Tovar-Pescador, J., Pozo-Vázquez, D., 2016. Assessing the Surface Solar Radiation Budget in the WRF Model: A Spatiotemporal Analysis of the BIAS and Its Causes. Monthly Weather Review 144(2), 703-711, http://dx.doi.org/10.1175/MWR-D-15-0262.1.
- Rummukainen, M., 2010. State of the art with Regional Climate Models. Wiley Interdisciplinary Reviews: Climate Change 1 (1), 82-96.
- Russak, V. 2009. Changes in solar radiation and their influence on temperature trend in Estonia (1955–2007). J. Geophys. Res., 114, D00D01, doi:10.1029/2008JD010613.
- Salgueiro, V., Costa, M. J., Silva, A. M., Bortoli, D., 2014. Variability of the Daily-Mean Shortwave Cloud Radiative Forcing at the Surface at a Midlatitude Site in Southwestern Europe. J. Climate 27, 7769–7780, http://dx.doi.org/10.1175/JCLI-D-13-00696.1.
- Salgueiro, V., Costa, M. J., Silva, A. M., Bortoli, D., 2016. Effects of clouds on the surface shortwave radiation at a rural inland mid-latitude site. Atmospheric Research, in press.
- Sanchez-Lorenzo A, Brunetti M, Calbo J, Martin-Vide J., 2007. Recent spatial and temporal variability and trends of sunshine duration over the Iberian Peninsula from a homogenized data set. J. Geophys. Res. 112: D20115, DOI: 10.1029/2007JD008677.
- Sanchez-Lorenzo, A, Calbó J, Brunetti M, Deser C. 2009. Dimming/brightening over the Iberian Peninsula: Trends in sunshine duration and cloud cover and their relations with

atmospheric circulation. Journal of Geophysical Research, 114, D00D09, doi:10.1029/2008JD011394.

- Sanchez-Lorenzo, A, Calbó, J Wild, M. 2013a. Global and diffuse solar radiation in Spain: building a homogeneous dataset and assessing their trends. Global and Planetary Change, 100, 343- 352.
- Sanchez-Lorenzo, A., M. Wild, and J. Trentmann. 2013b. Validation and stability assessment of the monthly mean CM SAF surface solar radiation dataset over Europe against a homogenized surface dataset (1983–2005). Remote Sensing of Environment 134 : 355-366.
- Sanchez-Lorenzo, A., M. Wild, M. Brunetti, J. A. Guijarro, M. Hakuba, J. Calbó, S. Mystakidis, and B. Bartok 2015. Reassessment and update of long-term trends in downward surface shortwave radiation over Europe (1939-2012). J. Geophys. Res. Atmos., 120, doi:10.1002/2015JD023321.
- Santabàrbara, J. M., Calbó, J., Baldasano, J. M., Esteve, J., Mitjà, A.,1996. Month-to-month variation of global solar radiation in Catalonia (SPAIN). Int. J. Climatol., 16, 711–721, doi:10.1002/(SICI)1097-0088(199606)16:6<711::AID -JOC42>3.0.CO;2-M.
- Santos, J. A., Rochinha, C., Liberato, M. L. R., Reyers, M., Pinto, J. G., 2015. Projected changes in wind energy potentials over Iberia. Renewable Energy, 75, 68-80. http://doi.org/10.1016/j.renene.2014.09.026.
- Santos-Alamillos, F. J., Pozo-Vázquez, D., Ruiz-Arias, J. A., Lara-Fanego, V., Tovar-Pescador, J., 2012. Analysis of spatiotemporal balancing between wind and solar energy resources in the southern Iberian Peninsula. Journal of Applied Meteorology and Climatology 51(11), 2005-2024, doi: 10.1175/JAMC-D-11-0189.1.
- Schwarz, M., D. Folini, S. Yang, Allan, P., Wild, M., 2020. Changes in atmospheric shortwave absorption as important driver of dimming and brightening. Nat. Geosci. 13: 110–115, https://doi.org/10.1038/s41561-019-0528-y.
- Silva VP, Silva RA, Cavalcanti EP, Braga CC, Azevedo PV, Singh VP, Pereira ERR., 2010. Trends in solar radiation in NCEP/NCAR database and measurements in northeastern Brazil, Solar Energy, 84, 1852–1862, doi: 10.1016/j.solener.2010.07.011.
- Skamarock, W. C., J. B. Klemp, J. Dudhia, D. O. Gill, D. M. Barker, W. Wang and J. G. Powers, 2005: A Description of the Advanced Research WRF Version 2. NCAR Tech Note, NCAR/TN–468+STR, 88 pp.

- Skamarock, W. C., Klemp, J. B., Dudhia, J., Gill, D. O., Barker, D. M., Duda, M. G., Huang X.-Y., Wang, W., Powers, J. G., 2008. A Description of the Advanced Research WRF Version 3. NCAR Technical Note, NCAR/TN-475+STR. Mesoscale and Microscale Meteorology Division, National Center for Atmospheric Research, Boulder, CO, USA.
- Sneyers, R., 1975. Sur l'analys estatistique des series d'observations. OMM, Note Tech, 143, 192p.
- Soares, P. M., Cardoso, R. M., Miranda, P. M., de Medeiros, J., Belo-Pereira, M., Espirito-Santo, F., 2012. WRF high resolution dynamical downscaling of ERA-Interim for Portugal. Climate Dynamics 39 (9-10), 2497-2522, doi 10.1007/s00382-012-1315-2.
- Soares, P. M., Cardoso, R. M., Semedo, Á., Chinita, M. J., Ranjha, R., 2014. Climatology of the Iberia coastal low-level wind jet: weather research forecasting model high-resolution results. Tellus A 66, http:dx.doi.org/10.3402/tellusa.v66.223777.
- Soares, Pedro M.M., Lima, Daniela C. A., Cardoso, Rita Nascimento, M., Manuel L., Semedo, Alvaro, 2017. Western Iberian offshore wind resources: More or less in a global warming climate?. Applied Energy 203, 72-90, https://doi.org/10.1016/j.apenergy.2017.06.004
- Stanhill G, Achiman O, Rosa R, Cohen S., 2014. The cause of solar dimming and brightening at the Earth's surface during the last half century: evidence from measurements of sunshine duration. J Geophys Res-Atmos, 119:10902–10911, doi:10.1002/2013JD021308.
- Stanhill, G and Moreshet S. 1992. Global Radiation climate changes: The world network, Clim. Change, 21, 57 – 75, doi:10.1007/BF00143253.
- Stanhill, G and Cohen, G. 2001. Global dimming: A review of the evidence for a widespread and significant reduction in global reduction with discussion of its probable causes on possible agriculture consequences. Agricultural and Forest Meteorology 107, 255-278. doi:10.1016/S0168-1923(00)00241-0.
- Stanhill, G, Cohen, S., 2008. Solar radiation changes in Japan during the 20th century:evidence from sunshine duration measurements. J Meteorol Soc. of Japan 86: 57−67, DOI: 10.2151/jmsj.86.57.
- Stauffer, D. R., Seaman, N. L., 1990. Use of four-dimensional data assimilation in a limited-area mesoscale model. Part I: Experiments with synoptic-scale data. Monthly Weather Review 118 (6), 1250-1277, http://dx.doi.org/10.1175/1520-0493(1990)118<1250:UOFDDA>2.0.CO;2

- Stephens, G., J. Li, C. Wild, M. Clayson, N. Loeb, S. Kato, T. L'Ecuyer, P. W. Stackhouse, M. Lebsock, and T. Andrews, 2012. An update on Earth's energy balance in light of the latest global observations, Nature Geoscience, 5(10), 691–696, doi:10.1038/ngeo1580
- Stjern, CW, Kristjánsson JE, Hansen AW. 2009. Global dimming and global brightening – an analysis of surface radiation and cloud cover data in northern Europe, International Journal of Climatology, 29, 643 – 653, doi:10.1002/joc.1735.
- Streets, D. G., Wu, Y., and Chin, M., 2006. Two-decadal aerosol trends as a likely explanation of the global dimming/brightening transition. Geophys. Res. Lett., 33, L15806, doi:10.1029/2006gl026471.
- Šúri, M., Hofierka, J., 2004. A New GIS-based Solar Radiation Model and Its Application to Photovoltaic Assessments. Transactions in GIS 8, 175–190, doi:10.1111/j.1467-9671.2004.00174.x.
- Šúri, M., Huld, T. A., Dunlop, E. D., Ossenbrink, H., A., 2007. Potential of solar electricity generation in the European Union member states and candidate countries. Solar energy 81 (10), 1295-1305, doi:10.1016/j.solener.2006.12.007.
- Tahir, Zia ul Rehman, Azhar, Muhammad, Mumtaz, Manhal, Asim, Muhammad , Moeenuddin, Ghulam, Sharif, Hanzalah and Hassan, Sohaib, 2020, Evaluation of the reanalysis surface solar radiation from NCEP, ECMWF, NASA, and JMA using surface observations for Balochistan, Pakistan, Journal of Renewable and Sustainable Energy 12, 023703 (2020); https://doi.org/10.1063/1.5135381.
- Tegen, I., Hoorig, P., Chin, M., Fung, I., Jacob, D. and Penner, J., 1997. Contribution of different aerosol species to the global aerosol extinction optical thickness: Estimates from model results. J. Geophys. Res., 102, 23895–23915.
- Toledano, C., Cachorro, V. E., Berjon, A., de Frutos, A. M., Sorribas, M., de la Morena, B. A. and Goloub, P., 2007. Aerosol optical depth and Ångström exponent climatology at El Arenosillo AERONET site (Huelva, Spain). Q.J.R. Meteorol. Soc., 133: 795–807. doi: 10.1002/qj.54.
- Träger-Chatterjee C, Müller RW, Trentmann J, Bendix J., 2010. Evaluation of ERA–40 and ERA-interim re-analysis incoming surface shortwave radiation datasets with mesoscale remote sensing data. Meteorologische Zeitschrift, Vol. 19, No. 6, p. 631 – 640, doi: 10.1127/0941-2948/2010/0466.
- Trigo RM., Osborn TJ., Corte-Real JM., 2002. The North Atlantic Oscillation influence on Europe: climate impacts and associated physical mechanisms, Climate Research, 20, 9-17.

- Trigo, Isabel Franco, 2006. Climatology and interannual variability of storm-tracks in the Euro-Atlantic sector: a comparison between ER–A40 and NCEP/NCAR reanalyses. Climate Dynamics 26: 127-143.
- Troccoli, A., Morcrette, J. J., 2014. Skill of direct solar radiation predicted by the ECMWF global atmospheric model over Australia. Journal of Applied Meteorology and Climatology, 53(11), 2571-2588. DOI: http://dx.doi.org/10.1175/JAMC-D-14-0074.1
- Twomey. S. A,. Piepgrass. M. and Wolfe. T. L., 1984. An assessment of the impact of pollution on global cloud albedo. Tellus, 36B. 356-366.
- Uppala, SM., *et al*., 2005, The ERA–40 re-analysis. Quarterly Journal of the Royal Meteorological Society, 131, 2961–3012. doi: 10.1256/qj.04.176.
- Valenzuela, A., Olmo, F. J., Lyamani, H., Antón, M., Quirantes, A., and Alados-Arboledas, L. 2012. Aerosol radiative forcing during African desert dust events (2005–2010) over Southeastern Spain. Atmos. Chem. Phys. 12, 10331-10351, doi:10.5194/acp-12-10331-2012.
- Vick, B.D., Myers, D.R., Boyson, W.E., 2012. Using direct normal irradiance models and utility electrical loading to assess benefit of a concentrating solar power plant. Sol. Energy 86 (12), 3519–3530, https://doi.org/10.1016/j.solener.2012.03.010.
- Von Neumann, J., 1941. Distribution of the Ratio of the Mean Square Successive Difference to the Variance. Ann. Math. Stat., 12, 367– 395.
- Von Storch, H., Langenberg, H., Feser, F., 2000. A spectral nudging technique for dynamical downscaling purposes. Mon. Wea. Rev. 128, 3664–3673.
- Wagner, F., Bortoli, D., Pereira, S., Costa, M. J., Silva, A., Weinzierl, B., Tegen, I., 2009. Properties of dust aerosol particles transported to Portugal from the Sahara desert. Tellus B 61 (1), 297-306, doi: 10.1111/j.1600-0889.2008.00393.x.
- Waldron, K.M, Peagle, J., Horel, J.D., 1996. Sensitivity of a spectrally filtered and nudged limited area model to outer model options. Mon. Wea. Rev. 124, 529–547.
- Wallace, J., and P. Hobbs, Atmospheric science an introductory survey, Academic press, 1977.
- Wang, K.,Q. Ma, Z. Li, and Wang. J., 2015. Decadal variability of surface incident solar radiation over China: Observations, satellite retrievals, and reanalyses. J. Geophys. Res. Atmos., 120, 6500–6514. doi: 10.1002/2015JD023420.

- Wang, Y., Wild, M., Sanchez-Lorenzo, A., and Manara, V., 2017. Urbanization effect on trends in sunshine duration in China, Ann. Geophys., 35, 839–851, https://doi.org/10.5194/angeo-35-839-2017, 2017.
- Wang, Y., and Wild, M., 2016. A new look at solar dimming and brightening in China. Geophysical Research Letters, 43.
- Wielicki, B. A., Barkstrom, B. R., Harrison, E. F., Lee III, R. B., Louis Smith, G., Cooper, J. E., 1996. Clouds and the Earth's Radiant Energy System (CERES): An earth observing system experiment. Bulletin of the American Meteorological Society 77 (5), 853-868, http://dx.doi.org/10.1175/1520-0477(1996)077<0853:CATERE>2.0.CO;2.
- Wijngaard, J. B., Klein Tank, A. M. G. and Können, G. P. 2003. Homogeneity of 20th century European daily temperature and precipitation series. Int. J. Climatol., 23: 679–692. doi: 10.1002/joc.906.
- Wild, M., A. Ohmura, H. Gilgen, and J. J. Morcrette, 1998. The distribution of solar energy at the Earth's surface as calculated in the ECMWF Re-Analysis. Geophys. Res. Lett. 25(23), 4373–4376. DOI: 10.1029/1998GL900175.
- Wild, M., 2001. Surface and atmospheric radiation budgets as determined in reanalyses, in IRS2000: Current Problems in Atmospheric Radiation. W.L. Smith and Yu. M. Timofeyev (Eds.). A. Deepak Publishing, Hampton, Virginia, p. 602-605.
- Wild, M., Gilgen, H., Roesch, A., Ohmura, A., Long, C. N., Dutton, E. G., Tsvetkov, A., 2005. From dimming to brightening: Decadal changes in solar radiation at Earth's surface. Science 308 (5723), 847-850.
- Wild, M., 2009. Global dimming and brightening: A review, J. Geophys. Res. 114, D00D16, doi:10.1029/2008JD011470.
- Wild, M., Trüssel, B., Ohmura, A., Long, C. N., König-Langlo, G., Dutton, E. G., and Anatoly, T., 2009. Global dimming and brightening: An update beyond 2000, Journal of Geophysical Research Atmospheres, 114, 895-896.
- Wild, M., 2010. Introduction to special section on Global Dimming and Brightening. J. Geophys. Res., 115, D00D00, doi:10.1029/2009JD012841.
- Wild, M, Schmucki, E., 2011. Assessment of global dimming and brightening in IPCC-AR4/ CMIP3 models and ERA–40, Climate Dynamics, 37, 1671-1688, doi: 10.1007/s00382-010-0939-3.
- Wild, M., 2012. Enlightening Global Dimming and Brightening.Bull. Amer. Meteor. Soc., 93, 27–37.doi: http://dx.doi.org/10.1175/BAMS-D-11-00074.1.

- Wild, M., *et al*., 2015. Projections of long-term changes in solar radiation based on CMIP5 climate models and their influence on energy yields of photovoltaic systems. Solar Energy 16: 12-24.
- Wild, M., Folini, D., Hakuba, M. Z., Schar, C., Seneviratne, S. I., Kato, S., Rutan, D., Ammann, C., Wood, E. F., and König-Langlo, G., 2015. The energy balance over land and oceans: an assessment based on direct observations and CMIP5 climate models, Clim. Dynam. 44, 3393–3429, doi:10.1007/s00382-014-2430-z.
- Wild, M., 2016. Decadal changes in radiative fluxes at land and ocean surfaces and their relevance for global warming. WIREs Clim Change 20, 7:91–107. doi: 10.1002/wcc.372.
- Wild, M., 2017. Towards Global Estimates of the Surface Energy Budget, Current Climate Change Reports, Volume 3, Issue 1, pp 87–97, https://doi.org/10.1007/s40641-017-0058-x.
- Wilmot, C.-S. M., Rappenglück, B., Li, X., and Cuchiara, G., 2014. MM5 v3.6.1 and WRF v3.5.1 model comparison of standard and surface energy variables in the development of the planetary boundary layer, Geosci. Model Dev., 7, 2693-2707, https://doi.org/10.5194/gmd-7-2693-2014.
- Wilson, P. R., 1994. Solar and Stellar Activity Cycles (New York: Cambridge University Press)
- WMO., 2008. Guide to Meteorological Instruments and Methods of Observation. WMO-No. 8, Seventh edition.
- Xia, X., 2010. A closer looking at dimming and brightening in China during 1961–2005, Ann. Geophys., 28, 1121–1132, doi:10.5194/angeo-28-1121-2010.
- Xia, X. A., P. C. Wang, H. B. Chen, and Liang, F., 2006. Analysis of downwelling surface solar radiation in China from National Centers for Environmental Prediction reanalysis, satellite estimates, and surface observations. J. Geophys. Res. 111, D09103, doi:10.1029/2005JD006405.
- Xue, Y., Janjic, Z., Dudhia, J., Vasic, R., De Sales, F., 2014. A review on regional dynamical downscaling in intraseasonal to seasonal simulation/prediction and major factors that affect downscaling ability. Atmospheric Research 147, 68-85, http://dx.doi.org/10.1016/j.atmosres.2014.05.001.
- Yang, D., Kleissl, J., Gueymard, C.A., Pedro, H.T.C., Coimbra, C.F.M., 2018. History and trends in solar irradiance and PV power forecasting: A preliminary assessment and review using text mining. Solar Energy, Volume 168, Pages 60-101 https://doi.org/10.1016/j.solener.2017.11.023.

- Yang, S., Wang, X. L., Wild, M., 2019. Causes of dimming and brightening in China inferred from homogenized daily clear-sky and all-sky in situ surface solar radiation records (1958–2016). J. Clim. 32, 5901–5913, DOI: 10.1175/JCLI-D-18-0666.1.
- Yhang, YB., Hong, SY., 2011. A study on large-scale nudging effects in regional climate model simulation. Asia-Pacific J. Atmos. Sci. 47 (235), doi:10.1007/s13143-011-0012-0
- You, Q., S. Kang, W.-A. Flügel, A. Sanchez-Lorenzo, Y. Yan, J. Huang, and J. Martin-Vide, 2010. From brightening to dimming in sunshine duration over the eastern and central Tibetan Plateau (1961–2005), Theor. Appl. Climatol., 101(3–4), 445–457, doi:10.1007/s00704-009-0231-9.
- You Q, Sanchez-Lorenzo A, Wild M, Folini D, Fraedrich K, Ren G, Kang S. 2013. Decadal variation of surface solar radiation in the Tibetan Plateau from observations, reanalysis and model simulations, Climate Dynamics 40, Issue 7-8, pp 2073-2086, doi: 10.1007/s00382-012-1383-3.
- Yu, H., Kaufman, Y. J., Chin, M., Feingold, G., Remer, L. A., Anderson, T. L., Balkanski, Y., Bellouin, N., Boucher, O., Christopher, S., DeCola, P., Kahn, R., Koch, D., Loeb, N., Reddy, M. S., Schulz, M., Takemura, T., and Zhou, M., 2006. A review of measurement-based assessments of the aerosol direct radiative effect and forcing. Atmos. Chem. Phys. 6, 613-666, doi:10.5194/acp-6-613-2006.
- Zeilik, M. and Gregory, S. Introductory Astronomy & Astrophysics, fourth edition, Saunders College Publishing. 1998. ISBN: 0030062284.
- Zhang X, Liang S, Wang G, Yao Y, Jiang B, Cheng J., 2016. Evaluation of the reanalysis surface incident shortwave radiation products from NCEP, ECMWF, GSFC, and JMA using satellite and surface observations. Remote Sens 2016;8:225.
- Zhao, L., X. Lee, and S. Liu, 2013. Correcting surface solar radiation of two data assimilation systems against FLUXNET observations in North America, J. Geophys. Res. Atmos., 118, 9552–9564, doi:10.1002/jgrd.50697.
- Zhou, Lian-Tong., 2011. Interdecadal Variability in Surface Solar Radiation over Northwest China and Its Possible Cause. Atmospheric and Oceanic Science Letters, 4:2, 103-108, DOI: 10.1080/16742834.2011.11446912.
- Zhou, Z, Lin, A, Wang, L, Qin, W, zhong, Y, He, L. 2019, Trends in downward surface shortwave radiation from multi-source data over China during 1984–2015. Int J Climatol. 2019; 1– 19. https://doi.org/10.1002/joc.6408.
- APREN, 2014: http://www.apren.pt/pt/projectos/nacionais/estudo-apren-deloitte/

- APREN, 2019: Anuário – Portugal precisa da nossa energia., (acessed: 23.09.2020)
- APREN: http://www.apren.pt/fotos/editor2/impacto_fer__relatorio_final_20140930.pdf
- CERES: https://ceres.larc.nasa.gov/data/
- DGAE: http://www.dgeg.pt/
- ECMWF: https://www.ecmwf.int/
- EUROSTAT: Europe 2020 indicators-climate change and energy. https://ec.europa.eu/eurostat/statistics-explained/index.php?title=Europe_2020_indicators_-_climate_change_and_energy, (Acessed: 24.02.2019)
- IDAE, 2016. Informe Estadistico Energias Renovables: http://informeestadistico.idae.es/t10.htm (accessed: 15.01.2017)
- IRENA: irena.org (accessed on 09/03/2020)
- Kipp & Zonen: http://www.kippzonen.com/ (accessed 15.09.2019)
- NOAA: https://www.ngdc.noaa.gov/stp/solar/ssn.html